6-30-2016

# Ligand-Induced Magnetic Changes In Metal Thin Films

Fiona Senta Oberbeck-Oxsher
*University of South Carolina*

# LIGAND-INDUCED MAGNETIC CHANGES IN METAL THIN FILMS

by

Fiona Senta Oberbeck-Oxsher

Vordiplom
Johannes Gutenberg Universität Mainz, 2007

---

Submitted in Partial Fulfillment of the Requirements

For the Degree of Doctor of Philosophy in

Chemistry

College of Arts and Sciences

University of South Carolina

2016

Accepted by:

Scott R. Crittenden, Major Professor

Thomas Vogt, Committee Member

Andrew B. Greytak, Committee Member

Stephen L. Morgan, Committee Member

Thomas M. Crawford, Committee Member

Lacy Ford, Senior Vice Provost and Dean of Graduate Studies

## DEDICATION

This work is dedicated to my parents, Renate and Arthur Oberbeck, for teaching me never to give up and never to lose sight of my dreams. It is also dedicated to my wonderful husband, Jerry Oxsher, who was my discussion partner for any chemical problem I encountered, but also the one who had my back in troublesome times. Their endless support and love gave me the strength to finish what I started.

Danke!

## ACKNOWLEDGEMENTS

Foremost, I would like to express my gratitude to my advisor, Dr. Scott Crittenden, for teaching me how to think out of the box. His guidance and support made me a better scientist. I would like to thank Dr. Thomas Crawford for his guidance in the magnetic world. My sincere thanks also go to all of my committee members, especially my committee chair, Dr. Thomas Vogt, for the encouragement, support, and advice throughout the last 6 years. A special thanks to Dr. Richard Webb for letting me use his instruments and for always having a word of advice. I would like to thank Dr. Bharat Kumar who spent countless hours discussing research and cultures with me. My thanks go to Dr. Brett Altschul, who managed to make a chemist understand Jackson. I also want to thank Dr. Qian Wang, Dr. Gary Horvath, Dr. Michael Bruckman, and Dr. Nisaraporn "Eve" Suthiwangcharoen for their training and mentorship in the virus work. Thank you, Dr. George Handy and Dr. Amelia Taylor-Perry for supporting me in my years as TA. A special thanks also goes to Dr. Monty Fetterolf and the chemistry faculty at USC Aiken for giving me the chance to be a "real" Professor. A big thank you goes to my dear friends Kathrin and Bea for a friendship that withstands thousands of miles. Last, but certainly not least, I would like to thank my wonderful friends Lauren, Tony, Adam, Swat, Jason, Nestor, Hannah, Ken, Gordon, Kevin, and Branfur for never having a dull moment in and out of the lab.

## ABSTRACT

The investigation of magnetic properties of thin films whose surfaces were modified by organic molecules shows that the addition of any functional group to the surface measurably changes the magnetic properties. The effect often scales with ligand strength and is not limited to surfaces with ferromagnetic properties. Improving upon the technique developed by Knaus *et al.* [1], a stable and sensitive device was developed to measure this magnetic effect using the planar Hall effect (PHE) in order to shed light onto controversial questions of purported paramagnetism of thiolated gold. There is a measureable non-diamagnetic response of thin gold layers when exposed to alkanethiols as well as other ligands such as alcohols, carboxylic acids, amines, and ketones.

This approach is not susceptible to contamination by external magnetic materials, unlike many of the previous measurements of anomalous gold-thiol magnetism. Significant efforts were devoted to exclude magnetic contaminations and are reported in chapters 4 and 5. The developed analysis system, a magnetic resistance measurement system (MaRMS), is stable, highly sensitive, and flexible. Our results and initial theoretical models open a door to a wide variety of magneto-chemical surface phenomena.

In the last few decades self-assembled monolayers (SAMs) on metal substrates have attracted attention for their ability to modify the physical properties of metal substrates [2, 3], for instance, the conductivity. The conductivity of gold is known to decrease significantly after the formation of SAMs on its surface. Recently, it has been suggested that the bulk diamagnetism of gold changed to paramagnetism after similar treatment [2, 3]. The measured values were extremely large and often ascribed to the susceptibility of non-diamagnetic contamination. The experimental techniques employed are very susceptible to contamination and hence it is difficult to rule it out. Therefore, a series of experiments not susceptible to contamination were performed and it was determined that the observed effects were due to magnetic changes in the gold or to systematic errors in the previous measurements. As presented in this dissertation, it was found that a change in magnetic properties of gold is indeed observable when the surface is modified via metal-organic bonds. In addition, it was demonstrated that a large number of different functional groups can cause this effect and that it is not exclusive to thiol ligands. Furthermore, the modification of magnetic properties for other metals was also shown.

The capability to make well characterized metal thin films has been developed, and the effect of a variety of organic surface modifications on the magnetic properties of metal thin films has been investigated. For these investigations a magnetic transport measurement technique (MTM) was used and a custom built instrument was developed and built.

First, measurements on cobalt, nickel, and Permalloy thin films will be discussed. The magnetic properties of these thin films were modified using the following molecules: ethanol, hexylamine, acetone, deionized water, 1-dodecylthiol, acetic acid, and hexane. The change in magnetism was recorded by measuring the planar Hall voltage of the sample.

For cobalt thin films in particular the reach of the PHE through the sample was determined by measuring thin films of varying thickness. It was demonstrated that the change of magnetic properties appears to reach much deeper into the metal sample than previously expected. An increasing effect was observed for up to 30 nm thickness of the thin film.

Also, the influence of the tail length was measured by applying different alcohols, ranging from methanol to hexanol. While methanol surprisingly had almost no effect on the magnetic properties, the longer alcohols showed a decreasing effect with increasing chain length. This shows that the choice of ligand for the surface modification cannot just be dictated by the head functional group, but one must consider the chain length as well.

Next, the change in magnetism of gold thin films and how it compares to other diamagnetic thin films, such as silver and copper, will be discussed. Induced magnetic moments in gold thin films and nanoparticles have been a popular topic in recent literature as will be discussed in chapter 3. Some of the reported magnetic moments for gold are extremely large, even when compared to the magnetic moment of iron. Although determining a quantitative value for the developed magnetic moment in gold is not possible with this technique, it was

definitively determined that gold can be manipulated into changing the size of its magnetic moment and developing a measureable non-diamagnetic magnetization. It was found that not only molecules with a thiol functionality have an effect on the magnetism of gold thin films, but that other ligands can also cause a change in magnetism. This was demonstrated by using the same series of small organic molecules as used previously on ferromagnetic thin films. This showed that surface-modified magnetism is more common than previously thought and by using less expensive materials and simpler measurements it can become an attractive method for inexpensive, yet widely applicable sensors in the medical field as well as novel digital storage devices.

## REFERENCES


1. Knaus, B.; Garzon, S.; Crawford, T.M. Alkenethiol induced changes in the magnetotransport properties of Co/Au bilayers. *J. Appl. Phys.* **2009**, *105*, 07A903

2. Trudel S. Unexpected magnetism in gold nanostructures: making gold even more attractive, *Gold Bulletin,* **2011**, *44*, 3

3. Love, J.C.; Estroff, L.A; Kriebel, J.K.; Whitesides, G.M: Self-assembled monolayers of thiolates on metals as a form of nanotechnology, *Chem. Rev.,* **2005**, *105*, 1103

# Table of Contents

# LIST OF FIGURES

## List of Abbreviations

AFM ..... Atomic Force Microscopy

EDX ..... Energy-Dispersive X-Ray Spectroscopy

emu ..... Electro-Magnetic Unit

EPR ..... Electron Paramagnetic Resonance

ESM ..... Electron Scanning Microscopy

ESR ..... Electron Spin Resonance

EXAFS ..... Extended X-Ray Absorption Fine Structure

fcc ..... face-centered cubic

*g* ..... Gravity Constant

G ..... Gauss

GC ..... Gas Chromatography

ICP ..... Inductively Coupled Plasma

MaRMS ..... Magnetic Resonance Measurement System

MFM ..... Magnetic Force Microscopy

$\mu_B$ ..... Bohr Magneton

mm ..... Millimeter

µm ..... Micrometer

MS ..... Mass Spectroscopy

nm ..... Nanometer

NMR ..... Nuclear Magnetic Resonance Spectroscopy

PHE ..... Planar Hall Effect

PIXE.....Particle Induced X-Ray Emission

PPMS..... Physical Property Measurement System

SAM ..... Self-Assembled Monolayer

SQUID ..... Superconducting Quantum Interfering Device

TEM .....Tunneling Electron Microscope

TF ..... Thin Film

UV-Vis.....Ultraviolet-Visible Spectroscopy

VSM .....Vibrating Sample Magnetometry

XANES..... X-Ray Absorption Near-Edge Spectrum

XAS..... X-Ray Absorption Spectroscopy

XMCD ..... X-Ray Magnetic Circular Dichroism

XPS..... X-Ray Photoelectron Spectroscopy

XRD .....X-Ray Diffraction

# CHAPTER 1

## INTRODUCTION

This dissertation will discuss the ligand-induced magnetic changes of metal thin films. It will be demonstrated that it is possible to modify the magnetic properties of gold as well as those of other metals such as silver, copper, cobalt, nickel and Permalloy. The strength of the modification is dependent on the ligand strength used to alter the surface of the metal. In contrast to the previous understanding that gold can only be modified with a thiol ligand and have a significant change in magnetic properties, it will be shown that other ligands such as alcohols, ketones, amines, and carboxylic acids can induce a similar effect. Silver and copper show the same magnetic changes as gold. Furthermore, a diamagnetic metal is not a necessity to change the magnetic properties. The ferromagnetic metal thin films of cobalt, nickel, and Permalloy show the same ability to be modified via a ligand layer on the surface as the diamagnetic metals. Again, the size effect is directly related to the ligand strength according to Pearson's HSAB concept. In addition, it will be demonstrated that the magnetic modification, which was so far believed to have a reach of about 1 nm, the length-scale of the magnetic effect appears to be about 10 nm. Also, it will be shown that the change in magnetization of the metal is not just dependent on the functional group directly in contact with the metal surface, but that the chain length also plays a significant role.

Magnetic transport measurements are a large and attractive research field. They are widely used in the electronics industry in sensors, switches, and read/write heads for hard drives [1-3]. The foundation of magnetic transport measurements is a variety of effects, such as the regular Hall effect, the anomalous Hall effect (AHE), and the planar Hall effect (PHE). Those effects are related to the magnetic anisotropy of various materials including metals, alloys, and oxides. In addition, many of these effects can influence each other. Electric and magnetic properties of materials are coupled, therefore, changes to one induce changes to the other. It was demonstrated, through the development of a highly stable and sensitive PHE sensor capable of detecting shifts in the local magnetic field on the order of 0.01 Oersted, that surface modifications to essentially any metal induce magnetotransport changes. Previous reports were confirmed of anomalous magnetic effects of thiol-capped gold, finding a change in magnetic properties, which is consistent with a para- or ferromagnetic response to gold thin film thiolation [1, 8-11]. Great effort was exerted toward the elimination of possible sources of magnetic material contamination and it is demonstrated that this cannot be the cause of the observed magnetic changes.

This work was inspired by a number of different reports of surface-modified magnetism in otherwise non-magnetic materials. For example, Elfimov *et al.* reported defect-induced magnetism in non-magnetic solids [4]. They calculated that a ferromagnetic ground state of calcium oxide could be created by introducing

dilute cation vacancies [4.5]. Density functional theory calculations [4] for such defects in zinc oxide suggested a magnetic moment similar to that of bulk iron [6].

The observation of magnetism in otherwise non-magnetic materials can be influenced by many external conditions, such as pressure or temperature to name a few [7]. Apart from potential contamination issues, the concentration of defects in the material of interest can play an important role. Therefore, despite the enticingly high theoretical moments reported in the literature [9, 11], the existence of magnetism in modified non-magnetic materials has yet to be convincingly demonstrated. Although controversial, since magnetism either is or is not present in a material, additional reports with similar observations in other previously assumed non-magnetic materials were published over the last two decades [20-22].

In this work, only those reports directly related to my work will be discussed. Beginning in 2003, a series of papers reported that gold thin films and gold nanoparticles switch from diamagnetic to paramagnetic when a thiolated self-assembled monolayer is formed [8-13]. For example, Carmeli *et al.* reported the appearance of magnetism in a 100 nm gold film after the deposition of thiols with different tail lengths, ranging from ethylthiol to a thiolated polyaniline [8]. Magnetic moments of several tens of Bohr magnetons per nanoparticle were reported. In addition, the magnitude of the magnetism effect in this publication was directly related to the size of the molecule used as ligand on the metal surface [8].

In 2010 Adeagbo *et al.* studied the effect of surface cleaning on the magnetic properties of various oxides and reported that for strontium titanate ($SrTiO_3$) they found an enhanced ferromagnetism after cleaning with ethanol, while

cleaning with acetone causes ferromagnetism to vanish [14,15]. Their theoretical calculations roughly confirmed their experimental findings. In their density function theory calculations, the magnetic moment was only present when the surface was terminated with titanium or oxygen and there was a vacancy of either one of these atoms. Further they reported that the adsorption of ethanol in the case of a titanium vacancy theoretically quenches the magnetic moment, while in the case of an oxygen vacancy the magnetic moment remains. Similar calculations were performed with acetone as adsorbent, however, it had no influence on the magnetic moment for either of the vacancies [16].

The work published for the magnetic changes report that the results are very difficult to reproduce [10, 11]. Because of this, it is hard to establish a correlation between the ligand and a change in magnetism. In addition, the molecules used for the SAM represent a very limited selection, which presents an additional problem in rationalizing a change in magnetism. The resulting magnetic moments vary over several orders of magnitude, making it difficult to extract a single answer from these values, but instead demonstrating that there is still a lack of understanding and experimental repeatability. The experimental techniques vary greatly and all suffer from possible sources of contamination of the sample. The majority of the measurements have been carried out using a superconducting quantum interference device (SQUID) [8-11, 13, 17], which gives information about the net magnetization of the sample. However, it lacks the ability to spot interference from contaminant atoms that might be present in the sample [10, 11, 18, 19].

Searching for a technique that does not suffer from these problems, Knaus *et al.* [13] first employed the PHE. Ogrin *et al.* [18] demonstrated that the net Hall effect as a function of the magnetic field shows a peak resulting from the planar Hall effect. This peak can shift in its position depending on the magnitude of the magnetic field to which the sample is exposed.

The PHE occurs due to a combination of electromagnetic effects and can be measured as a voltage perpendicular to the applied current. This measurement requires the sample and the applied magnetic field to be roughly, but not perfectly, perpendicular to each other, so that an in-plane component of the applied magnetic field is still present (**Figure 1.1**). By applying an external magnetic field, the magnitude of the in-field component can be changed. Eventually the in-field

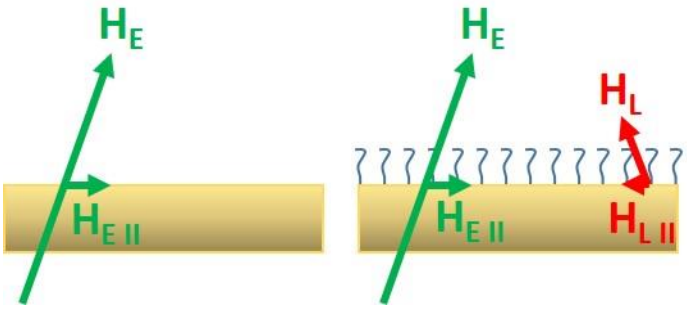


***Figure 1.1: Left: The sample is exposed to an externally applied magnetic field, $H_E$, which has an in-plane component, $H_{E\,II}$. Right: After the application of ligands on the sample there is an additional magnetic field, $H_L$, present, which also has an in-plane component, $H_{L\,II}$. The presence of the ligands on the surface and the additional magnetic field changes the net magnetic field that the sample experiences, and so the value of $H_E$ at which the PHE peak in the Hall voltage occurs. Here, as in most of my results, the additional field counteracts the externally applied field, resulting in a shift of the peak toward higher $H_E$.***

component becomes big enough to overwhelm the magnetization and cause it to snap around along the easy axis (see chapter 4.3), which causes the peak of the PHE used in this work. By adding a ligand layer, which modifies the magnetic properties, the net in-field component now includes an additional value for the surface modification. Therefore, the magnetization requires a different strength of the external field to snap along the easy axis and the peak shows up at a slightly shifted position. This change in peak position is the indicator for the change in magnetic properties of the sample. Therefore this technique was used as a reliable indicator to determine if the magnetic properties of metals can really be altered by a surface modification.

The goal was to conduct measurements that are not hampered by contamination, are very reproducible, and taken in a stable environment. Therefore, the focus of this work is on measurements in a custom designed instrument, the Magnetic Resistance Measurement System (MaRMS), which is similar in sensitivity to the Physical Property Measurement System (PPMS) but easier to use. Improvements on the previous measurements were made in several ways. First, a more stable, higher angular resolution measurement system compared to the PPMS was developed by designing MaRMS, which allows a pure surface measurement versus a volume measurement conducted in a SQUID. Second, the absence of magnetic contamination in the measurement is thoroughly examined; the effect is real. Third, it is shown that the effect is much more widespread than previously thought and demonstrates that it behaves consistently

with basic chemical facts, increasing with increasing ligand-strength according to the HSAB concept regardless of metal and ligand.

While the PPMS is a commercially available system with the capability to apply an external field of up to 9 T, it can be very cumbersome to use. Due to the large field, the sample must be placed in an enclosed cooled chamber and has to be removed in order to conduct the surface modification. The PHE is proportional to the angle of the applied magnetic field relative to the sample, therefore a stable sample setup is mandatory for successful measurements. It is not possible to reposition the sample holder in the exact same position, which causes a significant error. In MaRMS the sample is not enclosed and the surface of the metal layer can be modified without taking the sample out of the instrument. This allowed for the orientation at which I measured to be the same, which eliminates a significant error source in this set up compared to a PPMS. Just like the PPMS, MaRMS measures the sum of Hall effects occurring in a ferromagnetic metal layer before and after surface modifications, while being able to control the magnitude and the angle of an externally applied magnetic field up to 0.7 T. MaRMS enables measurements to be taken with great repeatability and with a sensitivity of 0.01 Oersted of the in-plane shift.

The absence of magnetic contaminants was verified through a variety of measurements, confirming that the effect is really due to the magnetic properties of surface-modified metals. Energy-dispersive X-ray spectroscopy (EDS) of the metal thin films was performed to show the absence of contamination by other magnetic materials. To demonstrate the purity of the small molecules employed

in the surface modifications, nuclear magnetic resonance (NMR) measurements as well as inductively coupled plasma mass spectrometry (ICP-MS) were used. This allows measurements to give a clear answer to whether or not the solvent layer is responsible for the change of the magnetic behavior of the metallic thin film.

To understand the PHE it is important to understand anisotropic magnetoresistance, which requires understanding of magnetic resistance and anisotropy. Therefore chapter 2 is a discussion of the fundamentals of magnetism leading to the PHE and anisotropic effects. Chapter 3 is a discussion of previous work, which inspired this project and chapter 4 and 5 will then summarize my results, including a discussion.

## 1.1 REFERENCES


1. Wolf, S. A.; Awschalom, D. D.; Buhrman, R. A.; Daughton, J. M.; von Molnár, S.; Roukes, M. L.; Chtchelkanova, A. Y.; Treger, D. M. Spintronics: A Spin-Based Electronics from the Furture, *Science,* **2001**, *294*, 1488

2. Versluijs, J. J.; Bari, M. A.; Coey, J. M. D. Magnetoresistance of Half-Metallic Oxide Nanocontacts, *Phys. Rev. Lett.,* **2001**, *87*, 026601

3. Zutic J. F.; Sarma, S. D. Spintronics: Fundamentals and Applications Rev. Mod. Phys. 76, 323 (2004).

4. Elfimov, I.S.; Yunoki, S.; Sawatzky, G.A. Possible path to a new class of ferromagnetic and half-metallic ferromagnetic materials. *Phys. Rev. Lett.* **2002**, *89*, 216403

5. Esquinanzi, P.; Hergert, W.; Spemann, D.; Setzer, A.; Ernst, A. Defect-induced magnetism in solids. *IEEE Trans. Magn.* **2013**, *49 (8)*, 4668

6. Adeagbo, W.A.; Fischer, G.; Ernst, A.; Hergert, W. Magnetic effects of defect pair formation in ZnO. *J. Phys.: Condens. Matter.* **2010**, *22*, 436002

7. Tippler, P. A. *Physik*, Spektrum Akademischer Verlag, Heidelberg, Berlin, Oxford 1994

8. Trudel, S. Unexpected magnetism in gold nanostructures: making gold even more attractive. *Gold Bull.* **2011**, *44*, 3-13

9. Carmeli, I.; Leitus, G.; Naaman, R.; Reich, S.; Vager, Z. Magnetism induced by the organization of self-assembled monolayers. *J. Chem. Phys.* **2003**, *118 (23),* 10372-10375

10. Crespo, P.; Litran, R.; Rojas, T.C.; Multigner, M.; de la Fuente, J.M.; Sanchez-Lopez, J.C.; Garcia, M.A.; Hernando, A.; Penades, S.; Fernandez, A. Permanent magnetism, magnetic anisotropy, and hysteresis of thiol-capped gold nanoparticles. *Phys. Rev. Lett.* **2004**, *93 (8)*, 087204

11. Hernando, A.; Crespo, P.; Garcia, M.A.; Fernandez Pinel, E.; de la Venta, J.; Fernandez, A.; Penades, S. Giant magnetic anisotropy at the nanoscale: Overcoming the superparamagnetic limit. *Phys. Rev. B* **2006** *74*, 052403

12. Vager, Z.; Naaman, R. Bosons as the origin for giant magnetic properties of organic monolayers. *Phys. Rev. Lett.* **2004**, *92 (8)*, 087205

13. Knaus, B.; Garzon, S.; Crawford, T.M. Alkenethiol induced changes in the magnetotransport properties of Co/Au bilayers. *J. Appl. Phys.* **2009**, *105*, 07A903

14. Khalid, M.; Setzer, A.; Ziese, M.; Esquinazi, P.; Spemann, D.; Poeppl, A.; Goering, E. Ubiquity of ferromagnetic signals in common diamagnetic oxide crystals. *Phys. Rev. B*, **2010**, *81 (21)*, 214414

15. Adeagbo, W.A.; Fischer, G.; Hergert, W. First-principle investigation of electronic and magnetic properties of $SrTiO_3$ (001) surfaces with adsorbed ethanol and acetone molecules. *Phys. Rev. B*, **2011**, *83*, 195428

16. Pavlenko, N.; Kopp, T.; Mannhart, J. Emerging magnetism and electronic phase separation at titanate interfaces. *Phys. Rev. B*, **2013**, *88*, 201104

17. Yamamoto, Y.; Miura, T.; Suzuki, M.; Nawamura, N.; Miyagawa, H.; Nakamura, T.; Kobayashi, K.; Teranishi, T.; Hori, H. Direct observation of ferromagnetic spin polarization in gold nanoparticles. *Phys. Rev. Lett.* **2004**, *93 (11)*, 116801

18. Ogrin, F.Y.; Lee, S.L.; Ogrin, Y.F. Investigation of perpendicular anisotropy of a thin film using the planar Hall effect. *J. Magn. Magn. Mater.* **2000**, *219*, 331-339

19. Garcia, M.A.; Fernandez Pinel, E.; de la Venta, J.; Quesada, A.; Bouzas, V.; Fernandez, J.F.; Romero, J.J.; Martin Gonzales, M.S.; Costa- Krämer, J.L. Sources of Experimental Errors in the Observation of Nanoscale Magnetism. *J. Appl. Phys.* **2009**, *105*, 013925

20. Crespo, P.; Litran, R.; Rojas, T.C.; Multigner, M.; de la Fuente, J.M.; Sanchez-Lopez, J.C.; Garcia, M.A.; Hernando, A.; Penades, S.; Fernandez, A.

Permanent magnetism, magnetic anisotropy, and hysteresis of thiol-capped gold nanoparticles. *Phys. Rev. Lett.* **2004**, *93 (8)*, 087204

21. Litran, R.; Sampedro, B.; Rojas, T.C.; Multigner, M.; Sanchez-Lopez, J.C.; Crespo, P.; Lopez-Cartes, C.; Garcia, M.A.; Hernando, A.; Fernandez, A. Magnetic and Microstructural Analysis of Palladium Nanoparticles with Different Capping Systems. *Phys. Rev. B* **2006**, *73*, 054404

22. Garitaonandia, J.S.; Insausti, M.; Goikolea, E.; Suzuki, M.; Cashion, J.D.; Kawamura, N.; Ohsawa, H.; Gil de Muro, I.; Suzuki, K.; Plazaola, F.; Rojo, T. Chemically Induced Permanent Magnetism in Au, Ag, and Cu Nanoparticles: Localization of the Magentism by Element Selective Techniques. *Nano Lett.* **2008**, *8*, 661-667

# CHAPTER 2

## MAGNETISM

There are many effects that are related to the magnetic anisotropy observed in metals, alloys and oxides. The origin of these effects is the spin-orbit coupling. While electron transport depends on the wave functions of the electrons and therefore on the basic shape of the orbital, only the spin is influenced by an externally applied magnetic field. Spin-orbit coupling connects the two components and therefore causes the applied magnetic field to have an influence on the electron transport. This makes the measurements presented in this work possible. Below, the basic types of magnetic behavior and their abstract description on terms of spin and domains are reviewed. The different Hall effects are then discussed, which make magnetic transport measurements possible.

### 2.1 TYPES OF MAGNETISM

The familiar macroscopic manifestation of magnetism can be explained microscopically by using the concept of spin. Due to the long range nature of magnetic forces, adjacent spins can couple resulting in macroscopic magnetization. Four types of magnetism can easily be explained using the coupling of spins. Three are static cases and one is dynamic. To understand the magnetic behaviors it is necessary to understand the microscopic source of spin.

The net spin is due to unpaired electrons in their respective orbitals. As a general rule there are twice as many electrons as there are orbitals. The exact state of each electron can be described with the use of four different quantum numbers. To understand the arrangement of the electrons in the atom it is important to know a few basic details of electron configuration. The principal quantum number, n, describes the shell of the atom and the azimuthal quantum number, l, describes the shape of the orbital in which the electron resides. The magnetic quantum number, $m_l$, describes the electrons energy state. The spin quantum number, $m_s$, describes the spin direction of the electron. It can only have two values: +/- ½. According to the Pauli Exclusion Principle and Hund's rule, if there are two electrons in one orbital they must have opposite spins, which causes their net spin to be zero. The set of quantum numbers is unique for each electron in the same atom [1].

In the dynamic case, the spin interaction energy is small compared to the thermal energy. This leads to weak coupling and therefore the spins are randomly oriented when no external magnetic field is present. Such materials are called paramagnetic. When a magnetic field is applied to paramagnetic substances the spins align with the field and relax back into random positions once the field is removed. Since the spins align with the field, the paramagnetic response is positive; the presence of a paramagnet causes a local enhancement of the magnetic field.

The three static cases can be macroscopically magnetized even without an external magnetic field present. In the first type a large number of spins next to

each other can be aligned in the same direction. These materials with a uniform spin alignment are called ferromagnetic (**Figure 2.1A**). The only elements that are ferromagnetic at room temperature are cobalt, iron and nickel.

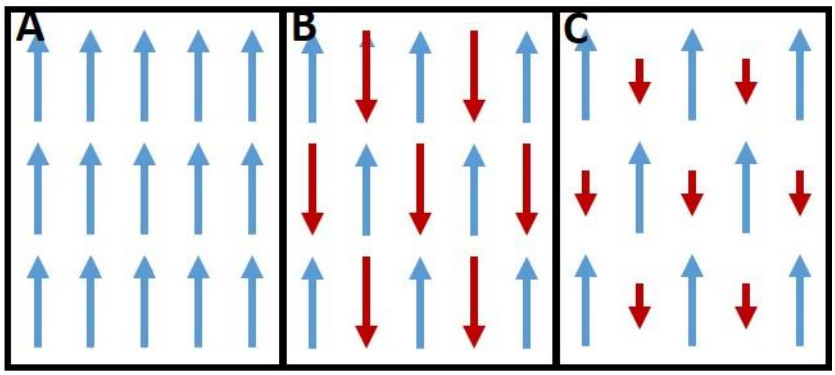


***Figure 2.1: Schematic drawing of the three static cases of magnetism: A) ferromagnetism, the case in which all spins are aligned in one direction, B) antiferromagnetism, the case in which neighboring spins point in opposite directions, and C) ferrimagnetism, the case in which neighboring spins do not only point in opposite directions but also have different magnitudes for the respective net spin.***

In the second static case the spins are also permanently aligned but neighboring spins in neighboring orbitals point in opposite directions (**Figure 2.1B**), which causes the net spin moment to be zero. These are antiferromagnetic materials. At room temperature the only antiferromagnetic element is chromium. Also, cobalt oxide is antiferromagnetic, which is important for this project due to the oxidation of the cobalt surfaces.

The third static type can be commonly found in oxides and alloys. For this case there are two sublattices that form the crystal structure. One sub-lattice with spins aligned in one direction and the second sub-lattice with spins aligned in the opposite direction (**Figure 2.1C**). Since the respective net spin of each sub-lattice

has different magnitudes the net spin of the entire material is non-zero. These are ferrimagnetic materials.

Any material that has entirely occupied or unoccupied orbitals should have a net spin of zero. When an external magnetic field is applied to these materials, they develop a magnetic moment in the opposite direction to the applied magnetic field. Such materials are called diamagnetic.

When a certain temperature is reached, the Curie temperature, the magnetic ordering in all three static cases vanishes and they become paramagnetic. The Curie temperature varies for the different types of magnetic materials.

The final type of magnetization requires a discussion of macroscopic physical objects, in particular the phenomenon of domain formation. A domain is a region of a magnetic material with uniform magnetization. In this particular region the spins are aligned with each other. Neighboring domains can align in different directions and are separated by domain walls. In those domain walls the spin orientation is much more likely to change, which moves the domain wall around. This allows the domain to change size. If there are several domains next to each other, which are randomly aligned, and an external magnetic field is applied, the domains with an orientation in the field direction grow at the expense of the others. This gives the impression of overall alignment in the field although the domains do not change directions (**Figure 2.2**). Magnetic domains do not coincide with crystal domains. Crystal domains are mainly shaped by defects in the crystal structure or parasite atoms. It is possible to have a number of crystal domains united in one

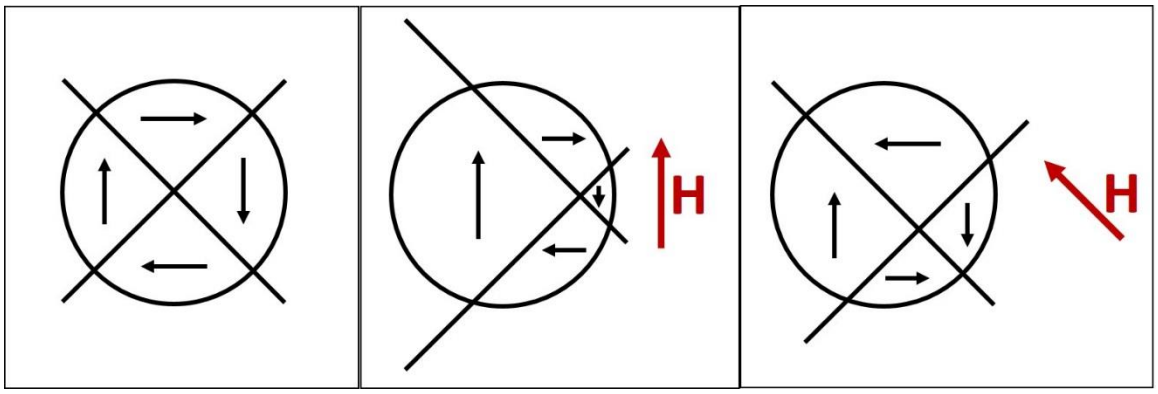


***Figure 2.2: Left: domain distribution without an external magnetic field present; middle and right: change in domain sizes caused by an applied external magnetic field.***

magnetic domain. The net spin per volume of a magnetic domain is referred to as the magnetization of this domain. Our particular sample is big enough to have many domains. The magnetization can reach a saturation point at which 100 % of the spins are aligned. However, the magnitude of the magnetization can vary for different materials since it depends on the net magnetic moment.

The existence of domains is crucial to understand super-paramagnetism, in which ferro- or ferrimagnetic materials can be organized in very small domains. These small domains are large enough to have a magnetic direction, yet small enough and insufficient coupling between the domains that the direction of the magnetization is not fixed. This is possible because the spin coupling in small domains is not strong enough to keep an orientation. Since the inter-domain coupling is weak, it appears as if a paramagnet is present.

## 2.2 HYSTERESIS

Hysteresis means that the response to an applied magnetic field depends on the previous magnetization of the material. This can be visualized by plotting

the externally applied magnetic field H, which is swept between $H_{max}$ and $-H_{max}$, against the magnetization M of the substance. Assuming one starts with an overall unmagnetized object, the magnetization initially increases approximately linearly with increasing magnetic field as shown by the dashed line. As the maximum is approached the magnetization eventually flattens out near the saturation magnetization. The net magnetization need not be equal to the applied field. It is due to the magnitude of the magnetic properties of the material. As the applied magnetic field decreases from its maximum value back to zero, the magnetization of the substance remains at a value slightly below the maximum value, which is called the remanence. The magnetization requires some additional magnetic field in the opposite direction to reach zero. This coercivity is the applied magnetic field needed in the reverse direction to drive the magnetization back to zero after it was saturated. All throughout this process, the domain sizes change in order to align the net moment with the new direction of the externally applied magnetic field. The actual shape of the hysteresis loop is caused by the coupling of the individual electrons. Initially the electrons have random directions and are not coupled. By applying an external field, the electrons are forced to point into the directions of the applied field and they couple. With an increasing applied field the number of coupled electrons increases and the domain grows. When the direction of the applied field changes, the electrons still remain in their most recent direction stabilized by the coupling. It takes a larger energy to move the direction of the coupled electrons than it did with the individual randomly aligned electrons.

Therefore, a retardation in the alignment with the applied field can be observed. This causes the shape of the hysteresis loop (**Figure 2.3**).

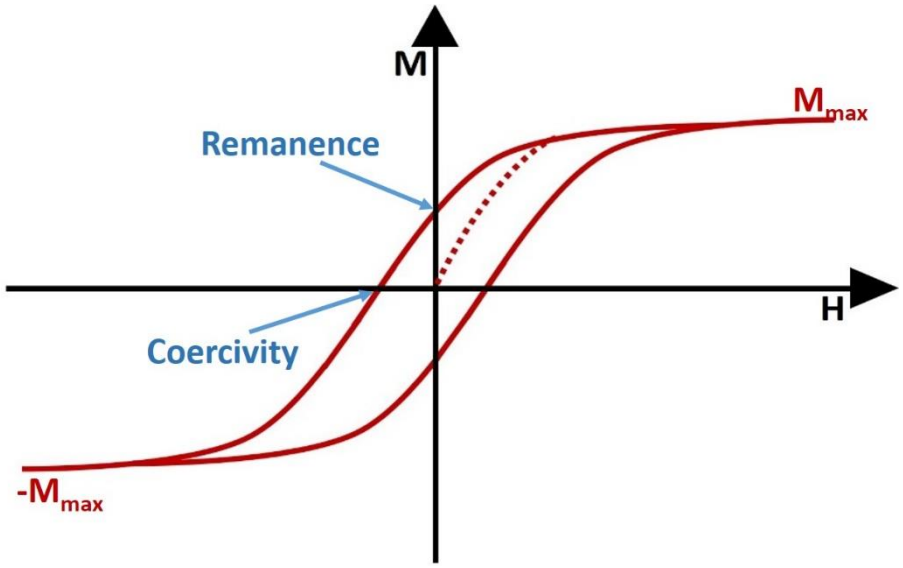


***Figure 2.3: Schematic drawing of a hysteresis curve, which shows how the magnetization M of a material is effected by an applied magnetic field H, including the remanence and the coercivity.***

## 2.3 Magnetic Anisotropy

The ease with which a magnetic material can have its magnetization set varies with the direction of that magnetization. The causes are manifold: crystal structure, macroscopic shape, mechanical stress, domain structure, et cetera. Often a small number of directions have low magnetization energy and these are called easy axes. This easy axis is bidirectional, which means the orientation along the axis, regardless of the direction, is equi-energetic. This allows a magnetization to flip along the easy axis. For this work, only the introduction of an easy axis during the deposition of the sample is important, therefore, the other examples will not be discussed. All measurements discussed in chapter 5 are

performed on systems with only one easy axis. Its presence is required to cause the appearance of a peak in the Hall voltage as the external field is swept through zero and past the peak position as discussed in chapter 4.

## 2.4 Hall Effects

In 1879, almost two decades before the electron was discovered, Edwin Hall discovered the presence of a voltage difference in the y direction across a gold leaf when a magnetic field was applied in the z direction of the sample with a current applied in the x direction [2] (**Figure 2.4**).

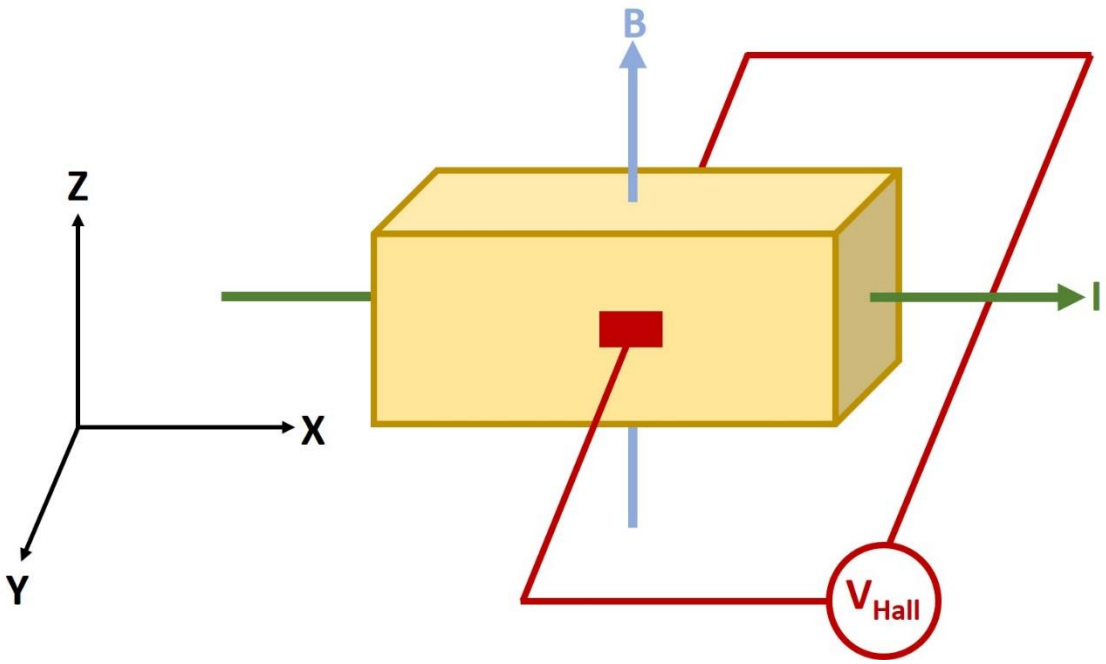


***Figure 2.4: Schematic drawing of Hall's initial experimental set up. A magnetic field, B, was applied perpendicular to the current, I, running through the metal sample. The resulting potential difference, $V_{Hall}$, was measured perpendicular to both, current and magnetic field.***

In the absence of an external magnetic field, the voltage difference would disappear. Hall attributed this difference in voltage to moving charges that are influenced by the presence of the magnetic field. He replicated this experiment with numerous other metals and demonstrated its general presence in metals. Mathematically the direction of the voltage can be determined by the cross product of the applied current I and the magnetic field B, and is the simplest example of spin-orbit coupling.

The effect is not limited to perpendicular magnetic or electric fields. The component of the field in the plane also causes a Hall voltage. This is called the PHE. The PHE requires the presence of a set magnetization. In ferromagnetic substances the applied magnetic field is only part of the net field the sample experiences, due to the internal magnetization of the material. The internal magnetization of the material is affected by the externally applied magnetic field, leading in turn to a Hall voltage. The regular classical Hall effect is due to the Lorentz force, which is the force a point charge experiences due to the presence of an electromagnetic field [1]. The third Hall effect is called the AHE and is purely quantum mechanical. The AHE is only significant in ferromagnetic materials because they are highly spin-coupled. The electrons experience a net field different from the external magnetic field due to the magnetization of the material.

## 2.5 Planar Hall Effect

The PHE is used in this work to measure the local magnetic field and determine whether or not metallic thin films change their magnetic properties when

a surface modification is performed. Therefore it is necessary to consider how to show the presence of the PHE in addition to the regular Hall effect. An equation is derived by following the suggestions from problem 6.15 in John David Jackson's "Classical Electrodynamics, 3rd Edition" [4], which leads to a very similar result as shown in a publication by Ogrin *et al.*[3]. The general form of the net electric field, **E**, can be derived as a function of the current density **J**, which is the electric current per unit area of the sample's cross section, and the magnetic field **H** by using a Taylor expansion of these two parameters. For this work, only an expansion of **J** to first order and of **H** to second order will be considered. Performing the Taylor expansion and collecting terms leads to

$$\begin{aligned}\mathbf{E} = {} & \rho_0 + \rho_1 \mathbf{H} + \rho_2 \mathbf{J} + (\rho_3 + \rho_4)\, \mathbf{H} \bullet \mathbf{J} + (\rho_5 - \rho_6)\, \mathbf{H} \times \mathbf{J} \\ & + (\rho_7 + \rho_8)\, (\mathbf{H} \bullet \mathbf{J})\, \mathbf{H} + \rho_9\, (\mathbf{H} \bullet \mathbf{H})\, \mathbf{H} + \rho_{10}\, (\mathbf{H} \bullet \mathbf{H})\, \mathbf{J} \\ & + (\rho_{11} - \rho_{12})\, \mathbf{H} \times (\mathbf{H} \times \mathbf{J}) + \rho_{13}\, \mathbf{H} \times (\mathbf{H} \times \mathbf{H}) + \rho_{14}\, \mathbf{J} \times (\mathbf{H} \times \mathbf{H}) \qquad \mathbf{(1)}\end{aligned}$$

**E** describes the net electric field in the system, **J** is the current density, **H** is the magnetic field, and the $\rho_i$ are the partial derivatives with respect to the current and the magnetic field evaluated at small **J** and **H**.

Equation 1 is the general mathematical result for a vector valued function, a function whose variable's range is set by multidimensional vectors, but **E**, **J**, and **H** are not arbitrary vectors. **E** and **J** are polar and **H** is axial, so many terms can be eliminated by demanding that the final mathematical result be consistent with the physics. A polar vector matches its mirror image upon reflection, while an axial

vector gains a sign flip under reflection. Since **E** is a polar vector, the final sum of all vectors must also be polar. Therefore, if an expression in this equation results in an axial vector it is automatically eliminated. Also, the same is true for scalars since the addition of a scalar and a vector does not result in a vector, which causes $\rho_0$, $\rho_1$ **H**, and $(\rho_3 + \rho_4)$ **H** • **J** to be eliminated from the equation. **J** is a polar vector, which allows $\rho_2$ **J** to stay. **H** is an axial vector, but since the cross product of an axial and a polar vector results in a polar vector, $(\rho_5 - \rho_6)$ **H** × **J** also remains in the equation. The dot product of an axial and a polar vector results in a pseudo-scalar, which changes sign under coordinate reversal. The multiplication of an axial vector with a pseudo-scalar results in a polar vector which restores parity and allows (**H** • **J**) **H** to stay. Parity is preserved for the dot product of two vectors of the same type, which results in a scalar that also preserves parity. Therefore $\rho_9$ (**H** • **H**) **H** is an axial vector and is eliminated while $\rho_{10}$ (**H** • **H**) **J** is a polar vector and stays. The cross product of two vectors that are aligned in the same direction is zero, which eliminates $\rho_{14}$ **J** × (**H** × **H**) and $\rho_{13}$ **H** × (**H** × **H**). $(\rho_{11} - \rho_{12})$ **H** × (**H** × **J**) can also be written as $(\rho_{11} - \rho_{12})$ (**H** • **J**) **H** – $(\rho_{11} - \rho_{12})$ (**H** • **H**) **J**. Since both of these terms are already present, only the different derivatives, symbolized by different $\rho_x$, must be considered. To simplify the derivatives of each remaining term are summed up and re-labeled, giving

$$\mathbf{E} = (\rho_\circ + \beta_1 H^2)\,\mathbf{J} + R_H\,\mathbf{H} \times \mathbf{J} + \beta_2\,(\mathbf{H} \cdot \mathbf{J})\,\mathbf{H} \qquad \textbf{(2)}$$

Since in the particular case presented in this work there is not just a magnetic field **H** to consider but actually the externally applied field **B** and the magnetization **M**

from the ferromagnetic metal thin film, the two components must be taken into consideration. Therefore the relationship $\mathbf{H} = \mathbf{B}/\mu_\circ + \mathbf{M}$ is used, which results in

$$\mathbf{E} = (\rho_\circ + \beta_1(\mathbf{B}/\mu_\circ + \mathbf{M})^2)\mathbf{J} + R_H(\mathbf{B}/\mu_\circ + \mathbf{M})\times\mathbf{J} + \beta_2((\mathbf{B}/\mu_\circ + \mathbf{M})\cdot\mathbf{J})(\mathbf{B}/\mu_\circ + \mathbf{M}) \quad \textbf{(3)}$$

However, following Ogrin [7], since the magnetization **M** is much larger than **B** in ferromagnetic materials, **B** will be neglected here. In addition it will be considered that **M** consists of its magnitude $|\mathbf{M}|$ and its unit vector $\boldsymbol{m}$. Considering this, the equation becomes

$$\mathbf{E} = (\rho_\circ + \beta_1 |\mathbf{M}|^2)\,\mathbf{J} + R_H|\mathbf{M}|\,(\boldsymbol{m}\times\mathbf{J}) + \beta_2|\mathbf{M}|^2(\boldsymbol{m}\cdot\mathbf{J})\,\boldsymbol{m} \quad \textbf{(4)}$$

To reproduce Ogrin's form of the result, the resistivities perpendicular and parallel to $\boldsymbol{m}$, $\rho_{II}$ and $\rho_\perp$, must be introduced and the terms in front of **J**, ($\boldsymbol{m}\times\mathbf{J}$), and ($\boldsymbol{m}\cdot\mathbf{J}$) $\boldsymbol{m}$ must be re-expressed in terms of them. Replacing these terms in equation 6 leads to the same result described by Ogrin *et al.* [3]

$$\mathbf{E} = \rho_\perp\mathbf{J} + \rho_H\,\boldsymbol{m}\times\mathbf{J} + (\rho_{II} - \rho_\perp)(\boldsymbol{m}\cdot\mathbf{J})\,\boldsymbol{m} \quad \textbf{(5)}$$

In the absence of a magnetization the second and third term would equal zero and the above equation would be reduced to Ohm's law. The current is scaled by the electrical resistivity with and without the presence of a magnetic field. The second term is the similar to the regular Hall effect with $\rho_H$ being the Hall resistivity. The final term is an additional magnetoresistance term in the direction of **m**. Knowing that the electric field **E** has components both parallel and perpendicular to **m**, as well as a Hall component allows to express **E** as:

$$\mathbf{E} = \rho_\perp\mathbf{J}_\perp + \rho_{II}\mathbf{J}_{II} + \rho_H\,\boldsymbol{m}\times\mathbf{J} \quad \textbf{(6)}$$

Since (***m*** • **J**) ***m*** is the vector projection $\mathbf{J}_{II}$ of **J** parallel to the unit vector **m** (**Figure 2.5**), the perpendicular component $\mathbf{J}_{\perp}$ can be described as the difference of **J** - $\mathbf{J}_{II}$

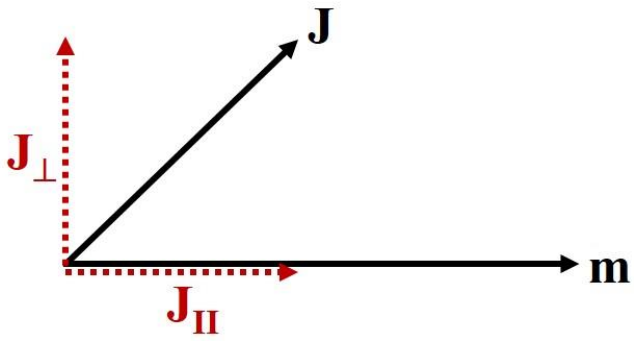


***Figure 2.5: Vector components of the current density J as parallel and perpendicular component to the magnetization M.***

or by directly replacing $\mathbf{J}_{II}$ as **J** - (***m*** • **J**) ***m***

$$\mathbf{E} = \rho_{\perp} (\mathbf{J} - (\boldsymbol{m} \cdot \mathbf{J}) \boldsymbol{m}) + \rho_{II} (\boldsymbol{m} \cdot \mathbf{J}) \boldsymbol{m} + \rho_{H} \boldsymbol{m} \times \mathbf{J} \qquad (7)$$

Rewriting the full terms allows one to see every single component:

$$\mathbf{E} = \rho_{\perp} \mathbf{J} - \rho_{\perp} (\boldsymbol{m} \cdot \mathbf{J}) \boldsymbol{m} + \rho_{II} (\boldsymbol{m} \cdot \mathbf{J}) \boldsymbol{m} + \rho_{H} \boldsymbol{m} \times \mathbf{J} \qquad (8)$$

From this the derivation of the term ($\rho_{II}$ - $\rho_{\perp}$) can be understood.

Since the above analysis is very involved, the problem is approached from a different vantage point to have a proof of concept. Therefore, the problem is approached by strictly using the rules of vector calculus. In vector calculations there can only be the regular multiplication of terms (*), the dot product (•), or the cross product (×). Using these three operations it is possible to go through the different orders and decide which ones can be used. To generalize the terms of the equation, □ is used as a place holders. It is mandatory however to regard the fact that the final result needs to be a polar vector and therefore the separate terms of the equations must all result in a polar vector. The first order would only exist

of one **H** and one **J**. For that multiplication would be excluded since for two vectors only cross products or dot products are acceptable. The later however would result in a scalar and therefore does not fit the desired pattern. Since it is only needed to expand **H** to second order, there would be three terms consisting of one **J** and two **H**s, which can be used with combinations of the three operations. The first set of combinations includes □×(□*□), □•(□*□), □*(□×□), or □*(□*□); none of which are possible since this would ask for the multiplication of two vectors, which is meaningless. The second set of combinations includes □•(□×□), □×(□•□), or □•(□•□), in which the first option would result in a scalar, since only polar vectors are relevant this is ruled out, the second/third option would ask for a cross/dot product with a scalar, which are meaningless. Therefore the second set is also ruled out. The third set holds the last two options which are □*(□•□) and □×(□×□), which are both possible. In the first option a vector would be scaled by the dot product and in the second option the double cross product would overall result in a vector. The term $\square_a \times (\square_b \times \square_c)$ can be written as $\square_b * (\square_a \bullet \square_c) - \square_c * (\square_a \bullet \square_b)$, leaving □×□ and □*(□•□) as the only possibilities. This shows that the first approach was indeed correct.

Since all of the calculations above were performed in a theoretical coordinate system, it is important to transfer this idea to the actually experimental setup used for this work. The coordinate system used for the above equations is defined by **J**, ***m***, and their cross product. For the sample coordinate system, all the variables remain, however, in the measurements presented, **J** has a fixed direction and cannot freely move around. The experiments measures the voltage

perpendicular to **J** in-plane. The presence of an easy axis gives ***m*** a bidirectional preferred alignment. The direction of ***m*** is influenced by the externally applied magnetic field, which is perpendicular to both, the direction of **J** and the measured voltage. The easy axis runs along the direction of J. By sweeping the externally applied field from positive values to negative values or vice versa, ***m*** is forced to flip to the opposite direction along the easy axis. During this flip, the in-plane component of ***m*** briefly aligns with the measured voltage, as shown in **Figure 2.6** by the dotted arrow, and a peak can be observed. By causing the applied magnetic field to change directions again, the process is inverted and ***m*** reverses its path. This causes a second peak with the same direction as the first, which is why either both peaks point up or both point down in the recorded plot.

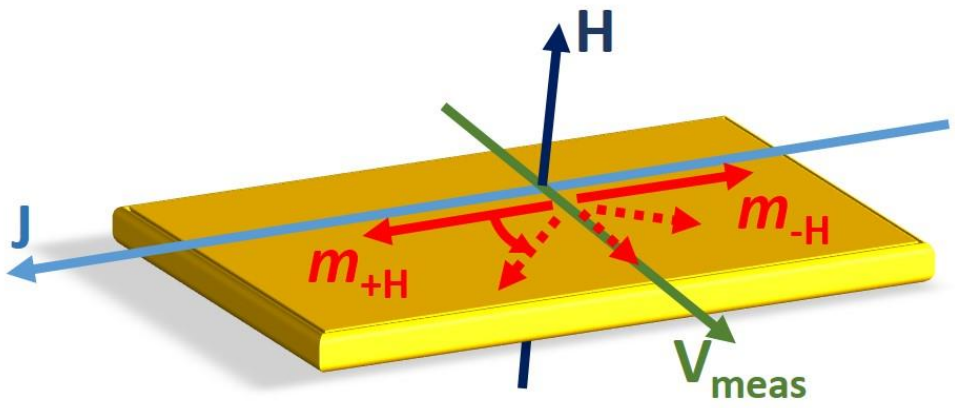


**Figure 2.6: Schematic of the alignment of *m* with the measured voltage, $V_{meas}$, during the direction flip of *m*, as shown by the dotted arrows.**

In conclusions the above derivation shows, that the part of **E** in the measured direction contains components that are dependent on the direction of **J** and ***m***. So is ***m*** flips its direction there should be a maximum in **E**, which causes a peak in the plotted data. This maximum is the key to the measurements

presented in this dissertation as the peak shifts in position when a surface modification via ligand deposition is performed.

## 2.6 REFERENCES


1. Tippler, P. A. *Physik*, Spektrum Akademischer Verlag, Heidelberg, Berlin, Oxford 1994

2. Hall E. On a new action of the magnet on electric currents. *Amer. J. Math.* **1879**, *2 (3)*, 287-292

3. Ogrin, F.Y.; Lee, S.L.; Ogrin, Y.F. Investigation of perpendicular anisotropy of a thin film using the planar Hall effect. *J. Magn. Magn. Mater.* **2000**, *219*, 331-339

4. Jackson, J. D. *Classical Electrodynamics 3rd Edition*, Wiley & Sons, Inc., New York 1998

# CHAPTER 3

## ANALYSIS OF PREVIOUS WORK

In this chapter the publications that are directly related to this work will be discussed, and potential problems with the presented data will be elaborated. It is important to state here that it is necessary to get a good idea of the published work up to date in order to understand the accomplishments achieved with this work, especially since this dissertation is a response to the controversy and perceived weaknesses of previous works.

Anomalous magnetic behavior of otherwise non-magnetic materials at room temperature has been observed by many groups and in many systems [1-33]. The work can be divided in two categories: interface effects and stabilized radical complexes. I studied surface induced magnetism and therefore I will not review the solution-phase assembly of stabilized radical complexes.

Because the magnetic effects are small, low dimensional systems must be employed to measure them, otherwise the properties of the bulk dominate the results. Work has been done on both 1D nanoparticles with a size range of 1-4 nm, and on 2D thin films with a thickness range of 0.2-100 nm. Both routes of investigation will be discussed.

To summarize the work to date in a few words, the following can be said:

1) Anomalous magnetic effects of palladium, gold, and zinc oxide nanoparticles are well established and understood. For all nanoparticles, the experimentally backed explanation is that the addition of capping molecules on the surface-induces d-shell vacancies in the surface atoms whose polarizability is sufficiently strong that it can overcome the diamagnetism of the bulk valence band electrons, resulting in both paramagnetic and ferromagnetic moments. For palladium, this explanation is not controversial as palladium is almost ferromagnetic to begin with. The study of zinc oxide began after the situation for palladium had stabilized, and so it too has not been controversial. Only the case of gold nanoparticles created some controversy, possibly because of the connection to the thin gold film claims, which will be discussed in this chapter.
2) A variety of thin film measurements of gold surfaces capped with thiolated ligands, which is also essentially the only 2D system studied, have found similar results. However, the para-/ferro-magnetic responses have extreme magnitudes and some of the reported magnetic moments have caused considerable controversy. Further, the theoretical explanations are problematic to say the least. To date there were three attempts of a theoretical explanation, however, one has been essentially retracted since [38-40], a second one is still being discussed [5, 15], and the third one is, so far, only accepted for metallic nanoparticles and not for thin films [2-13]. Finally, replication of the observed magnetic moments is intermittent [13] and has been strongly and convincingly criticized for its susceptibility to contaminant magnetic material [16, 23].

In addition to gold surfaces, a few groups have reported experimental and theoretical results for $SrTiO_3$ [27, 41] and other oxide surfaces [42]. They concluded, in case of $SrTiO_3$, that treatment of the surface with acetone induces magnetic moments at defect sites, while ethanol does not [27].

With one exception [34], the thin film studies have employed SQUID magnetometers and these are very susceptible to contamination due to their high sensitivity and unavoidable large sample volumes, coupled with a surface-dominated effect. The paper by Garcia *et al.* [16] essentially renders all SQUID measurements with the net magnetizations on the order of a hundred micro-emu highly suspect, absent a very careful handling and calibration procedure. No publication at this point has implemented such a procedure, therefore none of the SQUID measurements can be considered conclusive.

For low-dimensional systems, the magnetism of the surface can be a significant fraction of the total magnetic response of the system and is observable. For nanoparticles, the effect has an unsurprising and experimentally consistent theoretical explanation, whereas the situation for thin films is still troublesome.

Although no explanation can be offered at this time for the previously reported giant observed magnetic moments in thin films (hundreds of Bohr magnetons per atom), setting these few results aside, it can be noted that there is no particular reason to suppose that the same explanation applied to nanoparticles would fail to apply to thin films. Further, according to the understanding of the nanoparticle case, the stronger the interaction between ligand and metal surface, the stronger the expected increase in d-shell vacancies and consequent

localization of the displaced electrons and the stronger the surface polarizability. This is precisely what can be seen in the work of this thesis, as will be discussed in chapter 4 and 5.

A chronological ordered review of the relevant publications of nanoparticles will now be discussed, followed by essentially all of the work on thin film magnetism of gold. Only the most significant publications directly relevant to anomalous magnetic properties of capped thin films are covered. This includes a fair number of nanoparticles publications, since this work provides the current best theoretical explanation.

This literature review will be closed by the publication by Ogrin *et al.* [33] discussing the planar Hall sensor that I, following Knaus *et al.* [34], used to make the measurements in this work.

## 3.1 Observation of Induced Magnetism in Nanoparticles

Although this dissertation only shows measurements taken on metal thin films, in this following subchapter some publications about the same effect observed in nanoparticles will be discussed. Looking at these results can potential allow to develop a conclusive theory that is universal for all sample shapes.

### 3.1.1 Anomalous Magnetic Polarization Effect of Palladium and Gold Nanoparticles

In 1999 Hori *et al.* were perhaps the first to report an instance of anomalous magnetic properties for low-dimensional gold objects with exceedingly large

magnetic moments in palladium and gold [1]. The nanoparticles ranged in size between 2 to 4 nm and were encased in poly-N-vinyl-2-pyrrolidone (PVP), measured via SQUID at 4 K and 120K. The moments for a particle of 3 nm in diameter were equivalent to a net spin of 20, with palladium and gold yielding similar results. The suspension behaved superparamagnetically, i.e. both the palladium and gold nanoparticles, coated in PVP, displayed a permanent magnetic moment.

Hori *et al.* provide a lengthy discussion of potential theoretical explanations. However, since most of these explanations are only relevant to nanoparticles rather than thin films, which are the focus of this work, their theory will not be summarized. Importantly, they address the question of whether or not the effect can be due to free radicals, which would result from the chemical interaction of the metal nanoparticles with the ligand system. They conclude that this is not the case, based on the sharp peaks of the electron spin resonance (ESR) spectra of similar nanoparticle systems [2]. This possibly is relevant to later publications of this group, as well as to this work.

### 3.1.2 Anomalous Magnetic Polarization Effect of Palladium and Gold Nanoparticles

Using XANES, Zhang *et al.* determined in 2002 that weakly bound molecules on gold nanoparticles pushed excess electron density onto the gold surface atoms, while ligands with a thiol functional group extracted 0.07 electrons/atom from the d-shell relative to bulk [3]. This is in good agreement with

theoretically predicted 0.05 electrons/atom for $Au_{38}(SCH_3)_{24}$ [4]. This appears to be the first measurement showing the d-shell hole density varying with ligand bond strength for gold nanoparticles, which is central to the current theoretical explanation.

### 3.1.3 Anomalous Magnetic Polarization Effect of Palladium and Gold Nanoparticles

In 2004, Crespo *et al.* claimed a specific theoretical justification for their observed permanent magnetism in gold nanoparticles with a diameter of 1.4 nm [5]. The removal of d-shell electron density caused by thiolated ligands is given as the cause of the permanent moment behavior, while weakly bound molecules only displayed diamagnetic properties.

In this publication, the electronic properties of capped gold nanoparticles were studied via XANES, EXAFS, and EDX. The results are consistent with those published by Zhang *et al.*. Nanoparticles capped with thiolated ligands draw electrons out of the gold, while weakly bound molecules do not. In addition to Zhang *et al* [3]., Crespo *et al.* show a disappearance of a surface plasmon peak at 550 nm via UV-Vis absorption spectra, which indicates that surface 5d electrons have become at least partially localized.

Further, they show that gold nanoparticles with weakly bound ligands are diamagnetic, while equivalent systems with thiolated ligands display clear hysteresis curves. This persists up to 350 K and does not saturate in 1 T fields. They estimate a magnetic momentum of 0.036 $\mu_B$ per capped atom, which is again consistent with Zhang *et al*. It must be noted that the authors here substantially

overlap with Crespo *et al.* [5], wherein a highly problematic theory is presented to explain their observed extremely large magnetic moments per surface atom.

### 3.1.4 Direct Observation of Ferromagnetic Spin Polarization in Gold Nanoparticles

Published two months after Crespo *et al.* discussed above [5], Yamamoto *et al.* reported observation of ferromagnetic gold nanoparticles, this time using XMCD rather than SQUID to assess the situation, although they also analyze their samples with SQUID and compare the data to the results from XMCD, seeing consistent results [6].

Yamamoto *et al.* motivate their new approach by questioning a previous attempt of theirs, pointing out the susceptibility of SQUID measurements to contamination and its inability to identify the source of the measured net magnetic moment. In particular, they are concerned about unpaired electrons in the ligand system stabilizing the nanoparticles. They do not explain their change of opinion on this issue and do not address their previous comments about ESR [1]. Regardless, XMCD has an intrinsic advantage over SQUID, which is energy selectivity. Quoting Yamamoto *et al.* "XMCD allows the detection of the magnetic moments of a particular element through sensitivity to the difference between the up- and down-spin densities around the Fermi level." [6]. Since the Fermi level is significantly different for gold and iron, for example, is it possible to determine whether the source of magnetic moment, or actually the spin density asymmetry, is due to electrons associated with gold or some other contaminant atom. In this

case, XMCD unambiguously identifies the source of the magnetic moment with gold.

Yamamoto *et al.* find that gold nanoparticles have both a superparamagnetic and a Pauli paramagnetic response with a moment of 0.4 $m\mu_B$ per particle, 1.9 nm in diameter. They perform SQUID measurements along with XMCD-based ESM measurements and find comparable responses, including variation with temperature up to room temperature. They speculate that the observed non-diamagnetic responses of gold nanoparticles is due to size effects. In bulk gold diamagnetism is observed in all but the surface atoms, which become increasingly important as the size decreases. This suggests that the effect is intrinsic to the gold and the capping ligand has no effect, a claim that is inconsistent with essentially all subsequent data, including the data found in this work.

As with the paper by Hori *et al.* [1], most of the contents of Yamamoto *et al.* are not relevant to thin films or non-XMCD measurements, so there is no need to discuss them. However, it is important to point out that the evidence of abnormal magnetic susceptibility of nanoparticles, gold or not, is strong both experimentally and theoretically. It is not clear how to extend those models to the thin film case since the size of the nanoparticle effect peaks at diameters of 3 nm, whereas effects for thin films that are up to 80 nm thick could be seen in experiments conducted in this thesis. Further, some of the nanoparticle data is acquired at very low temperature, whereas the thin film measurements in this thesis are all performed at room temperature.

Notably, beyond using XMCD, ICP-MS was used to verify that contaminants account for less than the 5 ppm detection limit of the instrument and even 5 ppm of iron would be insufficient to explain their XMCD and SQUID data.

### 3.1.5 Diameter Dependence of Ferromagnetic Spin Moment in Gold Nanocrystals

Also in 2004, Hori *et al.* [7] (including Yamamoto) studied the dependence of the magnetic moment of gold nanoparticles with particle diameter, finding that it decays rapidly to essentially zero at 5 nm and is maximal at 3 nm. They also proposed to explain that the effect is due to Fermi holes, a theory that has since seen no further development.

The decay of an observable signal past 5 nm for nanoparticles highlights the most significant open question in the thin film case. It is still not clear how effects can be observed in thin films with a thickness of up to 100 nm [7].

### 3.1.6 Diameter Dependence of Ferromagnetic Spin Moment in Gold Nanocrystals

Besides gold, the magnetic properties of other metallic, and non-metallic, nanoparticles have been studied. As this work goes too far afield from the topic of this thesis, only a few relevant details will be selected here.

In 2006, Litrán *et al.* looked at the effect of adding capping molecules to palladium nanoparticles, both weakly (tetraalkylammonium salts) and strongly bound (alkane thiols), and saw similar results to the ones observed in gold nanoparticles. For palladium this is much less surprising as it is close to being

ferromagnetic anyway [8] and any chemical interaction that increases the electron density at the Fermi surface is likely to "push it over the edge" [8]. Hysteresis loops show slight permanent magnetism of about 100 Oe width for a 2000 Oe sweep for all the palladium nanoparticles studied. Litrán *et al.* suggest two mechanisms, the first being the excess electron density mentioned above, and the second the induction of 5d holes leading to localized, and hence, magnetically polarizable electrons near the surface, as was used to explain the gold results by the Japanese group.

### 3.1.7 Chemically Induced Permanent Magnetism in Gold, Silver, and Copper Nanoparticles: Localization of the Magnetism by Element Selective Techniques

In 2008, Garitaonandia *et al.* [9] extended the range of metal nanoparticles that display permanent magnetic moments when capped with thiolated ligands by looking at copper and silver as well as gold. They added Mössbauer spectroscopy, at 5 K, to the list of techniques that indicate a magnetic response located at the surface gold atoms for gold nanoparticles, although their method could not be used for copper and silver nanoparticles. In addition, XMCD measurements were performed on each type of nanoparticles, yielding quite large magnetic moments of 0.3 $\mu_B$ per nanoparticle for gold and silver, and 0.06 $\mu_B$ per nanoparticle for copper. They associate the smaller value for copper to diamagnetic copper (I) oxide ($Cu_2O$) and antiferromagnetic copper (II) oxide (CuO).

### 3.1.8 Chemically Induced Permanent Magnetism in Gold, Silver and Copper Nanoparticles: Localization of the Magnetism by Element Selective Techniques

In 2009, Garitaonandia *et al.* [10] reported results for gold nanoparticles with different alkane-thiol capping layers. However, they do not describe in any detail what their different nanoparticles were coated with, so it is difficult to draw any conclusions from their results other than that all alkanethiols are not created equal.

### 3.1.9 Ferromagnetism of Polythiophene-Capped Gold Nanoparticles

In 2011, Suzuki *et al.* [11] used VSM to measure the induced magnetic moment of polythiophene-capped gold nanoparticles, finding a magnetic moment about two orders of magnitude smaller than Garitaonandia *et al.* Potential sources of contamination were not discussed.

### 3.1.10 Magnetic Properties of Zinc Oxide Nanoparticles

A series of investigations have focused on palladium as well as zinc oxide nanoparticles, for a variety of reasons. The first such work was published in 2007 by Garcia *et al.* [12]. They find very similar behavior to palladium and gold; chemical modifications of the surface electron density resulting in the appearance of ferromagnetic behavior when the surface electrons are localized by strong bonds.

### 3.1.11 Induced Ferromagnetism in Copper and Manganese Thin Films Caused by Buckminster Fullerene Application, Measured by Muon Spin Rotation

In 2015, Al Ma'Mari *et al.* published measurements of the localized depolarization process of low-spin muons, which were implanted into copper and manganese thin films coated with Buckminster Fullerenes ($C_{60}$) [13]. Employing the measurement of the muon spin rotation allowed them to localize the magnetic changes in the first few layers of the metal thin film as well as the direct environment in the organic molecule close to the interface. They conclude that it is possible to overcome the Stoner criterion, which calculates the density of states at the Fermi level of a material. The Stoner criterion was so far the deciding factor if a substance would be ferromagnetic or not, and manipulate non-magnetic materials to control their magnetic properties.

## 3.2 Observation of Induced Magnetism in Thin Films

The following subchapter will present the literature discussing changes in magnetic properties observed in metallic thin films. The results from these publications are directly related to the work presented in this dissertation.

### 3.2.1 Ferromagnetism of Polythiophene-Capped Gold Nanoparticles

In 2003, Carmeli *et al.* [14] published the first results and explanation of induced paramagnetism in gold thin films. They showed that close packed organic

monolayers bonded via a thiol group to the gold thin film (100 nm) results in a large paramagnetic response, which is equivalent to a magnetization of several tens of Bohr magnetons per bonded ligand. All experiments were performed at room temperature. This is unprecedentedly large in comparison to 2-4 $\mu_B$ for iron and, in combination with the work of Hernando *et al.* discussed below [15], is the source of most of the skepticism of the thin film results.

Carmeli *et al.* investigated the effects of three ligands, two alkanethiols, and a polyalanine. They characterized the monolayers and verified their well-ordering by IR spectroscopy, ellipsometry, AFM, and XPS. Importantly, magnetic measurements were performed with a SQUID, which, due to a combination of high sensitivity and the fact that it measures the net magnetic moment of a fairly large volume while the sample is 2D, is susceptible to contamination. Using standard SQUID sensitivities, a cube of 5 μm on a side anywhere in the multi-$cm^3$ sample volume would yield the observed magnetization. As the samples must be removed from the SQUID to be coated with the ligands, there is ample opportunity for the inadvertent introduction of a microscopic amount of ferro- or even paramagnetic material. See Garcia *et al.* [15], discussed below, for further sources of error when measuring micro-emu moments with a SQUID. Further, not all samples yield an observable paramagnetic response.

However, Carmeli *et al.* assert that evidence, which shows that the observed paramagnetic response is a surface effect, is the clear contrast in induced magnetic moment between perpendicular and parallel external field orientation (**Figure 3.1**). The response of the film to a polarizing field applied

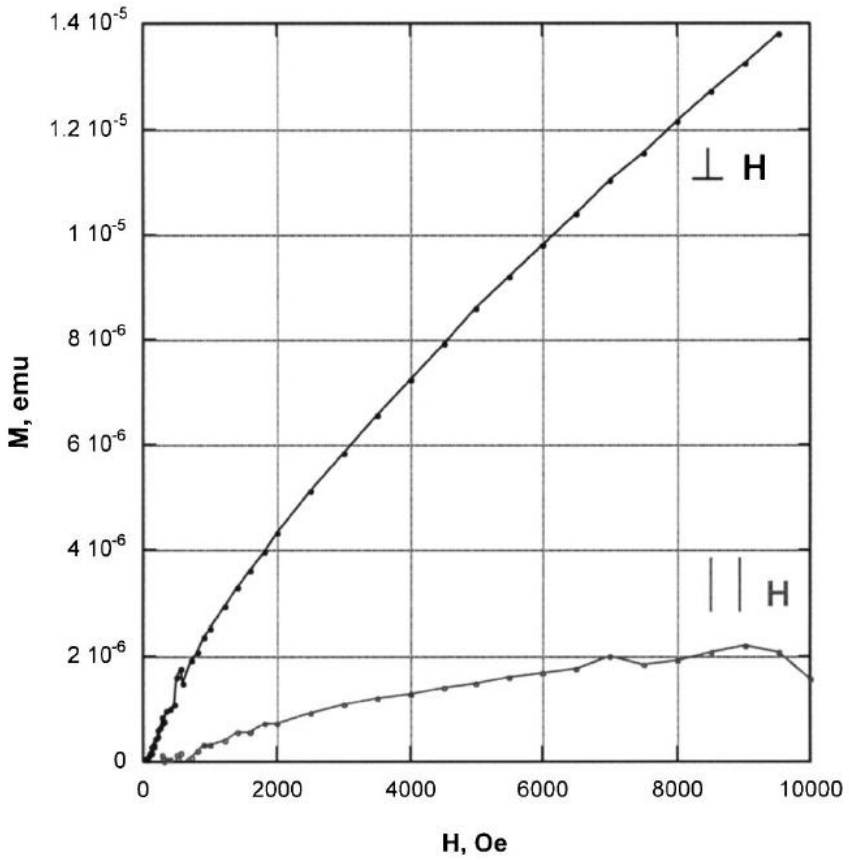


***Figure 3.1: Magnetization measurement vs. externally applied magnetic field at room temperature for octadecylthiol and ethylthiol on gold coated silica substrates. The magnetic field was applied perpendicular to the monolayer alignment and the samples were measured in a SQUID. Copyright 2003 by the American Institute of Physics***

parallel to the surface is seven times smaller than to one perpendicular to it. As the authors point out, the factor of seven difference does not take into account the strong demagnetization field of a thin film, which counteracts any perpendicular induced magnetic moments. The SQUID measures only the net magnetization and the demagnetization field would counter any surface moments and much smaller than the demagnetization field parallel to the surface. Therefore, the actual difference in parallel vs. perpendicular magnetic moments is larger than observed.

For this kind of magnetic response to be due to contamination, the contaminate must also be significantly anisotropic and oriented with the film, which seems unlikely. Carmeli *et al.* do not say if they had to remove the sample to reorient it. In addition, it is not mentioned whether all samples, that show an effect, display the same asymmetry. Further Garcia *et al.* [16] point out and show that sample positioning within the sensed volume can significantly affect the measured magnetic moments. Thus, this asymmetry is inconclusive for ruling out unauthentic signals.

Measuring the magnetic moment as a function of temperature shows what the authors characterize has a very small variation in magnetization, indicating possible ferromagnetic character. How this is consistent with paramagnetism is not explained.

Carmeli *et al.* theorized that the effect is due to charge transfer between the gold and the capping ligand, leaving unpaired electrons near the surface. Further, they note the obvious fact that this cannot explain the large magnetic moments seen and they therefore also speculate that the electrons (transferred to the capping ligand and away from the gold [17]) are trapped in the long tail of the capping molecules, leading to an enhanced magnetic polarizability.

This is vaguely consistent with Hori's speculations [1] but not with Yamamoto's explanation [6] discussed previously, which is essentially the current best explanation, minus the enhancement due to delocalization of the electrons in the alkane tails.

### 3.2.2 Observation of Magnetism in Gold Thin Films

In 2006, Reich *et al.* [18] showed thin film results with a non-SQUID measurement, finding either diamagnetic or paramagnetic responses at room temperature depending on the substrate. Interestingly, they point out that substrate smoothness differences are correlated with the magnetic properties. For rough surfaces, they saw paramagnetism, speculating that the thin film was behaving like isolated nanoparticles. But for flat surfaces, they observed a diamagnetic response, which is coherent with gold bulk properties.

### 3.2.3 Giant Magnetic Anisotropy at the Nanoscale: Overcoming the Superparamagnetic Limit

In 2006, Hernando *et al.* [15] studied gold thin films and found truly gigantic magnetic moments of 1,000 $\mu_B$ per atom for thiol-capped systems. Further, they proposed a novel and detailed theory in which well-organized long-chain monolayers, i.e. with long-range (100 nm) 2D crystalline order, play an essential part.

Although the paper has been cited 46 times as of July 2015, notably, no one has yet adopted the proposed theory. This is not surprising, as it appears to suffer from some serious problems. The model proposes an indirect polarization mechanism for the orbital moments; the first spins are polarized by an external field, then the orbitals are polarized by spin-orbit coupling. The problem is couplings to spin in the Hamiltonian can only arise from relativistic effects or through the exclusion principle. The polarized orbitals in the model are supposed

to be very large; hence the electrons should be weakly bound and slow moving, making a relativistic phenomenon highly disfavored. Moreover, the exclusion principle can only give rise to effective spin couplings when nearby electron states are heavily filled. This is ipso facto not the case if the spins and/or orbital state are heavily polarized. Therefore, there is no mechanism that seems capable of generating the strong spin-orbit interactions that the model would require. Further, the need for such an explanation only arises if the anomalous magnetic moments found are believed. It must be pointed out that these results are only found by various researchers in Spain working in overlapping groups, in particular, groups containing Hernando and Crespo.

All of the nanoparticle work, as well as work on other systems, such as the strontium titanate work discussed below, and the work in this thesis finds no such astonishingly large effects for thiolated ligands and can be explained with far less complex mechanisms. All this work finds a large effect associated with thiolation, but only relative to other molecules, not 100 times larger than pure iron.

Therefore, Hernando's results, experimental or theoretical, will not be discussed here in detail. It shall only be noted that there is a calculation error of $4\pi$, which is likely caused by conversion between the SI system and Gaussian units. This error causes all of their reported results to be too small by a factor of roughly 12.5. In addition it should be mentioned, that their reported gigantic magnetic moments (presumably measured via SQUID, although the origin of their data is not reported) is a major, perhaps even the greatest, source of controversy surrounding the gold thin film results.

### 3.2.3 Ubiquity of Ferromagnetic Signals in Common Diamagnetic Oxide Crystals

In 2010, Khalid *et al.* [19] published a detailed and extensive analysis of the magnetic properties of various oxide thin films. Through an analysis via XMCD, SQUID, XAS, EPR, and PIXE they thoroughly analyzed the sample properties and argue that the observed ferromagnetic signal (in addition to diamagnetic and paramagnetic ones from the bulk and impurities) comes from the surface.

However, they show no awareness of the work of Garcia *et al.* [15]. Their ferromagnetic curves are of the same order as those found by Garcia *et al.* and could be due to contaminants adhered to the Kapton tape often used to secure samples in the SQUID. Khalid *et al.* did not, however, use Kapton, instead using a varnish to secure the samples; but varnish can be quite sticky as well. They did use the standard plastic straw, which Garcia also showed could lead to ferromagnetic signals if deformed by a too-large or misaligned sample. Further, they calibrated the SQUID with the standard palladium calibration sample, which, presumably, is not the same shape as their oxide samples, though they do not elaborate. Again, Garcia showed that the shape and position of the sample affects the measured magnetic moment. One cannot calibrate a SQUID unless one's calibration sample is the same shape and is positioned the same as one's sample if one wants to measure micro-emu magnetizations [12].

It is therefore entirely possible that the tiny ferromagnetism response left, after subtracting the much larger dia- and paramagnetic moments from the bulk atoms, is simply an artefact.

### 3.2.4 Defect-Induced Ferromagnetism in Crystalline $SrTiO_3$

In 2011, Potzger *et al.* [20] demonstrated, that defects induced by ion irradiation can lead to ferromagnetic behavior in $SrTiO_3$ crystals.

## 3.3 Influence of magnetic Contamination

The presence of magnetic contamination could cause a sample to appear para- or ferromagnetic when, in reality, the magnetic properties of the sample stayed the same. In the following subchapter a number of publications discussing this problem will be presented.

### 3.3.1 Absence of Magnetism in Hafnium Oxide Films

In 2005, Abraham *et al.* [21] published an important contribution to the critique of SQUID measurements. They show that merely handling thin film samples with stainless-steel tweezers is enough to produce magnetic moments of $10^{-5}$ emu, which is on the same order as the net signal reported for many SQUID measurements on both nanoparticles and thin films.

### 3.3.2 Fe Impurities Weaken the Ferromagnetic Behavior in Gold Nanoparticles

In 2006, Crespo *et al.* [22] demonstrated that iron impurities incorporated within gold nanoparticles actually weaken the ferromagnetic response, rather than

strengthen it. This implies that any source of ferromagnetic contamination must be external to the nanoparticle themselves.

### 3.3.3 Sources of Experimental Errors in the Observation of Nanoscale Magnetism

One of the strongest arguments against contaminants being the source of the magnetization seen for thin films is the fact that sample rotation substantially reduces the observed hysteresis. However, in 2009, Garcia *et al.* [16] published a detailed investigation of sources of error when measuring very small magnetizations, concluding that small asymmetries in sample position upon rotation could explain these results. Further, the standard adhesive for securing samples in a SQUID is Kapton tape, which was shown here to yield measurable ferromagnetic hysteresis curves likely due to dust picked up from the environment. This is a very enlightening article for anyone measuring small magnetizations, as is the theoretical analysis by Stemenov *et al.* [23].

### 3.3.4 Magnetometry and Electron Paramagnetic Resonance Studies of Phosphine- and Thiol-Capped Gold Nanoparticles

In 2010, Guerrero *et al.* [24] added EPR to the list of techniques used to study capped gold nanoparticles, this time adding iron in solution. Again, they find permanent magnetism with SQUID measurements. They note that they use Kapton tape as a sample adhesive and do a baseline subtraction. It is not clear if

this explains the observed hysteresis since the reported magnetizations are on the order of 0.03 emu per gram of gold and no information on how much gold was in the sample is given. Therefore the actual observed magnetization is unknown. Garcia *et al.* [16] give a value of 10 micro-emu per cm of Kapton tape. Guerrero *et al.* state that they start, in one case, with 0.145 g of gold, but the solution volume is not mentioned. If it is 100 mL and their actual sample size in the SQUID is 1 mL, then they may have had 0.00145 g of gold, giving 0.0000435 emu = 43.5 micro-emu. This would require about 4 cm of Kapton tape, if that were the source of permanent magnetism. However, due to the lack of information in the publication, this calculation is mostly estimated conjecture but is quite close to a reasonable lower limit of 1 cm of Kapton. Thus, contamination cannot be ruled out, per Garcia *et al.* [15], which is not referenced by Guerrero although it was published nine months before Guerrero submitted their manuscript.

## 3.4 Theoretical Approaches

Various theoretical approaches for an explanation of the changes in magnetic properties of different materials have been made. The following subchapter will discuss the ones directly related to this dissertation.

### 3.4.1 First Principle Prediction of Vacancy-Induced Magnetism in Non-Magnetic Perovskite $SrTiO_3$

In addition to the work on metallic thin films and nanoparticles, there has been much interest in the magnetic properties of otherwise non-magnetic or

diamagnetic oxides. As this work is rather far from the work of this thesis, this discussion is limited to the most relevant highlights. In 2007, Shein *et al.* [25] presented computed models that predicted vacancy-induced magnetism in $SrTiO_3$. This appears to be the first of many computational efforts to show that surface modifications should induce magnetic changes in otherwise non-magnetic materials.

### 3.4.2 2011-2013, THE YEARS OF COMPUTATION

Beginning in 2011, a number of computational, mostly density function theory (DFT), papers began appearing. They show that normally diamagnetic materials can become para-/ferromagnetic when their surfaces are modified. As every paper seems to use a different approach with an apparently unlimited variety of algorithmic details and as they almost all reach essentially the same conclusion (non-diamagnetic responses should occur) only the most relevant papers are listed:

| | |
|---|---|
| 2007 | Shein *et al.* [25]<br>*Phys. Rev. Lett. A* 371, p. 155 |
| 2011 | Morozokovska *et al.* [26]<br>*Phys. B* 406, p. 1673 |
| 2011 | Adeagbo *et al.* [27]<br>*Phys. Rev. B* 83, p. 195428 |
| 2012 | Zhang *et al.* [28]<br>*J. Magn. Magn. Mater.* 324, p. 1770 |
| 2013 | Cuadrado *et al.* [29]<br>*J. Chem. Phys.* 139, p. 0.4319 |
| 2013 | Pavlenko *et al.* [30]<br>*Phys. Rev. B* 88, p. 201104R |
| 2013 | Glinchuk *et al.* [31]<br>*Thin Solid Films* 534, p. 685 |
| 2015 | Liu *et al.* [32]<br>*Mater. Chem. Phys* 160, p. 80 |

## 3.5 Publications that Inspired this Work

This literature review must conclude with the discussion of the two papers upon which the measurement technique for this work is based.

In 2000, Ogrin *et al.* [33] described a method for investigating the perpendicular anisotropy of a thin cobalt film with an easy axis employing the PHE. Since this is the basis of the technique used in this thesis, an extensive discussion will be provided in chapter 4, here only the essential details are highlighted.

Crucially, Ogrin *et al.* show theoretically and experimentally that there is a peak in the Hall voltage as an external field is swept from above to below the Hall bar plane and, due to hysteresis within the cobalt film, this peak occurs when the externally applied field is far from zero. Roughly, the position of the peak depends on the degree to which the external field is perpendicular to the Hall bar plane, moving outward toward infinity as the external field approaches absolute perpendicularity because the in-plane component of the field simultaneously goes to zero as perpendicularity is approached. When the in-plane component becomes large enough, the sample magnetization flips from one direction along the easy axis to the other, resulting in the large change of Hall voltage as the magnetization sweeps from one direction along the easy axis to the other.

In 2009, Knaus *et al.* [34] demonstrated that this angular dependence of the Hall voltage peak could be used to measure in-plane magnetic fields with almost arbitrarily high precision. Further, they used this technique to investigate the magnetic effect of cobalt-gold bilayers upon modification of the gold surface with a thiolated ligand, finding that the surface modification did change the position of

the peak. They concluded from this that the magnetic properties of the gold had been changed by the addition of alkanethiols. The position of the peak shifted slowly over a period of a few hours, which is consistent with the known reconstruction rate of long-chain alkane-thiol monolayers on gold surfaces. This is also consistent with Hernando's theory. Upon the application of ethanol, a peak shift sometimes occurred but did not evolve in time, suggesting that whatever process caused it had gone to completion in the time it took to re-measure the sample. Knaus *et al.* also note that peak motion variability was higher for samples stored in vacuum. Importantly, they showed that the well attested change in sample conductivity was not the cause of the peak motion by adding an insulating aluminum oxide ($Al_2O_3$) barrier between the cobalt and the gold. The Hall voltage peak still shifted but there was no vertical shift in the AHE slope, indicating a good insulating barrier had been formed.

Notably, the Ogrin-Knaus approach is not a volume measurement of a surface phenomenon and therefore is not nearly as susceptible to contamination issues as SQUID, although Knaus did not report any attempts to verify the purity of their samples and sample handling processes. However, they verified that sample cleanliness has a statistically significant effect on the change in magnetism.

## 3.6 REFERENCES


1. Hori, H.; Teranishi, T.; Nakae, Y.; Seino, Y.; Miyake, M.; Yamada, S. Anomalous magnetic polarization effect of Pd and Au Nanoparticles. *Phys. Lett. A* **1999**, *263*, 406-410

2. Teranishi, T.; Hori, H.; Miyake, M. ESR Study on Palladium Nanoparticles. *J. Phys. Chem. B* **1997**, *101 (30)*, 5774-5776

3. Zhang, P.; Sham, T.K. Tuning the electronic behavior of Au nanoparticles with capping molecules. *Appl. Phys.* Lett **2002**, *81*, 736-738

4. Häkkinen, H.; Barnett, R.N.; Landman, U. Electronic Structure of Passive $Au_{38}(SCH_3)_{24}$. *Phys. Rev. Lett.* **1999**, *82*, 3264

5. Crespo, P.; Litran, R.; Rojas, T.C.; Multigner, M.; de la Fuente, J.M.; Sanchez-Lopez, J.C.; Garcia, M.A.; Hernando, A.; Penades, S.; Fernandez, A. Permanent magnetism, magnetic anisotropy, and hysteresis of thiol-capped gold nanoparticles. *Phys. Rev. Lett.* **2004**, *93 (8)*, 087204

6. Yamamoto, Y.; Miura, T.; Suzuki, M.; Nawamura, N.; Miyagawa, H.; Nakamura, T.; Kobayashi, K.; Teranishi, T.; Hori, H. Direct observation of ferromagnetic spin polarization in gold nanoparticles. *Phys. Rev. Lett.* **2004**, *93 (11)*, 116801

7. Hori, H.; Yamamoto, Y.; Iwamoto, T.; Miura, T.; Teranishi, T.; Miyake, M. Diameter Dependence of Ferromagnetic Spin Moment in Gold Nanocrystals. *Phys. Rev. B* **2004**, *69*, 174411

8. Litran, R.; Sampedro, B.; Rojas, T.C.; Multigner, M.; Sanchez-Lopez, J.C.; Crespo, P.; Lopez-Cartes, C.; Garcia, M.A.; Hernando, A.; Fernandez, A. Magnetic and Microstructural Analysis of Palladium Nanoparticles with Different Capping Systems. *Phys. Rev. B* **2006**, *73*, 054404

9. Garitaonandia, J.S.; Insausti, M.; Goikolea, E.; Suzuki, M.; Cashion, J.D.; Kawamura, N.; Ohsawa, H.; Gil de Muro, I.; Suzuki, K.; Plazaola, F.; Rojo, T. Chemically Induced Permanent Magnetism in Au, Ag, and Cu Nanoparticles: Localization of the Magentism by Element Selective Techniques. *Nano Lett.* **2008**, *8*, 661-667

10. Garitaonandia, M.; Goikolea, E.; J.S.; Insausti, Suzuki, M.; Kawamura, N.; Ohsawa, H.; Gil de Muro, I.; Suzuki, K.; Cashion, J.D.; Gorria, C.; Plazaola, F.; Rojo, T. Thiol-capped ferromagnetic Au nanoparticles investigated by Au $L_3$ X-ray absorption spectroscopy. *J. Appl. Phys.* **2009**, *105*, 07A907

11. Suzuki, K.; Zhang, H.; Saito, K.; Garitaonandia, J.S.; Goikolea, E.; Insausti, M. Ferromagnetism of Polythiophene-Capped Au Nanoparticles. *J. Appl. Phys.* **2011**, *109*, 07E328

12. Garcia, M.A.; Merino, J.M.; Fernandez Pinel, E.; Quesada, A.; de la Venta, J.; Ruiz Gonzales, M.L.; Castro, G.R.; Crespo, P.; Llopis, J.; Gonzales-Calbet, J.M. Hernando, A. Magnetic Properties of ZnO Nanoparticles. *Nano Lett.* **2007**, *7*, 1489-1494

13. Al Ma'Mari, F.; Moorsom, T.; Teobaldi, G.; Deacon, W.; Prokscha, T.; Luedkens, H.; Lee, S.; Sterbinsky, G.E.; Arena, D.A.; MacLaren, D.A.; Flokstra,

M.; Ali, M.; Wheeler, M.C.; Burnell, G.; Hickey, B.J.; Cespedes, O. Beating the Sonter Criterion using Molecular Interfaces. *Nature,* **2015**, *524*, 69-73

14. Carmeli, I.; Leitus, G.; Naaman, R.; Reich, S.; Vager, Z. Magnetism induced by the organization of self-assembled monolayers. *J. Chem. Phys.* **2003**, *118 (23),* 10372-10375

15. Hernando, A.; Crespo, P.; Garcia, M.A.; Fernandez Pinel, E.; de la Venta, J.; Fernandez, A.; Penades, S. Giant magnetic anisotropy at the nanoscale: Overcoming the superparamagnetic limit. *Phys. Rev. B* **2006**, *74*, 052403

16. Garcia, M.A.; Fernandez Pinel, E.; de la Venta, J.; Quesada, A.; Bouzas, V.; Fernandez, J.F.; Romero, J.J.; Martin Gonzalez, M.S.; Costa-Krämer, J.L. Sources of Experimental Errors in the Observation of Nanoscale Magnetism. *J. Appl. Phys.* **2009**, *105*, 013925

17. Häkkinen, H. The Gold-Sulfur Interface at the Nanoscale. *Nat. Chem.* **2012**, *4*, 443-455

18. Reich, S.; Leitus, G.; Feldman, Y. Observation of Magnetism in Au Thin Films. *Appl. Phys. Lett.* **2006**, *88*, 222502

19. Khalid, M.; Setzer, A.; Ziese, M.; Esquinazi, P.; Spemann, D.; Pöpple, A.; Goering, E. Ubiquity of Ferromagnetic Signals in Common Diamagnetic Oxide Crystals. *Phys. Rev. B* **2010**, *81*, 214414

20. Potzger, K.; Osten, J.; Levin, A.A.; Shalimov, A.; Talut, G.; Reuther, H.; Arpaci, S.; Bürger, D.; Schmidt, H.; Nestler, T.; Meyer, D.C. Defect-Induced

Ferromagnetism in Crystalline $SrTiO_3$. *J. Magn. Magn. Mater.* **2011**, *323*, 1551-1562

21. Abraham, D.W.; Frank, M.M.; Guha, S. Absence of Magentism in Hafnium Oxide Films. *Appl. Phys. Lett.* **2005**, *87*, 252502

22. Crespo, P.; Garcia, M.A.; Fernandez Pinel, E.; Multigner, M.; Alcantara, D.; de la Fuente, J.M.; Penades, S.; Hernando, A. Fe Impurities Weaken the Ferromagnetic Behavior in Au Nanoparticles. *Phys. Rev. Lett.* **2006**, *97*, 177203

23. Stamenov, P.; Coey, J.M.D. Sample Size, Position, and Structure Effects on Magnetization Measurements using Second-Order Gradiometer Pickup Coils. *Rev. Sci. Inst.* **2006**, *77*, 015106

24. Guerrero, E.; Munoz-Marquez, M.A.; Fernandez, A.; Crespo, P.; Hernando, A.; Lucena, R.; Conesa, J.C. Magnetometry and Electron Paramagnetic Resonance Studies of Phosphine- and Thiol-Capped Gold Nanoparticles. *J. Appl. Phys.* **2010**, *107*, 064303

25. Shein, I.R.; Ivanovskii, A.L. First Principle Prediction of Vacancy-Induced Magnetism in Non-Magnetic Perovskite $SrTiO_3$. *Phys. Lett. A* **2007**, *371*, 155-159

26. Morozovska, A.N.; Eliseev, E.A.; Glinchuk, M.D.; Blinc, R. Surface-Induced Magnetism of the Solids with Impurities and Vacancies. *Phys. B* **2011**, *406*, 1673-1688

27. Adeagbo, W.A.; Fischer, G.; Hergert, W. First-Principle Investigations of Electronic and Magnetic Properties of $SrTiO_3$ (001) Surfaces with Absorbed Ethanol and Acetone Molecules. *Phys. Rev. B* **2011**, *83*, 195428

28. Zhang, Y.; Hu, J.; Cao, E.; Sun, L.; Qin, H. Vacancy Induced Magnetism in $SrTiO_3$. *J. Magn. Magn. Mater.* **2012**, *324*, 1770-1775

29. Cuadrado, R.; Puerta, J.M.; Soria, F.; Cerda, J.I. A First Principle Study of Thiol-Capped Au Nanoparticles: Structural, Electronic, and Magnetic Properties as a Function of Thiol Coverage. *J. Chem. Phys.* **2013**, *139*, 034319

30. Pavlenko, N.; Kopp, T.; Mannhart, J. Emerging Magnetism and Electronic Phase Separation at Titanate Interphases. *Phys. Rev. B* **2013**, *88*, 201104(R)

31. Glinchuk, M.D.; Eliseev, E.A.; Khist, V.V.; Morozovska, A.N. Ferromagnetism Induced by Magnetic Vacancies as a Size Effect in Thin Films of Non-Magnetic Oxides. *Thin Solid Films* **2013**, *534*, 658-692

32. Liu, Y.; Zhou, W.; Wu, P. Tuning of Magentism of $SrTiO_3$ by Site-Specific Doping. *Mater. Chem. Phys.* **2015**, *160*, 80-86

33. Ogrin, F.Y.; Lee, S.L.; Ogrin, Y.F. Investigation of perpendicular anisotropy of a thin film using the planar Hall effect. *J. Magn. Magn. Mater.* **2000**, *219*, 331-339

34. Knaus, B.; Garzon, S.; Crawford, T.M. Alkenethiol induced changes in the magnetotransport properties of Co/Au bilayers. *J. Appl. Phys.* **2009**, *105*, 07A903

35. Trudel, S. Unexpected magnetism in gold nanostructures: making gold even more attractive. *Gold Bull.* **2011**, *44*, 3-13

36. Crespo, P.; de la Presa, P.; Marin, P.; Multigner, M.; Alonso, J.M.; Rivero, G.; Yndurain, F.; Gonzalez-Calbet, J.M.; Hernando, A. Magnetism in Nanoparticles: Tuning Properties with Coatings. *J. Phys. Cond. Matt.* **2013**, *25*, 484006

37. Nakamura, T.; Suzuki, M. Recent Progress of the X-Ray Magnetic Circular Dichroism Technique for Element-Specific Magnetic Analysis. *J. Phys. Soc. Jap.* **2013**, *82*, 021006

38. Vager, Z.; Naaman, R. Bosons as the origin for giant magnetic properties of organic monolayers. *Phys. Rev. Lett.* **2004**, *92 (8)*, 087205

39. Hernando, A.; Garcia, M.A. Comment on “Bosons as the Origin for Giant Magnetic Properties of Organic Monolayers. *Phys. Rev. Lett.* **2006**, *96*, 029703

40. Vager, Z.; Naaman, R. In Response. *Phys. Rev. Lett.* **2006**, *96*, 029704

41. Adeagbo, W.A.; Fischer, G.; Ernst, A.; Hergert, W. Magnetic effects of defect pair formation in ZnO. *J. Phys.: Condens. Matter.* **2010**, *22*, 436002

42. Elfimov, I.S.; Yunoki, S.; Sawatzky, G.A. Possible path to a new class of ferromagnetic and half-metallic ferromagnetic materials. *Phys. Rev. Lett.* **2002**, *89*, 216403

# CHAPTER 4

## EXPERIMENTAL APPROACH

This series of experiments stems from a very simple thought. Having ferromagnetic thin films with a given magnetization means that a number of electrons have spins aligned in a certain direction. Applying an organic thin film to the surface causes metal organic bonds between the organic ligands and the surface metal atoms, which effects some of these spin-aligned electrons. The occupation of these electrons and orbitals must have an influence on the magnetization and alters it, which was measured. The PHE was employed to measure a change in magnetism in the metal thin film. The measurement is a comparison measurement. The PHE peak position before exposure to a ligand is compared to that after. The ligand affects the surface electrons and thereby the surface magnetization. This results in a slightly different total magnetic field felt by the rest of the sensor. Therefore the PHE peak will occur at a slightly different external field H. The following experimental set up was employed.

### 4.1 MAGNETIC MEASUREMENT SYSTEMS

In this dissertation a custom system for the measurement of the peak caused by the PHE is introduced. The design of the magnetic resistance measurement system (MaRMS) is greatly based on the workings of a physical

property measurement system (PPMS) and to understand the connection between the two instruments, as well as the reason for the new design, first, some work performed on the PPMS will be discussed, followed by the design and measurements in MaRMS.

### 4.1.1 Physical Property Measurement Systems (PPMS)

Since these experiments follow the initial work performed by Brad Knaus [6], a reproduction of his experiments was performed. For this purpose, the physical property measurement system (Quantum Design) was used, which can create magnetic fields up to 9 Tesla.

Samples with 30 nm of cobalt topped by 30 nm of gold were measure both in a manually adjustable sample holder and an automated one. The manual sample holder was fixed perpendicular to the magnetic field and only a very small adjustment of the sample angle was possible. The automated holder could be rotated 360° in steps of 0.15°. Measurements were performed under reduced pressure and at room temperature. A constant current of 1 mA with a frequency of 10 k Hz was applied along the long side of the sample and the magnetic field was swept over a range of -3 Tesla and 3 Tesla. However, it became obvious that the angle adjustment in the automated sample holder was not as accurate as advertised by the manufacturer, mainly due to gear-wheel mechanics. While the manually adjustable sample holder showed slightly better results, it was a much longer process to find a good peak. During the performance of the experiment it was found that the measured peaks shifted their position whenever the sample

holder was taken out of the PPMS in order to apply a self-assembled monolayer. Therefore a test series was performed for both sample holders in which the position of the sample was kept steady, and only the sample holder was taken out of the PPMS and replaced into the same position without any chemical modifications to see if this would cause a shift. The data showed that even without a self-assembled monolayer the peaks shifted slightly, which led to the conclusion that the mounting and dismounting of the sample holder in the PPMS is not a stable process and therefore this is not an adequate technique to get conclusive data. Therefore a more stable custom system was built. Nevertheless, a sweep of a 6 Tesla field was performed in the PPMS which allows to see all of the Hall effects (**Figure 4.7**).

### 4.1.2 Magnetic Resistance Measurement Systems (MaRMS)

The magnetic resistance measurement system (MaRMS) used for the measurements of this dissertation was custom designed to ensure a stable measuring environment. The driving idea for this set-up was to build a simple table top version of the PPMS. To create a stable magnetic environment around the sample it was important to have sufficiently large magnet poles with a pole gap large enough to insert a sample holder. The sample holder needed to be significant larger than the sample holder in the PPMS in order to introduce better control over the angular adjustment of the sample. In addition, a deposition system was created, consisting of a piezo crystal to evaporate the ligands and a house

vacuum connection to create an airflow over the sample, as can be seen conceptually in **Figure 4.1**. The real MaRMS can be seen in **Figure 4.2**.

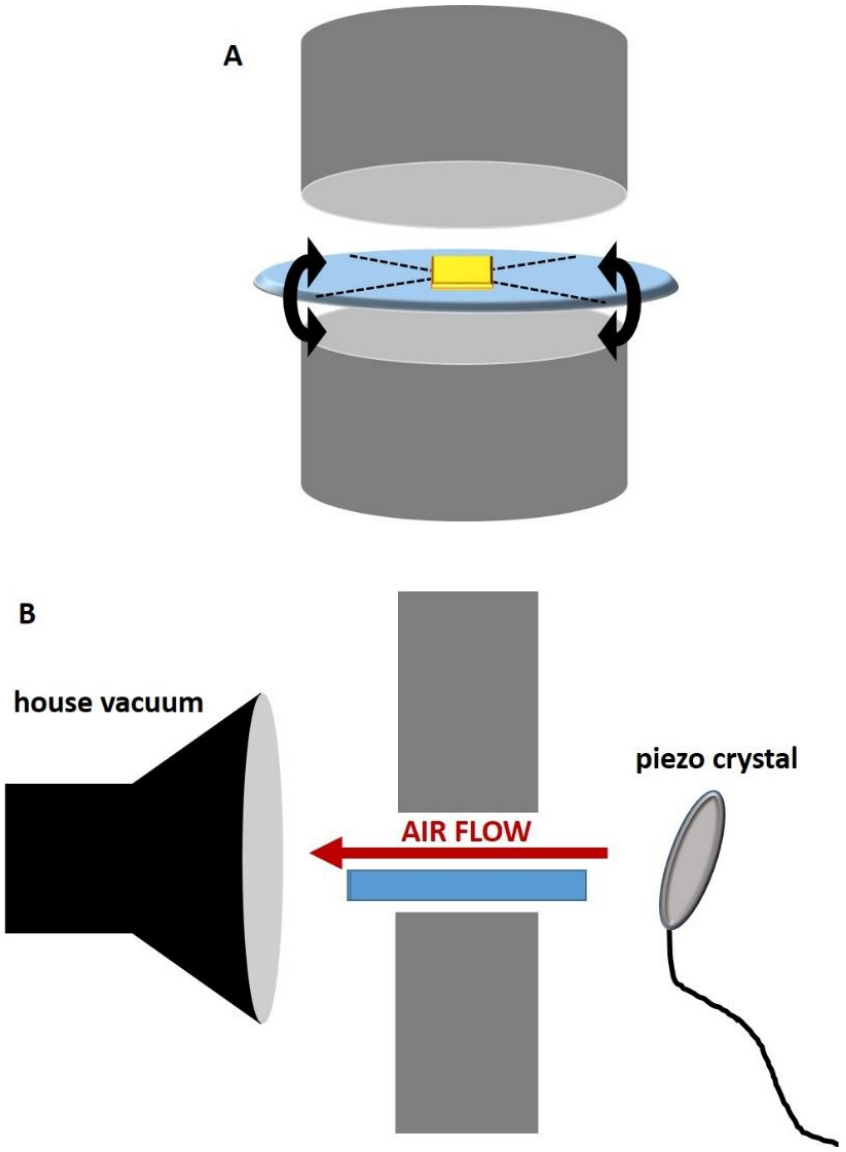


***Figure 4.1: 2D sketch of the sample placement (gold square) between the magnet poles with the angle adjustment of the sample holder in two directions for better angle control relative to the magnetic field. B) a flow trap (left), which is connected to the house vacuum, creates an air channel, allowing to guide the chemical over the sample holder (middle) after evaporation over the piezo crystal (right).***

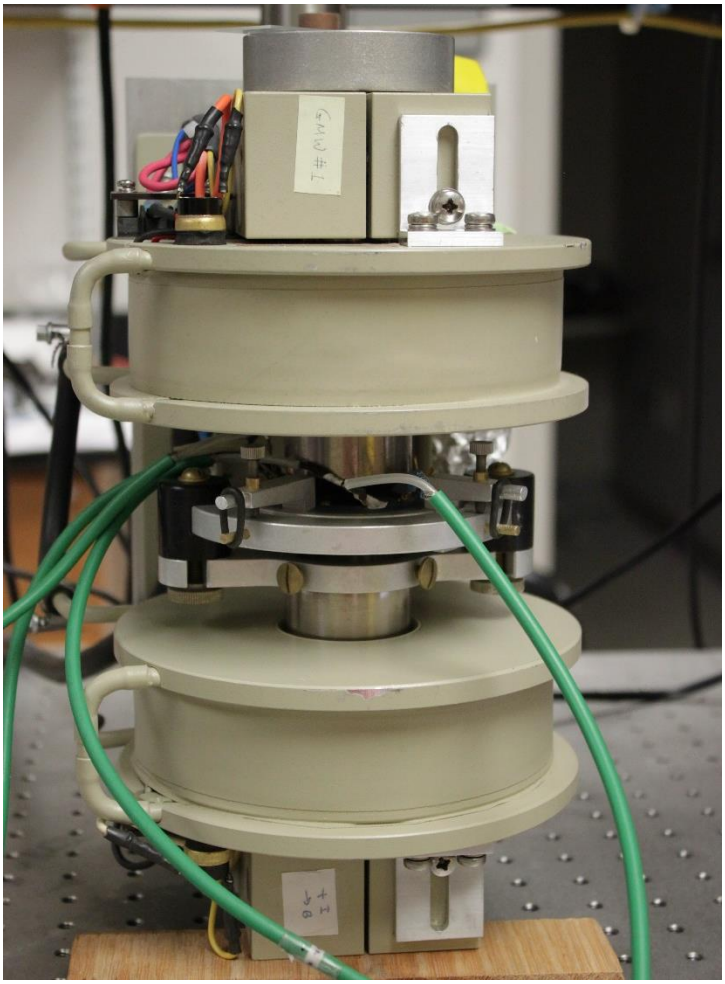

***Figure 4.2: The Magnetic Resistance Measurement System (MaRMS) with its custom sample holder.***

The MaRMS setup consisted of a Kepco bipolar operational power supply/amplifier. This power supply controlled the magnetic field of a model 3470 electromagnet by GMW Magnet Systems with a pole diameter of 45 mm. The pole magnet was adjusted to a pole gap of 15 mm, in which a custom sample holder was inserted. The custom sample holder allowed angle adjustment in x- and y-direction. A Stanford Research System, Model SR830 DSP lock-in amplifier supplied a DC current through the sample and allowed to read out the Hall voltage simultaneously. The hardware controller existed of a BNC 211 brake-out box, a

PXIe-1062Q chassis, as well as a PXI-6251 M Series multifunctional DAQ card, all by National Instruments. A custom virtual instrument was designed in LabView to control the power supply and read from the lock-in amplifier. The circuit drawing is shown in **Figure 4.3**. In this circuit, $V_M$, from the National Instruments DAQ

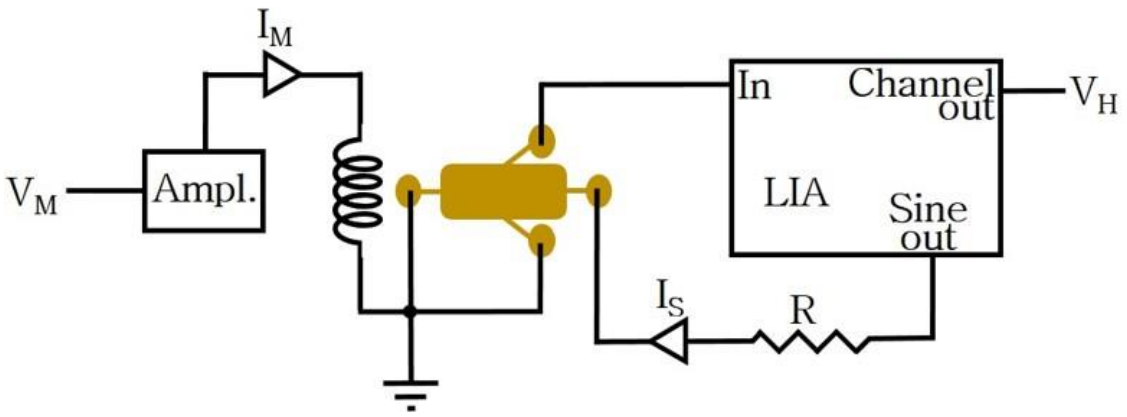


***Figure 4.3: Circuit diagram of the MaRMS set up as described in detail in the apparatus section. Briefly, the Hall bar is connected to a lock-in amplifier that supplies an AC current and measures the transverse Hall voltage, while an electromagnet applies a varying external field. A ballast resistor ensures a sufficiently low current through the Hall bar thin film to avoid thermal damage.***

hardware, is converted onto a current, $I_M$, through the electromagnet by the voltage controlled power supply (Ampl). This allows the control of the magnetic field that is applied to the sample. The lock-in amplifier (LIA) produces a constant amplitude 2 V, 2 kHz AC voltage at "Sine Out", which is applied to a series circuit consisting of a 2 kΩ ballast resister, R, and my sample, yielding a final sample current $I_S$. The LIA simultaneously measures the amplitude of the net Hall voltage perpendicular to $I_S$, which also oscillates at 2 kHz since the driving voltage at Sine Out does. This amplitude is the "Signal", $V_H$, which is scaled, by additional LIA settings, to be roughly 1 V and so requires further processing to convert back to an actual Hall voltage across the sample. The applied magnetic field H was swept in strength

between ±6000 Oersted with a frequency of 0.03 Hz. Each run measured 10,000 data points over two full sweeps of the magnetic field starting at 0 Oersted. Since the signal strength varied with the net resistance of the sample, the lock-in sensitivity was adjusted for each run to ensure the best signal-to-noise ratio. All samples were measured under ambient conditions in this custom magnetic resonance measurement system (MaRMS).

The angle between the sample and the applied magnetic field could be adjusted by two screws on the custom sample holder, which allowed adjustment in x- and in y-direction (**Figure 4.1A**). The system was designed with an 80 threads per inch screw. One turn of the screw resulted in an angular adjustment of 4 mrad. It was determined that the smallest adjustment was 1/8 of a turn of the screw, which resulted in a resolution of 0.5 mrad. The piezo crystal and the control electronics were extracted from a commercially available humidifier by Crane, called Elephant Ultrasonic Cool Mist Humidifier "Elliot". A large hose ending with a funnel was connected to the vacuum suction of the local laboratory hood. The open funnel end was placed to one side of the sample holder, while the piezo crystal and two fans were placed on the other side. The combination of the fans and the suction of the hood created an air channel around the sample holder, which guided the evaporated chemical vapors over our sample (**Figure 4.1B**). A picture of MaRMS can be seen in **Figure 4.2**.

## 4.2 Sample Preparation

All metal thin film samples were prepared in a multi-step procedure. While the preparation itself required attention for details, it was also very important to

ensure the cleanliness of the sample before it was measured in MaRMS. In the following subchapter the preparation as well as the cleaning process will be discussed. In addition, the chemicals used for the measurements as well as their purity will be discussed.

### 4.2.1 Patterning Metals

For the experiments three Hall bars per sample with an area of roughly 0.75 $mm^2$ (500 µm x 1500 µm) were patterned using positive photolithography (**Figure 4.4**). To create a pattern this way, 2 mL of the positive photoresist S1811 was applied onto a clean, nonconductive silica wafer and spun it down for 40 seconds at 4000 rpm, before it was baked for 1 minute at 110 °C. The pattern was burned into the positive photoresist film by exposing it to blue light with a wavelength of 436 nm (g-line) for 3 seconds. Afterwards the wafer was placed in a solution of 5 parts DI water and one part Developer 351 and stayed there for 45 seconds before it was rinsed with DI water to stabilize the film.

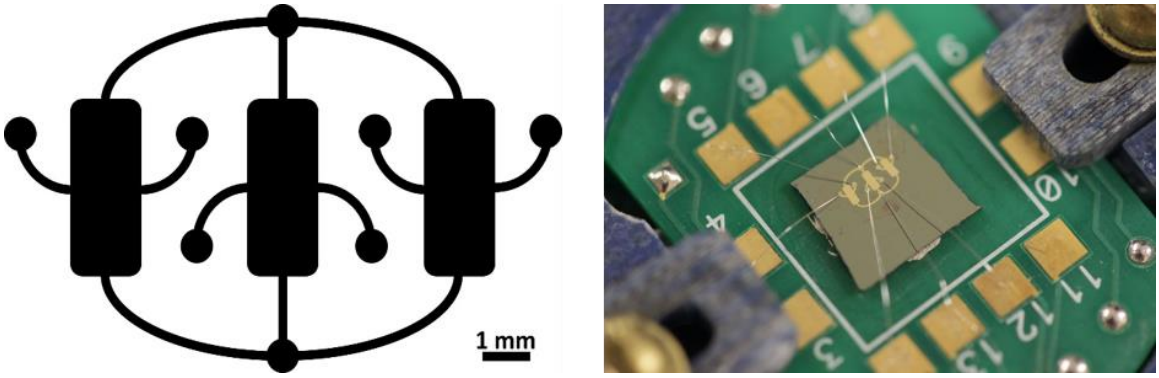


***Figure 4.4: left: Sample outline of the three-Hall bar sample. Wire bonds are made at the round pads, ensuring that the bonding process does not change the shape of the Hall bar or the effective location of the measurement point. Each Hall bar is measured separately. Right: picture of an actual sample showing the trio sample wired onto the sample holder.***

The metal thin films were deposited onto a silica wafer via electron beam deposition under reduced pressure ($10^{-6}$ Torr) with a deposition rate of 1 Å/s. During the evaporation of the metals an easy axis was introduced along the current direction by placing the sample between two magnets with 40 pounds pull force. The photoresist was removed with remover 1165, then rinsed in acetone, ethanol, and DI water, before they were immediately dried under nitrogen flow. The silica wafer was glued onto a sample holder using silver paint and the electrodes of the metal thin film were wire-bonded to the electrodes of the sample holder using aluminum wires. This sample holder was then in turn place in our custom set up. Ensuring the measurement of a clean sample, a cleaning procedure was developed to avoid dried solvent residues on the sample. For this, the sample was rinsed with acetone, ethanol, and DI water and immediately tried under a nitrogen stream. If the sample was left to air dry, a residue that was visible with the naked eye was formed on the sample surface (**Figure 4.5**). Using the piezo crystal for the deposition, a similar residue for the solvents was never observed.

***Figure 4.5: The sample wafer before (left) and after (right) cleaning with solvents when not tried with nitrogen immediately.***

### 4.2.2 CHEMICALS

All chemicals were used as received. The metal pellets (Ag, 99.99 %; Au, 99.999 %; Co, 99.95 %; Cu, 99.999 %; Ni, 99.995 %; $Ni_{80}Fe_{20}$, 99.95 %) were received from Kurt J. Lesker Company. The chemicals for the positive photolithography (Photoresist S1811, Developer 351, and Remover 1165) were by Dow Chemicals, the deionized (DI) water was provided by a local DI source, the silver paint (PELCO® Conductive Silver 187) was received from Ted Pella, Inc., the wire to connect the sample electrodes to the sample holder was a 1 % Si/Al alloy with a diameter of 0.00125 inches by Ametek®, the silicon wafer used was 3" in diameter and 2 mm thick with a 200 nm oxide layer, by Silicon Quest International. All following chemicals were tested for trace metals by NMR and EDS before and after application to the piezo crystal. No contamination for any ferromagnetic element was found prior or past the application. 1-dodecylthiol, 98 %, was received from Acros Organics, benzyl alcohol, certified, was received from Fischer Scientific, methanol, 99.8 %, ethanol, ≥ 99.5 %, propanol, 99.5 %, hexanol, 98 %, glacial acetic acid, ≥ 99.5 %, acetone, ≥ 99.9 %, hexylamine, 99 %, and hexane, 95 %, were received from Sigma-Aldrich. All liquids used as ligands were measured by NMR and ICP-MS. The spectra can be found in Appendix B.

## 4.3 EXAMPLE DATA EXPLAINED

In order to give an understanding of the collection of the data, in the following chapter theoretical data collection as well as the data analysis will be discussed.

### 4.3.1 Theoretical Data Explained

The MaRMS is designed to perform comparative measurements of the PHE under ambient conditions. The PHE can be measured as part of the sum of Hall effects in form of a voltage perpendicular to current density. The plot is a combination of the regular Hall effect, the AHE, and the PHE as shown in **Figure 4.6** for a sweep between -6 T and +6 T. The regular Hall effect is a linear plot (**Figure 4.6A**) and due to the drift of electrons caused by the application of an external magnetic field. The AHE is due to quantum mechanics and generally start with a plateau, then increases and ends in a plateau as can be seen in **Figure 4.6B**. The PHE signal addition is only caused when the magnetization changes directions and briefly aligns with the measured voltage in-plane, which causes a maximum in the voltage and is shown as a peak (**Figure 4.6C**).

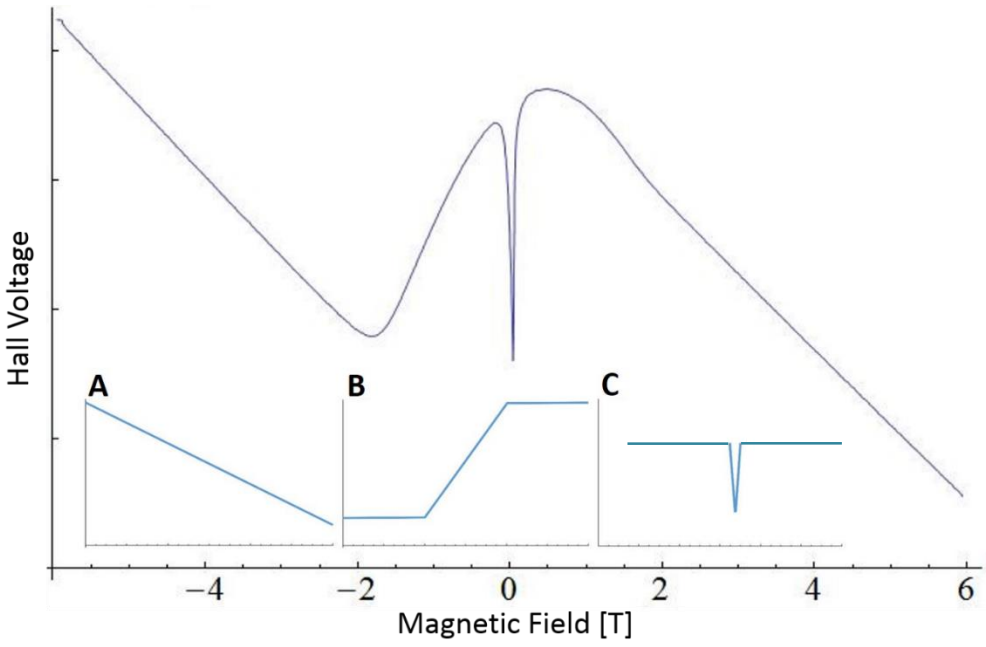


***Figure 4.6: Graph for a sweep from -6 T to +6 T. Inset are the different Hall effects, which dictate the shape of this graph. A) regular Hall effect, B) anomalous Hall effect, and C) planar Hall effect.***

Knowing that the sensor for this work is the ferromagnetic layer of the sample, it is also known that hysteresis is always present throughout the measuring process. When plotting a hysteresis curve, the magnetization, M, of the sample is plotted versus the externally applied magnetic field, H. The magnetization of the sample has in general only two directions, positive or negative, on the hysteresis plot. Although the hysteresis curve can shift in various ways, for example by having a magnetization before the system is first charged up, the direction of the magnetization M only changes, when the value for the magnetization changes its sign and therefore, when M crosses zero. This seems to be a rather obvious observation but it is of vital importance to understand the connection with the measured peaks. The peaks employed for the measurements of this dissertation are caused by a direction change in magnetization of the sample. It was concluded, that the position of the peaks is directly related to the hysteresis of the sample and occurs exactly when the magnetization crosses zero.

Often, the measured hysteresis curve is shifted in its coordinate system, so to understand the various ways that the hysteresis curve can be shifted, a scheme of all cases is shown in **Figure 4.7**. The most commonly thought about hysteresis curve is the one for a material that has no initial magnetization and without any external magnetic field applied. This case is presented on the top center. As discussed previously, there would be an initial magnetization taking place, which is not presented in this figure. Once a saturation magnetization is reached and the system is cycled between an external field of a given positive and negative value for H, the presented hysteresis curve would be observed.

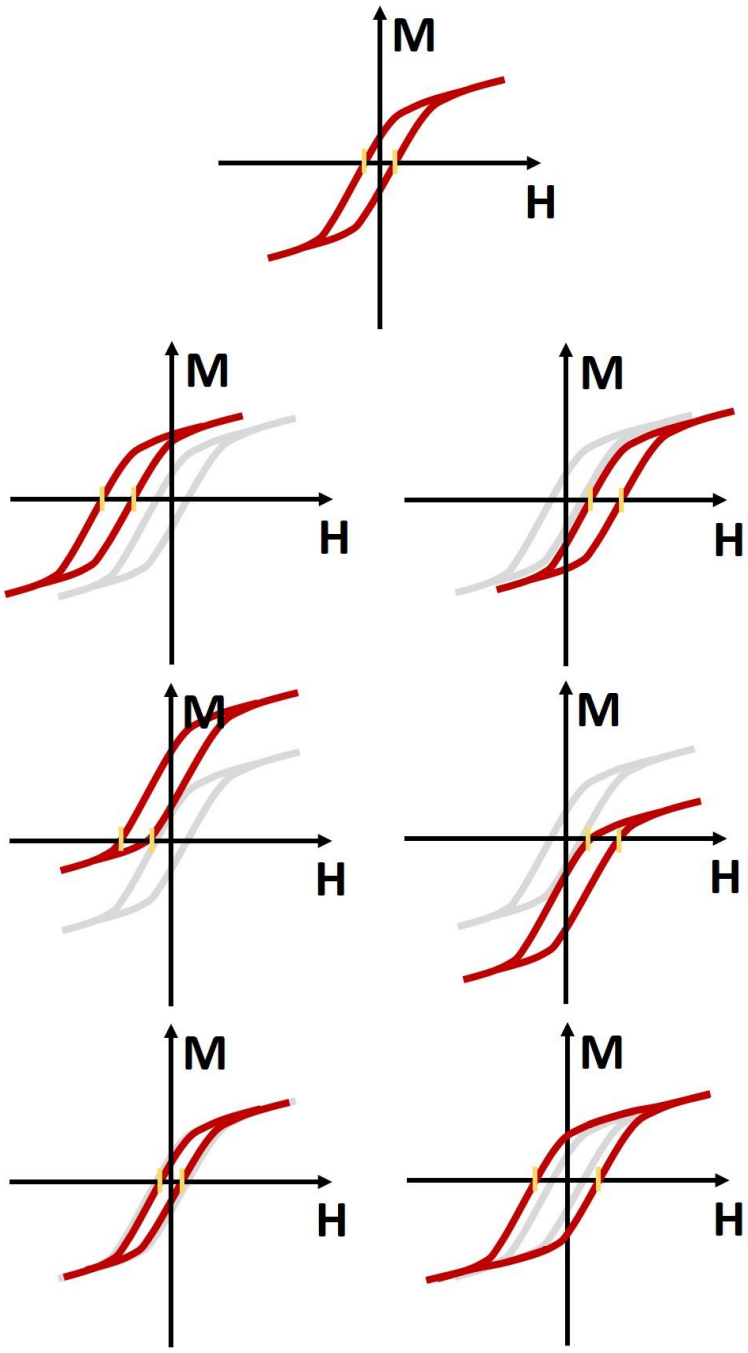


***Figure 4.7: Schematic of possible shifts for a hysteresis curve when magnetization M is measured for a certain applied magnetic field H. First line: ideal hysteresis curve with no initial magnetization M and cycled between equal values of +/- H. Second line: hysteresis curve with no initial magnetization cycled between significantly different values for +H and –H. Third Line: hysteresis curve cycled between equal values of +/- H but with an initial magnetization present in the material. Last line: change in magnetic properties can cause the width of the hysteresis curve to be wider or narrower than the initial case. Yellow bars indicate zero crossing points.***

The images in the second row show hysteresis curves that are created when a material has no initial magnetization, but the externally applied magnetic field is cycled between significantly different values, where the negative value is larger than the positive one for the left plot and vice versa for the right plot. Having different values for the positive and negative maximum of the applied magnetic field shifts the hysteresis curve to the left or the right along the x-axis.

The third line shows the hysteresis curves for samples with previous positive, on the left, or negative magnetization on the right. Starting with an initial magnetization present in the system simply shifts the hysteresis curve up or down.

If the peaks shift, knowing the previous discussed relationship, this means that the hysteretic properties of the sample change. All of the previous discussed cases can happen, as well as a change in width of the hysteresis curve, which is shown in the last line of **Figure 4.7**. A change in width of the hysteresis curve generally indicates a change in magnetic hardness.

### 4.3.2 Real Data Explained

Since this data had to be analyzed in an elaborate process, the different steps of analysis as well as the thoughts taken into consideration to understand the data will be discussed below as well as the steps taken to ensure data accuracy and repeatability.

#### 4.3.2.1 Extracting Data

The observed raw data consists of two full sweeps of the magnetic field. **Figure 4.8** shows the raw data as collected during the measurement. On top the applied magnetic field is shown over the time of the measurement. In the middle the net Hall voltage as measured is shown over the time of the measurement. On the bottom only a part of the data is taken into consideration. Although it was one full sweep, it is important to look at a sweep after the initial magnetization to get a consistent result from an already magnetized sample. In this last graph, the Hall voltage is plotted versus the applied magnetic field.

The change of the applied magnetic field causes the magnetization direction to align with the field. However, due to the hysteresis of the ferromagnetic metal this realignment does not occur at 0 Tesla like for the externally applied magnetic field. Rather the magnetization of the cobalt keeps the overall magnetization of the system steady until the coercive field strength is reached, which is the point when the magnetization switches direction. This particular direction change causes the peak measured in this dissertation. A change of magnetization due to the surface modification causes a change in the net magnetic field experienced by the ferromagnetic metal, which, in turn, causes a shift in the peak position of the PHE. To analyze the change in magnetization a full sweep cycle was analyzed, in which the applied magnetic field changes between ±0.6 Tesla to ensure a set magnetization of the sample. In a full sweep two peaks can be observed, one to either side of 0 Tesla.

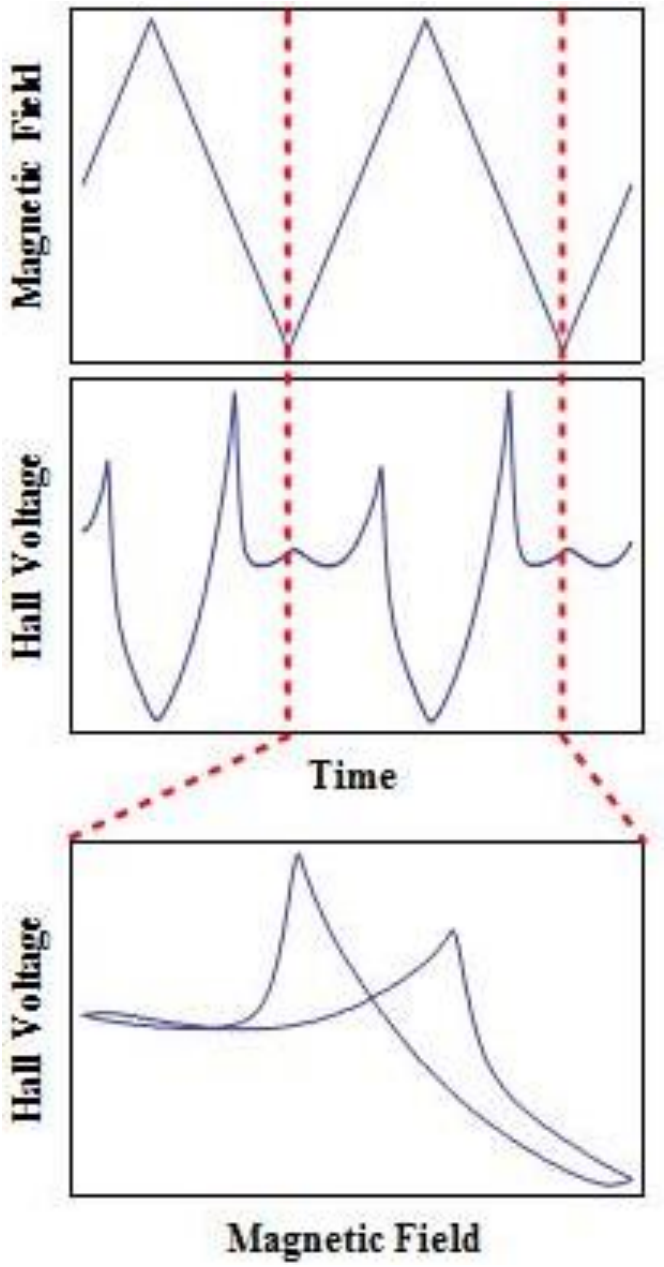


**Figure 4.8: Schematic indicating the experimental procedure. A) The magnetic field is swept linearly between two symmetric extrema. B) The Hall voltage is recorded for the entire sweep but only the portion between the second and third extremum is normally analyzed. Initial responses are variable because the magnetization of the sample is initially random, not having been exposed to ~1T external fields. Subsequent responses match the initial one, and so are not shown in any of the remaining figures. C) The result, showing a full sweep with increasing and decreasing segment of the applied field and the measured Hall voltage as an x-y plot. Depending on the direction of the applied magnetic field with respect to the current direction, the peak can point up or down.**

#### 4.3.2.2 Accuracy of Angular Adjustment

The process of recording the baseline was the same for every measurement. Adjusting the angle of the applied magnetic field relative to the sample, a nicely shifted peak was found and a baseline was recorded.

To have a reasonable sensitivity on the measurements it was mandatory to find a well-defined peak with a peak location at roughly 0.2 T or greater. For this, a full sweep was recorded, plotted, and the sample angle was adjusted relative to the applied magnetic field by adjusting the custom sample holder. The peak shifts during such an adjustment for half a sweep can be seen in **Figure 4.9**. Once a well-defined peak with decent shift was found, the data was recorded. Every sample was measured before and after the ligand application.

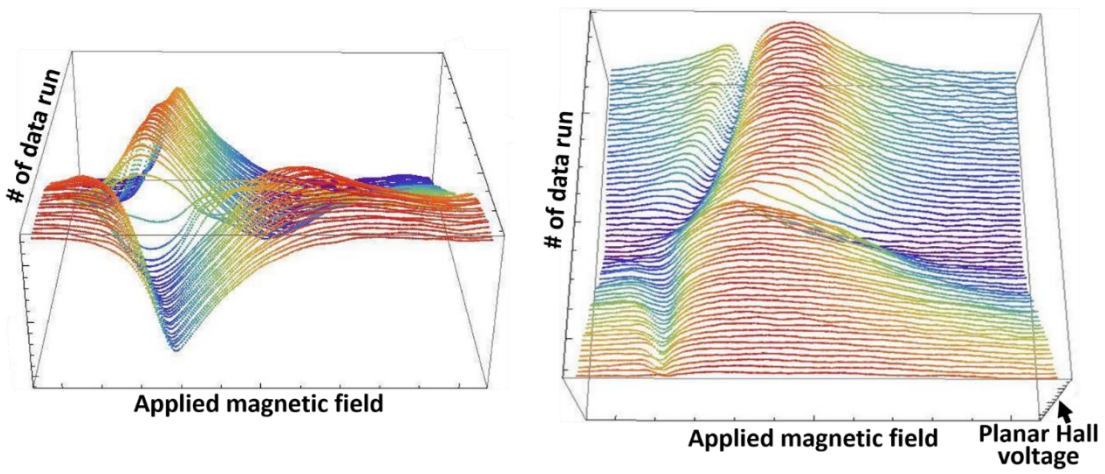


***Figure 4.9: Left: frontal view and right: top view of a 3D plot of the peak movement in MaRMS during the process of finding an adequate peak.***

#### 4.3.2.3 ACCURACY OF PEAK POSITION

To ensure the accuracy of the peak position, each measurement was repeated five times (**Figure 4.10**). As an initial confirmation measurement the sample was left chemically untreated in MaRMS and measured in different time

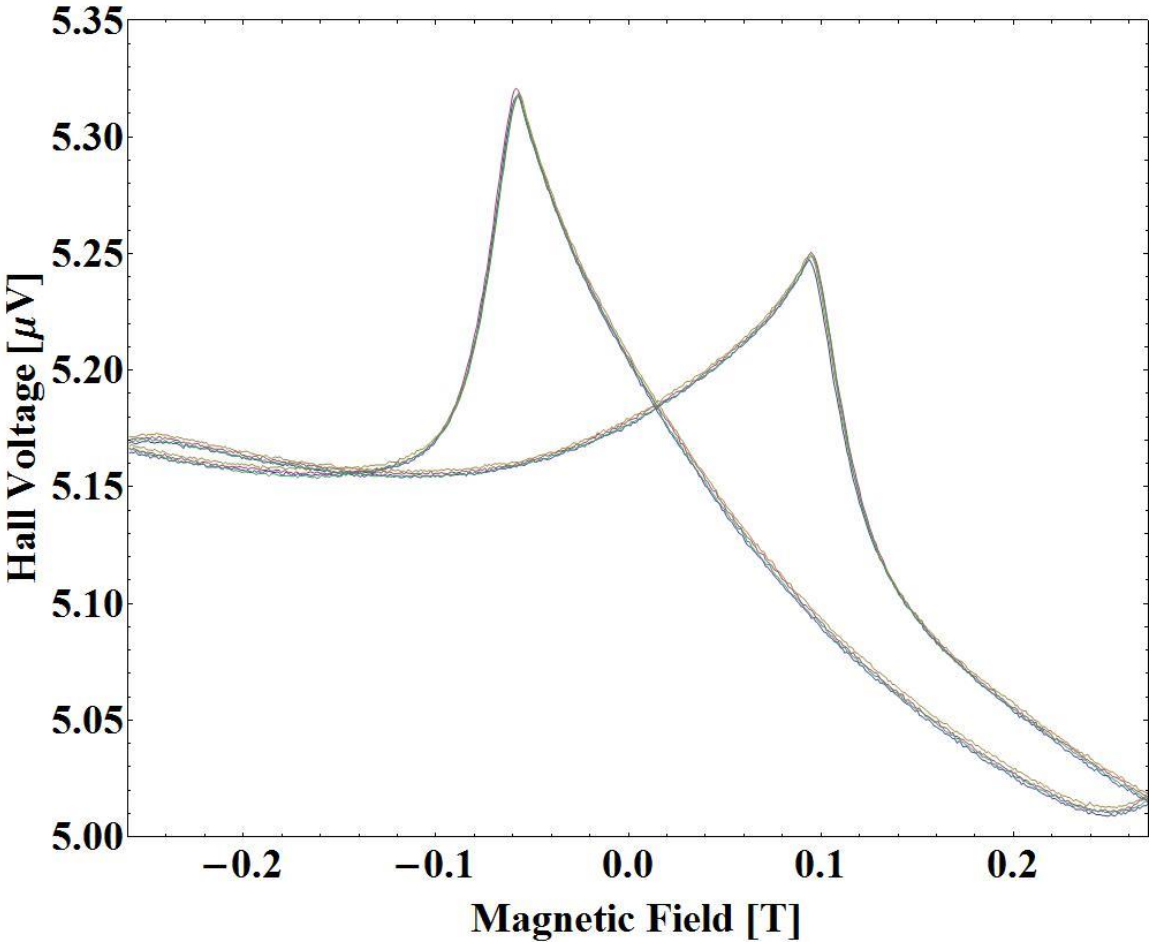


***Figure 4.10: To determine an accurate peak position, each measurement was repeated 5 times as shown above.***

intervals of up to 21 hours to see if the environment could have any effect on the peak shift. The peak was stable in its position (**Figure 4.11**), which allowed the conclusion that the environment in the room, especially the humidity, had no effect on the sample. This experiment was repeated frequently over night or when not

in use. After the baseline was recorded, the liquid of interest was vaporized over the piezo crystal and incubated for 30 minutes before the sample measurement was repeated. Generally each data set consists of 5 measurements, which ensured a steady peak.

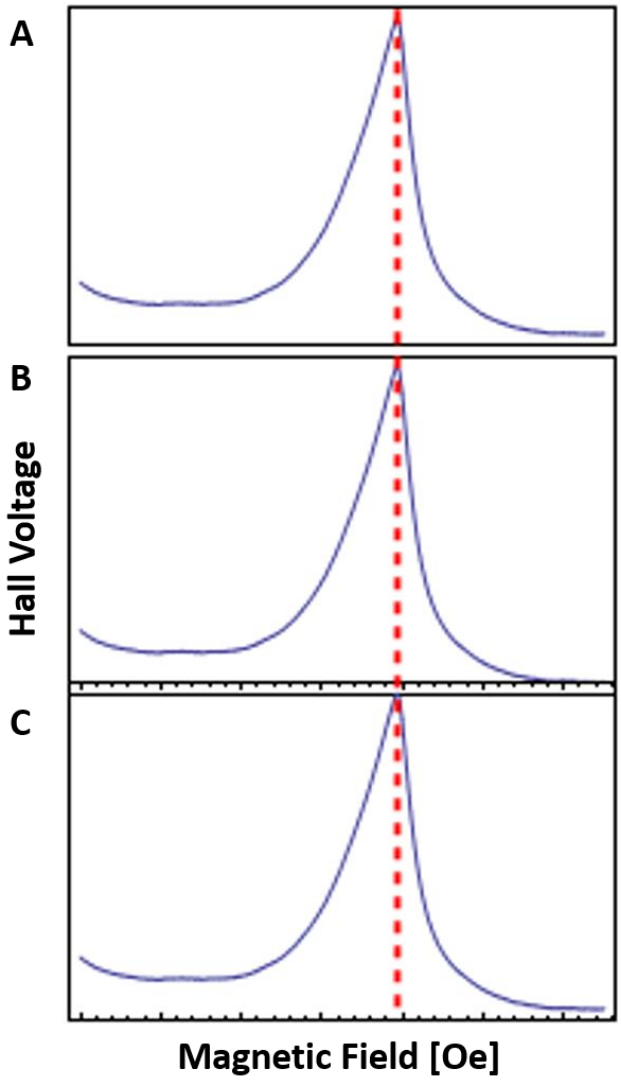


***Figure 4.11: Comparison of the peak caused by the planar Hall effect at A) the initial measurement, B) after 4 hours, and C) after 21 hours. The peak did not move at all.***

#### 4.3.2.4 DATA ANALYSIS

After the experiment, the data was imported into Wolfram Mathematica and analyzed (for code see Appendix B). Using a manipulative graph, in which the strength of the magnetic field was plotted versus the Hall voltage, the peak position was determined by finding the peak maximum manually. Since some peaks had a rather broad shape, it was sometimes difficult to decide on a position, which caused a random error and therefore an increase in the standard deviation of the mean. The standard deviation of the mean, $s_{\bar{x}}$, was calculated using the following equation:

$$s_{\bar{x}} = \frac{\sqrt{\frac{\sum_{i=1}^{N}(x_i - \bar{x})^2}{N-1}}}{\sqrt{N}} \quad \textbf{(9)}$$

N represents the total number of sample runs, $x_i$ is the individual sample value, and $\bar{x}$ is the mean of all sample values.

Measuring with a small magnetic field, compared to the PPMS, only two of the Hall effects were visible. The PHE, which was used to measure the shift, and the net HE, caused by the AHE and the regular HE. This net HE was visible as the slope on which the PHE peak is sitting. One consideration for the changed peak position must be a possible slope change of the net HE. If there is a peak in data and a line shift is added, then the position of the peak will shift up slope. It is important that the shift caused by the magnetic changes is significantly larger than the shift caused by the slope change. To show this, the slope was compared before and after the deposition of the ligand. As shown in **Figure 4.12**, only a negligible change in slope could be found that is not on the size range of the change in peak position and therefore the peak shift must be due to the PHE.

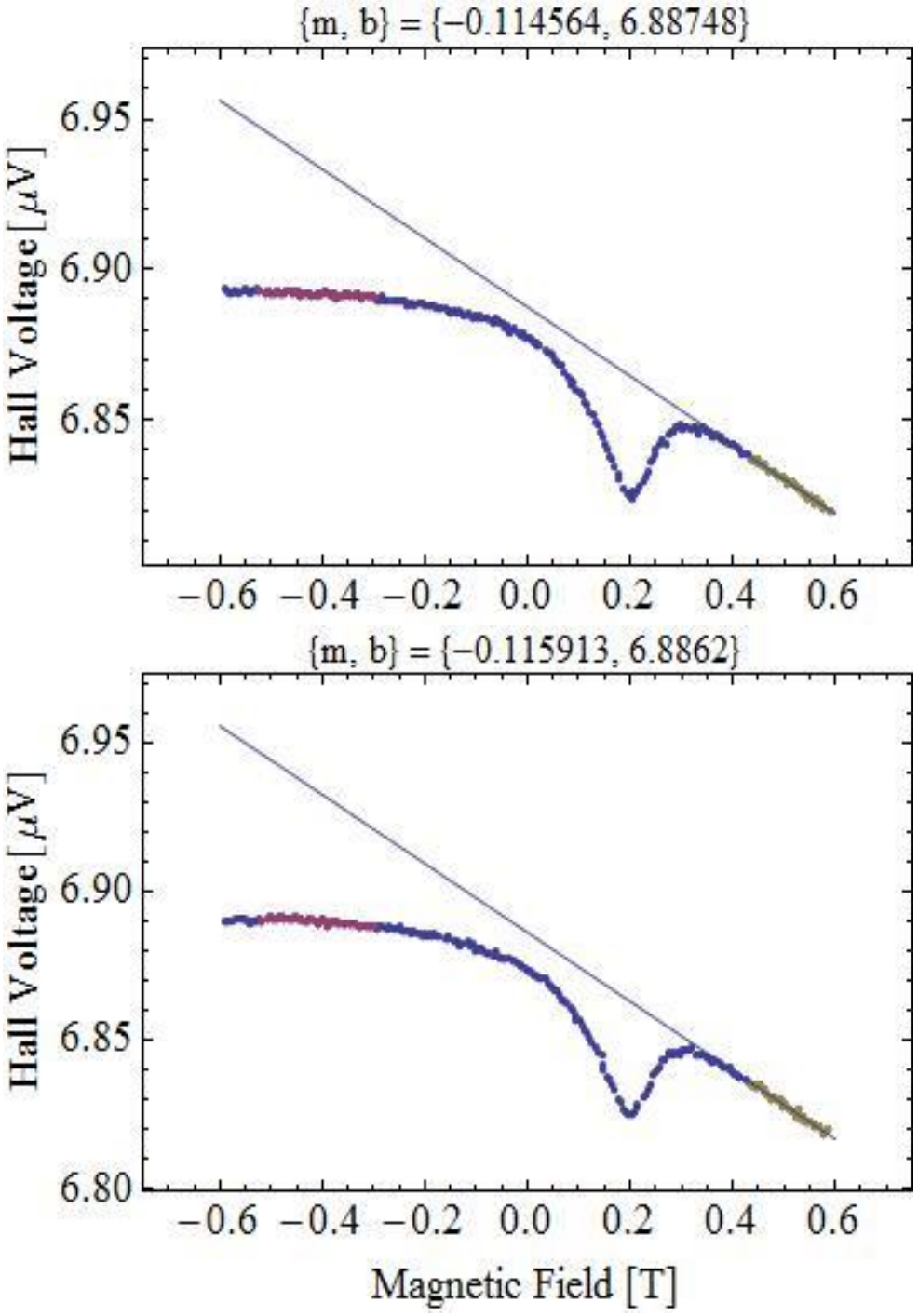


***Figure 4.12: Comparison of the slope caused by the AHE before (top) and after (bottom) the deposition of a ligand. The slope only changes by 1.35 × $10^{-3}$ μV/T, which is over a ten-fold smaller than the change in peak position and it is therefore negligible.***

Using a full sweep between ±0.6 Tesla, both peaks must be taken into account. Because of that, all peak pairs were centered for the analysis by subtracting the initial midpoint of the pair. This is equivalent to declaring that any asymmetry is a systematic error and removable. If this is not done, the relative shifts are different for the left and the right peak, which leads to difficulties of definition and interpretation.

The results for all measurements will be presented below in relative motion, measured in percent. The relative motion is often more meaningful as, in absolute terms, the location of the peak can vary by a factor of five due to the sample alignment and the variety of ferromagnetic materials studied. From the geometry and model, the location of the peak depends on the angle between the sample plane and the applied magnetic field. Therefore, the component of the applied magnetic field in-plane varies when the position of the peak varies, making it difficult to compare two measurements with significantly varying initial peak positions.

To get a better understanding of the actual peak movement and what it means, the peak position for 30 nm cobalt thin film both before (lighter) and after (dark) the application of ethanol were plotted, as well as the midpoint of the two peaks (**Figure 4.13**).

Without further analysis it seems obvious that the majority of peaks move closer to 0 Tesla after the application of ethanol. In addition, it must be mentioned that each sample consists of three Hall bars, which are generally measured consecutively. Therefore, all peak sets of three are from the same sample. Non-

triplet results are from samples where one or more Hall bar did not yield any data for various reasons. This argues strongly that the individual Hall bars are not independent. Instead the results depend on the entire sample rather than the bar itself.

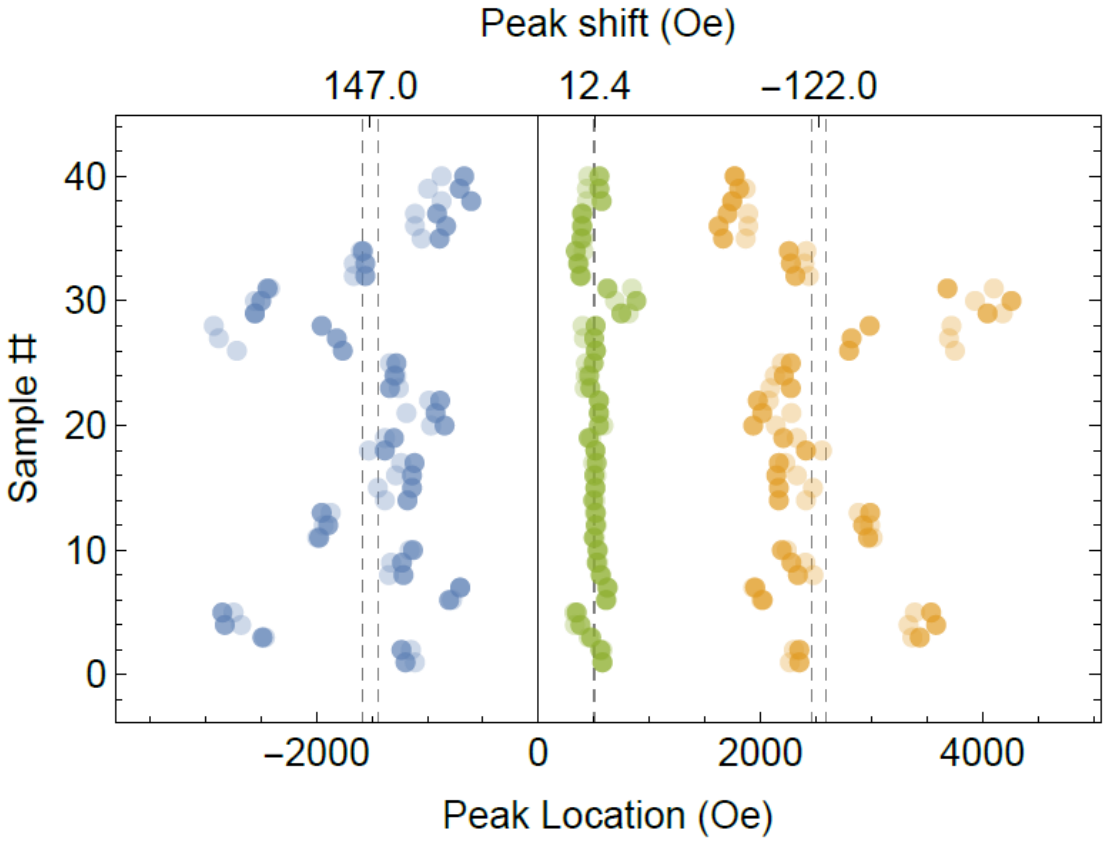


***Figure 4.13: Peak location of left and right peak in blue and orange, respectively, before (light) and after (dark) the application of ethanol on a 30 nm cobalt thin film, with the midpoint location in green. The ligand application causes the peak to shift closer to the midpoint and therefore decreases the width between the two peaks, which is generally associated with a material becoming magnetically softer. The dotted lines indicate the average peak shift for both sides in Oersted.***

An analysis of all midpoints of all samples acquired over 14 months show that the midpoints are similar for samples measured at similar times, suggesting equipment systematics. Some possible causes could be residual magnetic polarization of the iron poles or slightly calibration errors in the output of the power

supply. The midpoints scatter much less than the left and the right peak and are slightly shifted to the right, which causes them have positive values of roughly 500 Oersted rather than 0 Oersted. Some of this offset can be explained by varying sample position in the magnetic field, which was measured by a second researcher. However, it does not account for the entire 500 Oersted.

Seeing that the absolute peak position varies greatly with the sample geometry and therefore is hard to compare, only the width between the left and the right peak and its relative percent change will be taken into consideration for the analysis of this work, as well as the change in midpoint.

Although this measurement does not yet allow for the calculation of a definite value for the magnetic moment of a compound, it does give a conclusive answer for changes in magnetism.

## 4.4 Resistivity of Metal Layers

Anecdotal evidence suggested that thin metal films produced by thermal evaporation onto cold substrates do not form continuous layers until thicknesses reach about 30 nm. Therefore, an attempt was made to ascertain fil quality as a function of thickness via conductivity measurements. A four-point measurement was performed on samples, which were identical in size and shape to the ones used for the MaRMS measurements. The only difference existed in the fact that there was only one metal thin film bar instead of three per sample. To be able to measure the resistivity of a thin film that potentially interrupted by holes, all samples were measured on a 30 nm cobalt layer. This measurement was

performed in the absence of a magnetic field. As shown in **Figure 4.14**, a current was applied along the long axis of the metal bar and a voltage was measured perpendicular to the current direction. By dividing the measured voltage by the applied current the resistance of the sample was calculated. First the resistance of the bare cobalt layer was measured and the resistivity of which was calculated using the equation

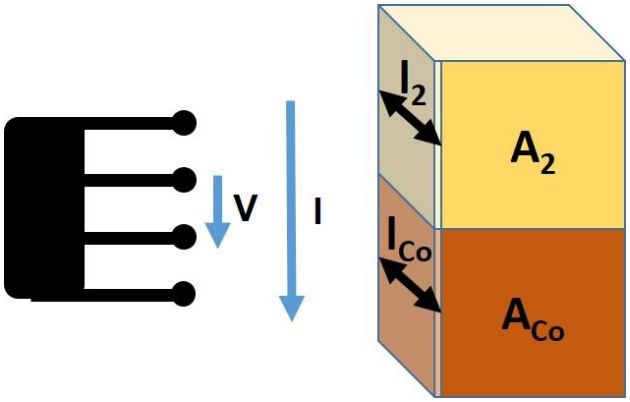


***Figure 4.14: Left: Sample outline for resistivity measurements with indication of current and voltage direction. Right: schematic drawing showing the length, l, and the area, A, of the different metal layers, which were used as variables in the calculation of the resistivity.***

$$\rho_{Co} = \frac{R * A_{Co}}{l_{Co}} \quad \textbf{(10)}$$

$\rho_{Co}$ is the desired resistivity, R is the measured resistance of the sample, $A_{Co}$ is the area of the sample face (height multiplied by the width of the layer), and $l_{Co}$ is the length of the cobalt layer. The resistivity that was calculated for cobalt was later used to calculate the resistance of other metals, which formed a top layer on the cobalt film.

To measure the top metal of the bilayer, the same experiment was performed and the following equation was used to calculate the resistance

$$\rho_2 = ((\frac{1}{R_{total}} - \frac{A_{Co}}{\rho_{Co} * l_{Co}})\frac{l_2}{A_2})^{-1} \quad \textbf{(11)}$$

$\rho_2$ is the desired resistivity of the top layer, $R_{total}$ is the measured net resistance of the sample, $\rho_{Co}$ is the previously calculated resistivity of the cobalt sublayer, $A_{Co}$ is the area of the cobalt layer face (height multiplied by the width of the layer), $A_2$ is the area of the top layer (height multiplied by the width of the layer), $l_{Co}$ is the length of the cobalt layer, and $l_2$ is the length of the top layer.

The cobalt layer was topped by copper, silver, and gold, respectively. For each individual metal 6 samples were prepared with different thicknesses of the top metal, ranging from 10 nm to 200 nm. As can be seen in **Figure 4.15**, all three metals started off with a high resistivity which dropped and reached saturation. For copper and silver, the saturation point was reached at roughly 20 nm, while for the gold the saturation was reached around 30 nm. All resistivities after the saturation point are roughly comparable to the literature values [1]. The high resistivities for the low thicknesses indicate that there is indeed not a homogenous layer present. Because of this, the majority of experiments was performed with a 30 nm thin layer.

## 4.5 References

1. Lide, D. R., ed. *CRC Handbook of Chemistry and Physics, 85th Edition*, CRC Press, Boca Raton, 2004

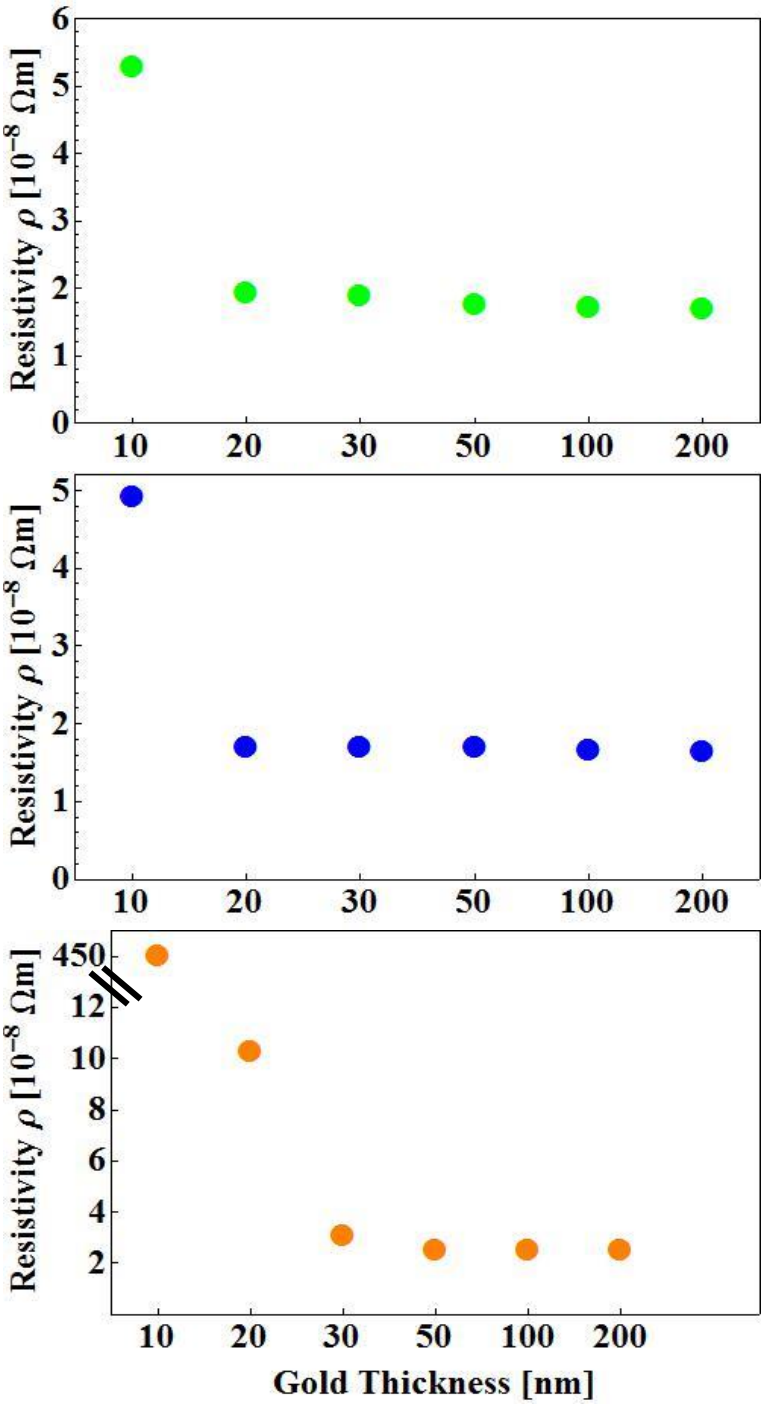


***Figure 4.15: Resistivities for copper (top), silver (middle), and gold (bottom) thin films with varying thicknesses. A non-uniform thin film with holes present causes an increased resistivity. Once a uniform layer is reached, the resistivity saturates.***

# CHAPTER 5

## RESULTS

In the following chapter the experimental results will be discussed. The first subchapter will elaborate on measures taken to ensure the absence of contamination. Next, the verification of the presence of a surface modification layer as well as an easy axis will be demonstrated and the ligand-substrate stability will be discussed. After that all the experimental results from the MaRMS measurements will be discussed and analyzed. It will be shown that the manipulation of the magnetic properties of a cobalt thin film has a reach of roughly 10 nm. It will be demonstrated that large variety of functional groups can cause a change in magnetic properties although the effect scales with the ligand strength roughly in line with Pearson's HSAB concept. While the functional group can have a significant effect on the magnetic properties, it will be shown that the tail of the ligand also plays an important role. Widening the selection of metal serving as planar Hall sensor, the influence of the various functional groups on nickel and Permalloy will be demonstrated. Having shown that ferromagnetic metal thin films can very well be manipulated via surface modification, next, the same will be shown for diamagnetic metal layers. The change of magnetic properties caused by the surface modifications of copper, silver, and gold will be discussed. Since thiol is the chosen ligand for gold in a large number of publications, as was discussed in chapter 3, a study with various gold thicknesses of gold on cobalt will

be shown and a comparison to an identical experiment with ethanol will be performed. As last subchapter potential future work will be discussed.

## 5.1 Contamination and Verification

The main source of potential error is contamination of the sample or the ligand solution. In addition, judging from the literature review, it seems to be difficult to produce repeatable results. Therefore this work has gone to great length to guarantee the purity and repeatability of the experiments. In the following chapter the measures taken to avoid these potential errors will be discussed first, and then the various measurements that were conducted for this thesis.

### 5.1.1 Contamination

Since potential contamination of the metal thin film or the applied ligand liquid were an important potential source of error for the results reported in literature, this subchapter will show the absence of such. In the metal thin films the absence of parasite materials will be shown via energy dispersive spectra analysis and in the ligand liquids via nuclear magnetic resonance as well as inductively coupled plasma-mass spectrometry. In addition it will be shown that even a large amount of paramagnetic iron (II) chloride (aq) has no effect on the magnetic properties of the sample.

#### 5.1.1.1 EDS Analysis

Bearing in mind that the samples are created in a multi-user deposition chamber, the first concern is the contamination of these metal patterns. To show the absence of parasite atoms, energy dispersive spectra (EDS) of different cobalt and gold samples were recorded. To achieve a good sensitivity, all samples were tested to 10,000 counts. As expected, the silica substrate can be found in all of the sample spectra in form of signal for silicone and oxygen due to the penetration depth of the EDS, which reaches way past the sample thickness. In addition, carbon was detected, which resulted from the tape that affixed the sample to the holder. All samples were measured with a FEI Quanta 200 SEM and the spectra can be found in Appendix C. Overall it was shown that no impurities in form of other metals are present in the thin film samples.

#### 5.1.1.2 NMR Analysis

After showing the purity of the metal samples, the next concern was the purity of the ligand liquids. To show the ligand purity, nuclear magnetic resonance (NMR) spectra were recorded for each ligand prior and past application over the piezo crystal. For this, the ligands were dissolved in an appropriate deuterated solvent and measured in a Bruker Avance III HD at 300 MHz. The recorded spectra were identical for the ligands collected prior and past the application over the piezo. For all spectra, it was shown that no impurities are present in the liquid according to the present peaks. The spectra can be found in Appendix D with an explanation for the chemical shift.

#### 5.1.1.3 Confirmation of Contamination Absence via ICP-MS

Contamination of the ligand liquid by trace metals has to be considered, which could not be verified by NMR. Therefore, ICP-MS was performed of ligand samples prior and past the application via the piezo crystal to find the quantity of ferromagnetic trace metals in the liquids used. Samples of the ligand liquids were taken prior and past evaporation over the piezo crystal. Before the sample were injected into the ICP-MS system, all of them were run through a syringe with a metal needle just like used in the original experiment, in case this caused any contamination.

**Table 5.1 ICP-MS data for ferromagnetic trace metals in used liquids**

| | Cobalt [ppb] | Iron [ppb] | Nickel [ppb] |
|---|---|---|---|
| DI water | 0.09 | 4.87 | 1.01 |
| Ethanol | 0.13 | 6.15 | 0.94 |
| Acetone | 0.08 | 2.16 | 1.76 |
| Hexane | 0.05 | 9.92 | 0.96 |
| 1-Dodecylthiol | 0.84 | 35 | 9.52 |

To form a monolayer of iron on the sample it would require roughly 1 ppm of iron, assuming a liquid thickness of 1 mm on top of the sample. Results from the ICP-MS show that the used liquids have less than 40 ppb, and often only a few ppb, of ferromagnetic metals present. Since the sensitivity to magnetically active contaminants is not known for MaRMS, it is mandatory to explore whether 40 ppb of iron is detectable and therefore could cause the peak shift.

#### 5.1.1.4 Introduction of Iron (II) Chloride layer on top of Cobalt

Knowing from the ICP-MS measurement that there are a few ppb of iron, nickel, and cobalt present in each of the ligand bottles, it is important to establish a detection limit for ferromagnetic substances on the surface of the metal thin film. To disqualify the influence of ferromagnetic atoms, an aqueous iron (II) chloride solution in DI water was prepared with a concentration of 0.056 mol/L, which equals one $Fe^{2+}$ ion per thousand water molecules. The presence of a paramagnetic ion should add to the net magnetic field experienced by the Hall voltage when an external magnetic field is applied.

Although a large number of ions were present in the solution, only the peak shift for water (discussed in chapter 5.2) was observed. The presence of the salt on top of the cobalt had no influence on the peak position. Looking at the sample

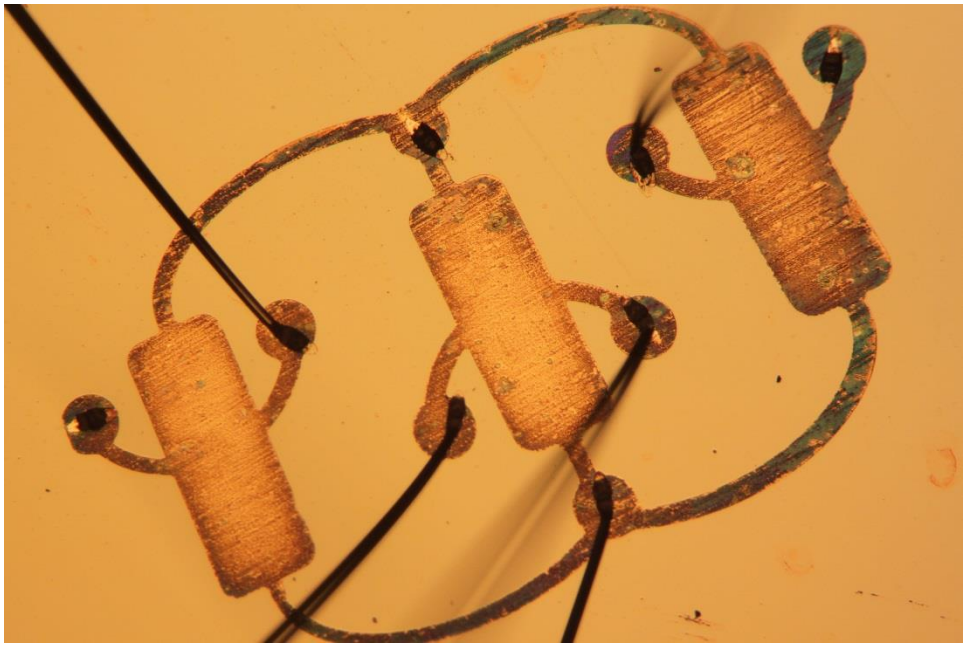

***Figure 5.1: Picture of a cobalt thin film sample after application of 0.056 M aqueous iron (II) chloride, photographed through an optical microscope.***

under an optical microscope, the salt layer on top of the sample was clearly visible (**Figure 5.1**). Since no movement was observed other than the water, the organometallic bond must have a much larger strength than random paramagnetic particles sitting on top of the surface without any direct bonds to the sample.

### 5.1.2 VERIFICATION

Another vital factor to prove that the MaRMS measurements are not flawed is the verification of the presence of an easy axis in the metal thin film sample. To do so, vibrating sample magnetometry was performed, in which the sample is measured at different alignments relative to the applied magnetic field and it was determined that one orientation indeed has a magnetically harder axis than the other. In addition, to verify the presence of a ligand layer on the metal thin film after the evaporation over the piezo crystal, a scratch test using an atomic force microscope was performed and will be discussed. Also, the ligand-substrate stability will be discussed and it will be shown that the peak shift caused by the ligand has settled after about 15 minutes and remains steady for at least 90 minutes.

#### 5.1.2.1 EXISTENCE OF AN EASY AXIS

Having a custom sample holder in the deposition chamber to introduce an easy axis in the sample it was necessary to prove that one axis is preferred over the other. Therefore a vibrating sample magnetometer (VSM) measurement was performed on the cobalt samples. In this measurement, a sample is uniformly

magnetized in a magnetic field, then the sample is physically vibrated in a sine wave fashion. A voltage is induced in nearby pick-up coils, which is proportional to the magnetic moment of the magnetized sample. By plotting this data versus the applied magnetic field, it is possible to obtain the hysteresis curve for a material. In the case of the cobalt Hall bars, VSM was performed twice: once the sample was aligned with the field lines, and the second time it was set perpendicular to the field line of the applied magnetic field. The resulting data clearly showed a difference in the ease of magnetization, proving that indeed an easy axis was created in the samples. If the easy axis aligns with the applied magentic field, the hysteresis loop shows a large opening and it saturates quickly. Overall, the hysteresis loop has a rather square shape in this case. If the applied magnetic field aligns with a hard axis instead, the hysteresis loop will take more of an S shape and the opening in the loop will vanish entirely. As can been seen in **Figure 5.2**, the sample did have an easy axis, although it was not perfectly aligned with the field in this case. Since the sample was aligned on the VSM sample holder by using the orientation of the Hall bar as a guide, it can be concluded that the easy axis did not run perfectly along the Hall bar axis. However, the use of the 40 lb pull force magnets is sufficient for the introduction of an easy axis for these measurements.

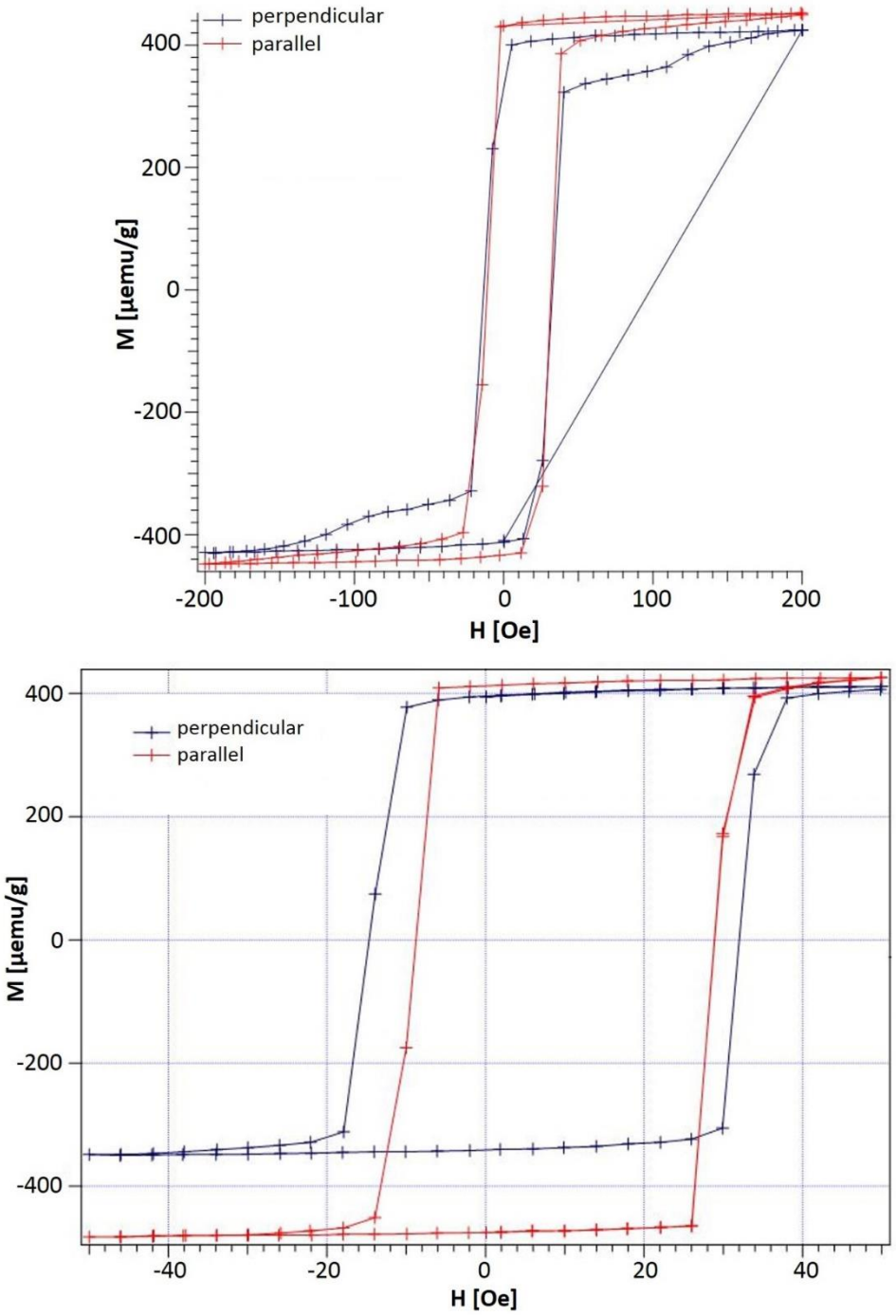


***Figure 5.2: Top: hysteresis curve for the 30 nm Co thin film for a applied field of +/- 200 Oe measured in increments of 11 Oe, bottom, hysteresis curve for same sample for a applied field of +/- 50 Oe measured in increments of 4 Oe Application of the magnetic field B along the sample showed evidence of a hard axis (red), while alignment of the magnetic field B across the sample showed the presence of an easy axis (black).***

### 5.1.2.2 Deposition of a Thin Solvent Layer

The solvent layer was applied by vaporizing the liquid over the piezo crystal and guiding it over the sample by controlling the air flow around the sample and creating an air channel as previously discussed. The sample was allowed to sit for 15 minutes to guarantee a dry surface after the ligand application.

As confirmation for a deposition of ligands on the thin film surface, a scratch test via atomic force microscopy (AFM) was performed. For this purpose, after performing the post deposition measurements, the sample was scanned under the

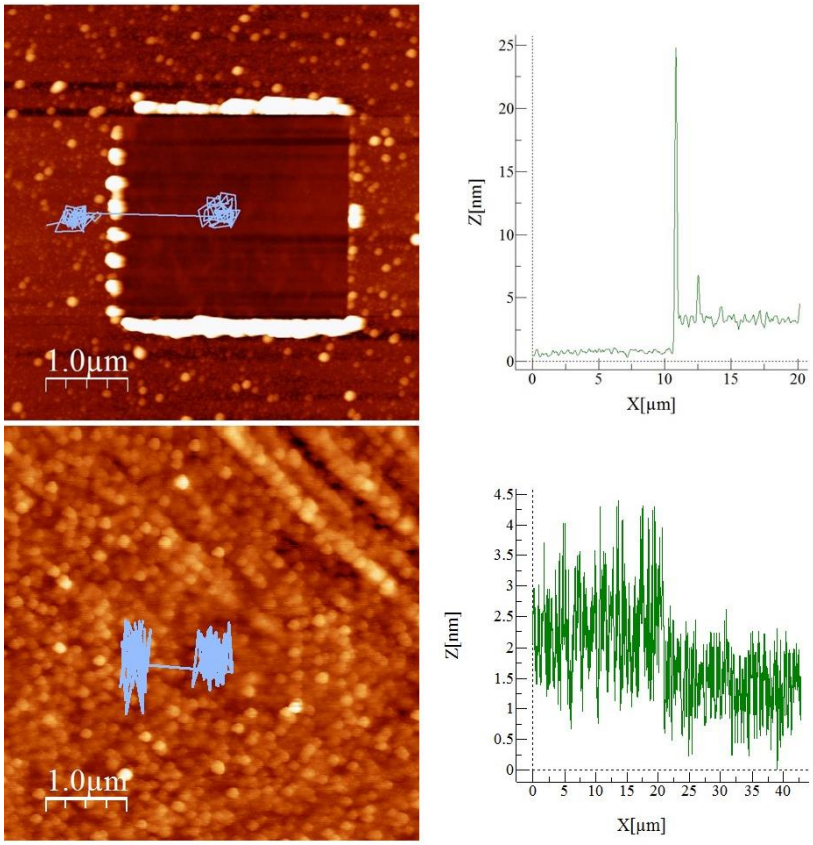


***Figure 5.3: Images of AFM scratch tests on the left with height profiles on the right. The top data is an exemplary scratch test on a purchased flat gold sample, the bottom data is a scratch test after ethanol deposition on a 30 nm cobalt thin film.***

AFM in the tapping mode. Once a smooth area was found, the cantilever was forced onto the surface of the sample in contact mode, which caused the ligand layer to be scratched off. For this it is important to use just enough force to remove the ligand, yet little enough to not scratch the soft gold layer. Once the ligand layer is removed, the sample is scanned again in tapping mode and the height difference between the exposed surface and the ligand layer is measured. As shown in **Figure 5.3**, the samples did not permit a clean height measurement. The main cause for this is that the surface was very rough. Regardless, the scratch test did confirm a deposition of roughly 1 nm on the metal surface.

#### 5.1.2.3 Ligand-Substrate Stability

Knaus *et al.* reported in their publication, that the peak shift slowly settles over a time frame of three hours after a surface modification was performed [1]. To be able to compare my results from the MaRMS to the ones received from a PPMS a similar study was performed. The initial baseline was measured, the ligand was applied using the piezo crystal to vaporize the liquid, after 15 minutes the sample was measured, and after 90 minutes the sample was measured again. As shown in **Figure 5.4**, the shift of the peak after the deposition is clearly visible, but then the peak remains in its position, even after 90 minutes. For the experiment in the PPMS, as shown by Knaus *et al.* [1], the ligand could only be deposited out of a dilute ethanol solution and therefore some time might be required to see a deposition form on the substrate. For this work, only pure ligands were deposited via vapor deposition, which might have enabled a quicker deposition.

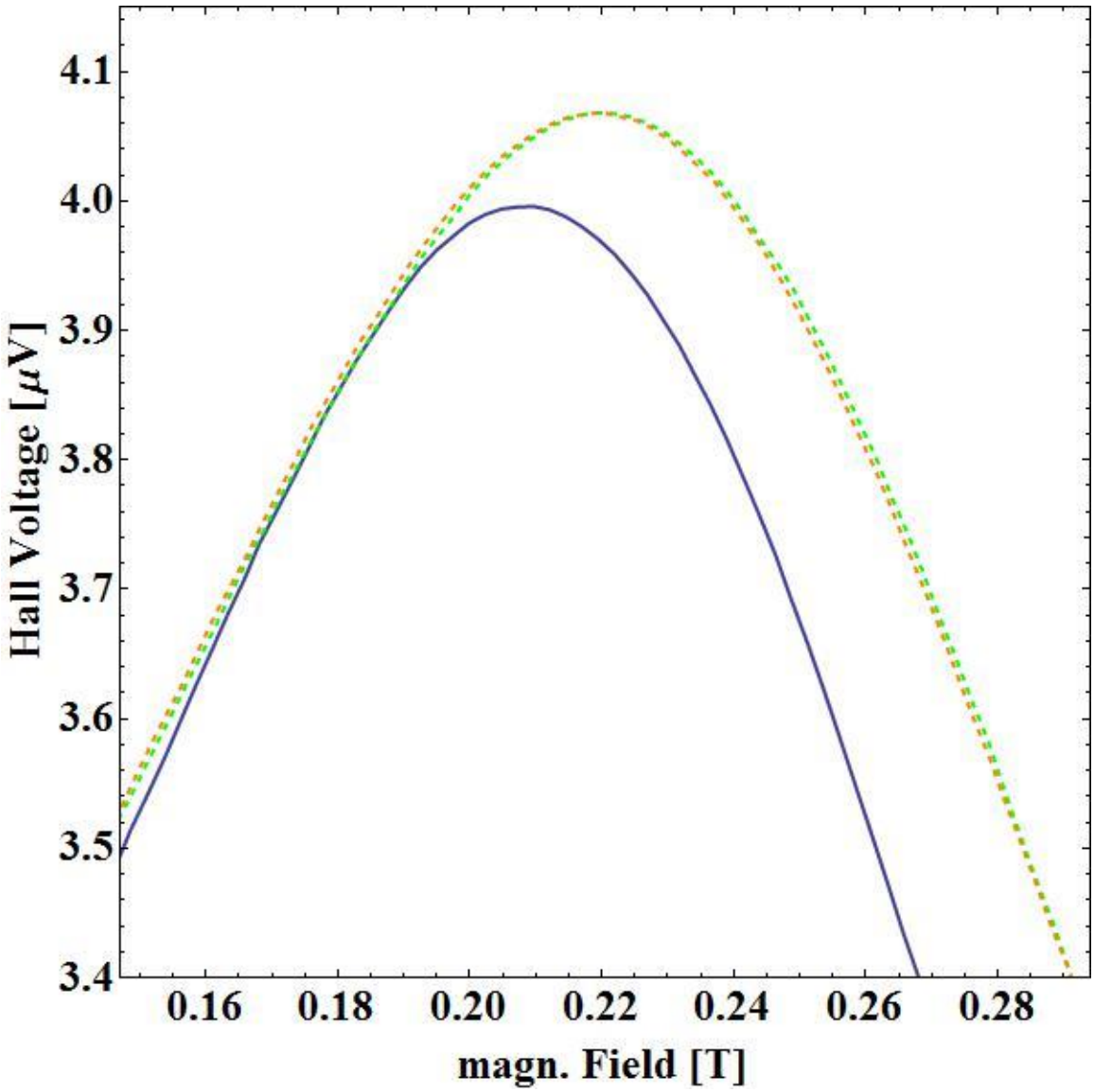


***Figure 5.4: Planar Hall effect before (blue) and after (dashed) the deposition of ethanol onto 30 nm Co. The green dashed line is 15 minutes after the deposition and the orange dashed line* is after additional 90 minutes. This shows, that the peak remains in a steady position after a ligand was deposited.**

## 5.2 Ferromagnetic Thin Films

The MaRMS Measurements depend highly on the ability to observe a peak caused by the PHE. Since the PHE can only be observed in ferromagnetic metals it is important to explore a variety of such metals to show that this technique can be used as reliable sensor system. The three ferromagnetic elements under standard conditions are iron, nickel, and cobalt. While nickel and cobalt are good candidates for the MaRMS experiments, iron has unpredictable oxidation rates and stages, which rules it out for this work as all measurements are performed at a regular atmosphere. Instead Permalloy was chosen to serve as a third representative for the ferromagnetic group. It will be shown that all three metal thin films can be manipulated via surface modification. The magnitude of the change in magnetic properties of the thin film roughly correlates with the HSAB concept.

### 5.2.1 Cobalt

Since this work was inspired by the work of Knaus *et al.*, their sample set-up was used to identify important measurements [1]. Their sample generally consisted of a cobalt layer topped by a gold layer. Since the cobalt layer is the actual sensor in this experiment it is important to explore, if the magnetic properties of cobalt itself can be manipulated by applying a ligand layer on the surface. Since indeed a number of functional groups have a significant impact on the magnetization of the cobalt, it was important to show how deep the effect reaches through the metal layer. It will be demonstrated that ethanol causes a reach of at

least 30 nm through the metal sample. Also, the influence of different chain length as tail groups on an alcohol as head group will be demonstrated.

#### 5.2.1.1 Variation with Film Thickness

Assuming that the modification only takes place on the surface, it was investigated how deep the magnetization change reaches through a cobalt thin film. This is particularly of importance to gain a better understanding of the magnetic moments reported in literature [2-5]. The nanoparticle work showed effects vanishing at a diameter of 10 nm and theory suggests a surface effect spin coherence lengths in gold are on the order of 1 nm and even less for silver and copper [6].

To find out the interaction distance between the ligand and the metal atoms, a measurement was performed on different thicknesses of the cobalt thin film ranging from 10 nm to 50 nm. For all measurements ethanol was applied to the surface as ligand of choice. As presented in **Figure 5.5** this experiment showed that the change in magnetization varies only very little with increasing thickness and, if anything, only drops in strength for the 50 nm thick cobalt sample. The samples with 10 nm to 30 nm of cobalt have a change in width between the two peaks that is rather stable. For the 40 nm sample it is hard to draw a conclusion because the standard deviation is so very large compared to the other samples. The sample with 50 nm of cobalt clearly has a significantly smaller change in the width between the two PHE peaks. Considering that all reaction conditions were constant, this leads to the conclusion that the change of the magnetic properties

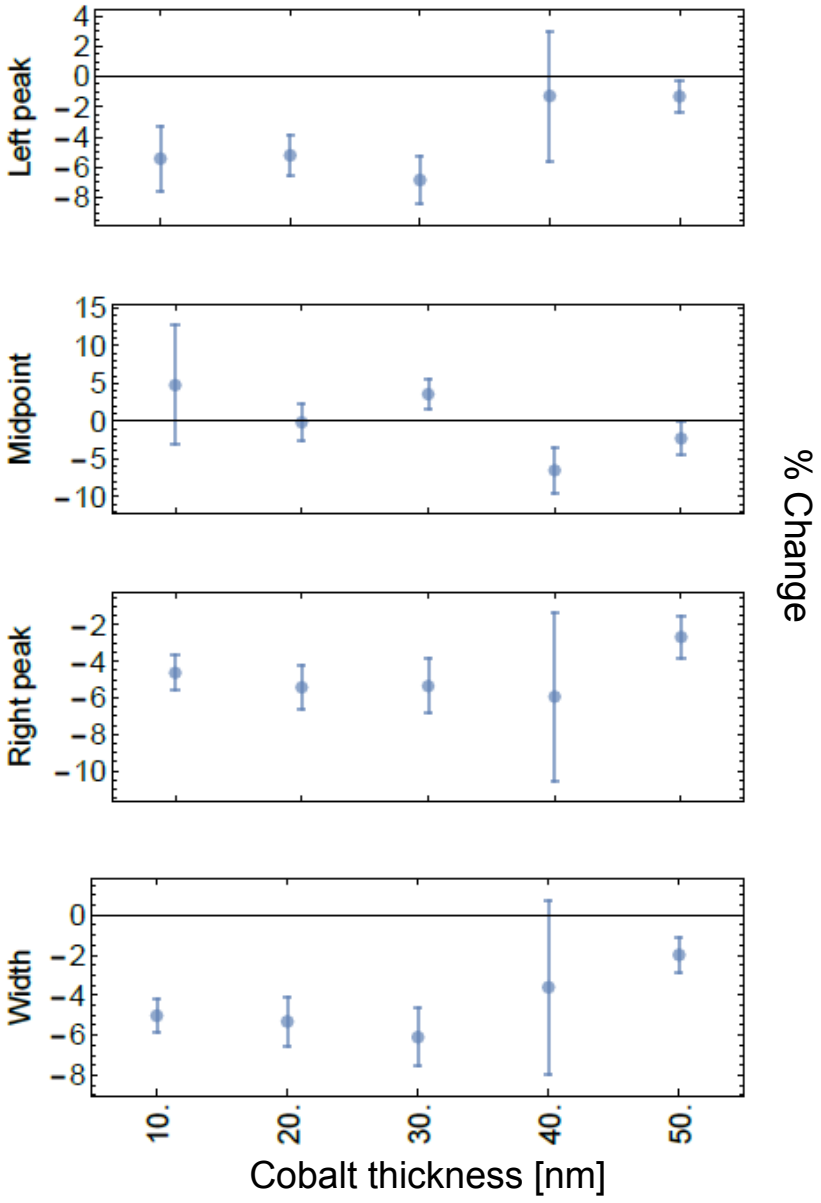


***Figure 5.5: Change in left and right peak, as well as the midpoint and the width between the two peaks for varying cobalt thickness after the application of ethanol on the surface. The error bars indicate the standard deviation of the mean.***

has a very larger reach of 30 nm into the sample, which has never been shown before. But, since it does decreases in strength with increasing thickness of the metal thin film, the cause of the effect must be a surface phenomenon. The data

cannot be explained with a dipole on the surface, because the total energy of interaction should vary approximately like $1/r^2$. The data as shown can be explained by having the effect present, but changing the surface to volume ratio causes a decrease in the change in peak-to-peak width. Due to the fact that wire bonding on thin films with a thickness less than 30 nm is cumbersome and the effect decreases with increasing thickness, all following measurements were performed on 30 nm of the pure metal. Statistical Analysis was performed via ANOVA single factor analysis and a p-value of p=0.809 was determined for the comparison of all data sets. This p-value indicates that, in this simple analysis, there are no significant differences between the data sets. It is possible that more sophisticated analysis will yield more statistical information. However, the lack of theoretical understanding of the effect suggests that determining the correct statistical procedure cannot yet be done. See appendix F for complete tables of pairwise T-tests and groupwise ANOVA p-value results.

#### 5.2.1.2 Variation with Ligand Tail Length

Considering that not only the functional group, often considered the head group, might have an influence, but that the tail of the ligand might also be significant, considering that it can have a significant influence on the electron density in the head group, alcohols with various tail lengths were measured to see the influence of the remaining molecule. Alcohols were chosen for their physical properties. Most of the short alcohols are liquid at room temperature, while the same is not true for other functional groups. Therefore, methanol, ethanol,

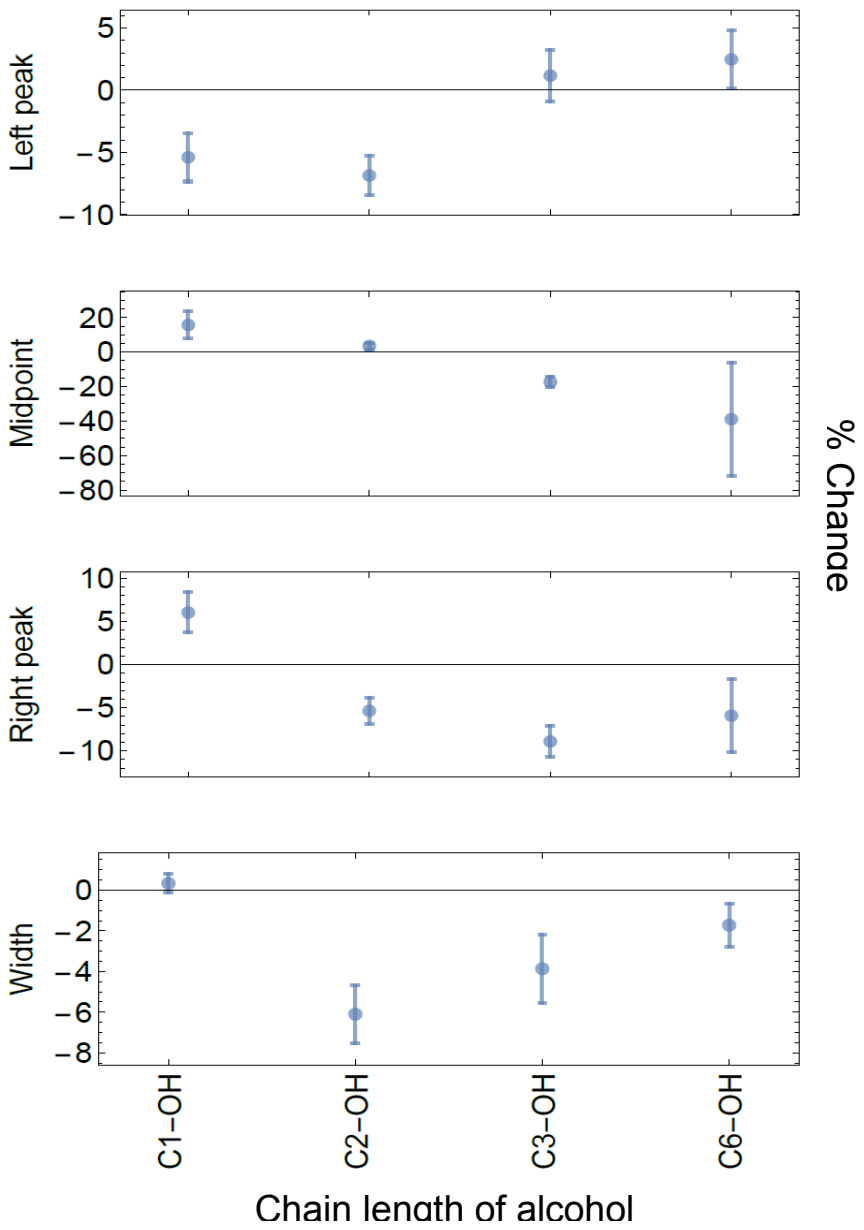


***Figure 5.6: Change in left and right peak, as well as the midpoint and the width between the two peaks for 30 nm cobalt thin films after the application of various alcohols with increasing tail lengths on the surface. The error bars indicate the standard deviation of the mean.***

propanol, and hexanol were applied to the 30 nm cobalt thin film. The midpoint first has a shift to the right and gradually changes to a shift to the left with changes of up to 40%. This is unseen for any of the other measurements. For methanol, the width almost does not change at all, while for ethanol a maximum in width

change is reached, which slowly decreases again with increasing tail length. This suggests that the tail length very clearly does have an effect on the change in magnetization of the thin film. However, for the following measurements it was difficult to stay with the same tail length for all functional groups, since some of the ligands would have been very hazardous, very expensive, or in a gaseous state, which would have prevented a deposition using the piezo crystal. Therefore the tail length was neglected when choosing the ligands and strictly safety and convenience were the deciding criteria. Statistical Analysis was performed via ANOVA single factor analysis and a p-value of p=0.125 was determined for the comparison of all data sets. This p-value indicates that, in this simple analysis, there are no statistically significant differences between the data sets. Again, see appendix F.

In addition, an attempt was made to deposit phenol to see if the presence of a phenyl ring with its high electron density might have an influence on the change in magnetization. However, since the melting point of phenol is higher than the other alcohols, evaporation over the piezo crystal was not possible and therefore it could not be measured.

#### 5.2.1.3 Variation with Ligand Strength

To see if different functional groups influence the size of the change in magnetization, a variety of chemicals were chosen to guarantee a different interaction strength with the metal surface, according to the hard and soft acid and base theory by Ralph G. Pearson [7]. One important criteria for all chemicals was

that they had to be liquids with a viscosity similar to water to be able to evaporate them over the piezo crystal. The chosen chemicals were acetic acid, ethanol, hexylamine, 1-dodecylthiol, acetone, DI water, and hexane. Considering that the HSAB concept is based on the electron density of the functional group, the chosen chemicals can be roughly grouped in the hard group with a high electron density and the soft group with a low electron density in the functional group. The hard group consists of the alcohol (ethanol), the carboxylic acid (acetic acid), and the amine (hexylamine), which is the least hard of the three. The soft group consists of the ketone (acetone) and the thiol (1-dodecylthiol). The DI water would be considered an intermediate between the two groups. Hexane, although classically not mentioned in this concept, has only carbon-carbon bonds and carbon-hydrogen bonds, which have no particularly high electron density and therefore the hexane is proposed very soft. All ligands are the base in this concept since in the trivial chemical view, they donate an electron-pair for the complex bond. The metals can also be classified as hard and soft, again based on the electron density. For this a typical trend in the periodic table can be followed which has an increasing hardness from left to right and from bottom to top. As shown in **Figure 5.7** the different functionalities indeed varied greatly in their influence on the magnetization. Acetic acid has the strongest influence with a change in width of over 6 %, while hexane has basically no influence. The peak shifts and change in width between the two peaks for the different functional groups roughly follow the trend of the HSAB concept for the application on a 30 nm cobalt thin film. This suggests that the previously stated hypothesis of being able to predict the size of

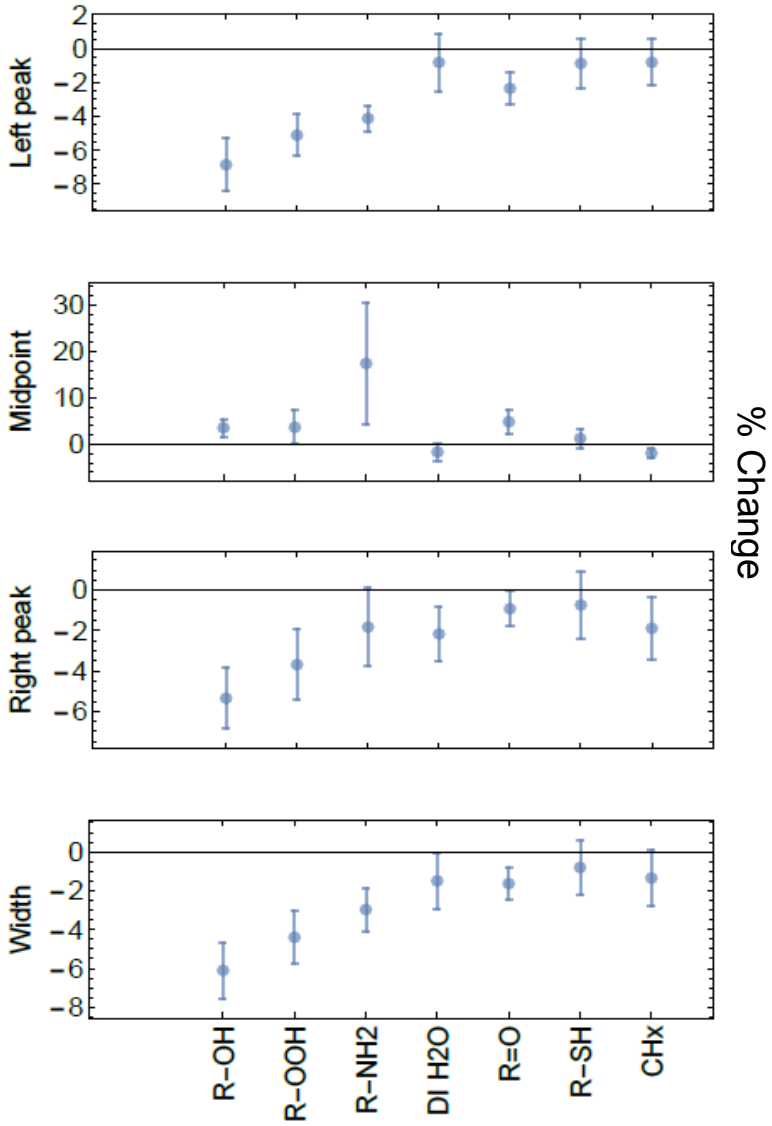


***Figure 5.7: Change in left and right peak, as well as the midpoint and the width between the two peaks for 30 nm cobalt thin films after the application of various ligands with different functional groups on the surface. The error bars indicate the standard deviation of the mean.***

the effect by considering the ligand strength is true and it opens up the more predictable experimental approach. Statistical Analysis was performed via ANOVA single factor analysis and a p-value of p=0.085 was determined for the comparison

of all data sets. This p-value indicates that, in this simple analysis, there are no statistically significant differences between the data sets. Again, see appendix F.

#### 5.2.1.4 Ligand Substitution

Following classic concepts of organometallic chemistry, the question arose, whether a ligand substitution can take place on the surface. This is a very important question due to the fact that any surface modification would already have to be a substitution. During the preparation of the sample a number of chemicals are used to create the photolithography pattern, to lift off the photo resist, and to clean the sample. Any of these chemicals could have already created a metal ligand bond and occupy the surface atoms before the measurements were even performed. Therefore none of the measurements start with an actual clean surface, but all of them are ligand substitutions. To show that more than one replacement is possible, a series of experiments was performed in which the baseline was measured and then a number of ligands were applied one at the time, and the sample was measured between each new application. Various combinations of ligands were chosen. First, DI water was chosen as first ligand, followed by a deposition of ethanol, followed by DI water again. The first DI water deposition pushed the peak by the typical shift of ~1 %. The following ethanol deposition pushed it further to have the typical shift of ethanol of ~4 % (**Figure 5.8**). However, the last deposition of DI water did not change the peak again. Therefore a substitution of ligands is indeed possible, but a weaker ligand cannot displace a ligand with a stronger attraction. In a second set experiments, a

deposition of ethanol was followed by more ethanol. The peak shifted by the common ~ 4 % and remained there, even though more ethanol was deposited. This suggests, that a certain saturation can be reached with the first application of a strong ligand.

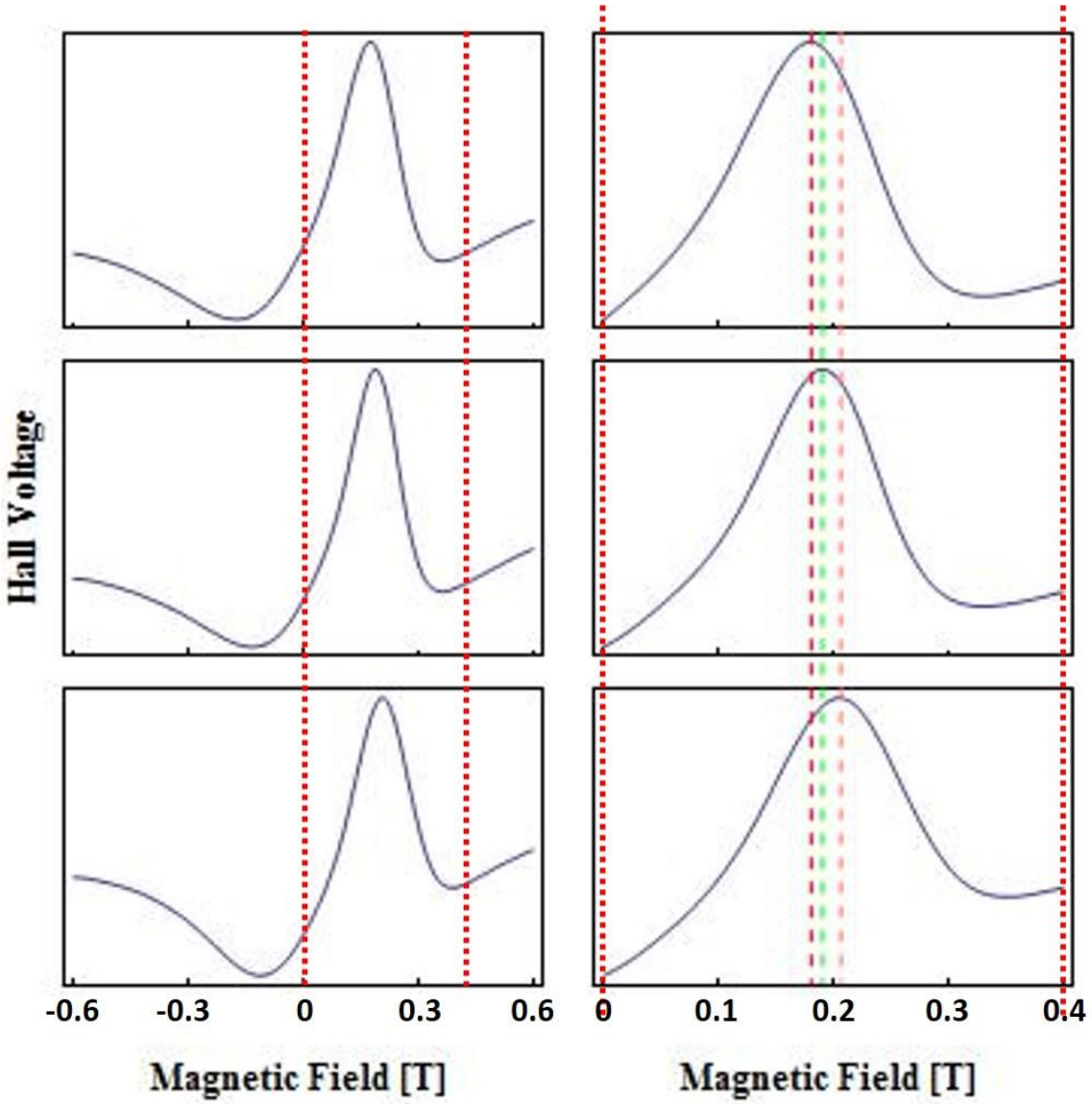


***Figure 5.8: Top: baseline shift of the PHE peak, middle: shift of PHE peak after deposition of DI water, and bottom: shift of PHE peak after additional deposition of ethanol. Ligand substitution allows the shift to be further pushed out.***

**Table 5.2 Periodic Table of the Elements with Magnetic Properties**

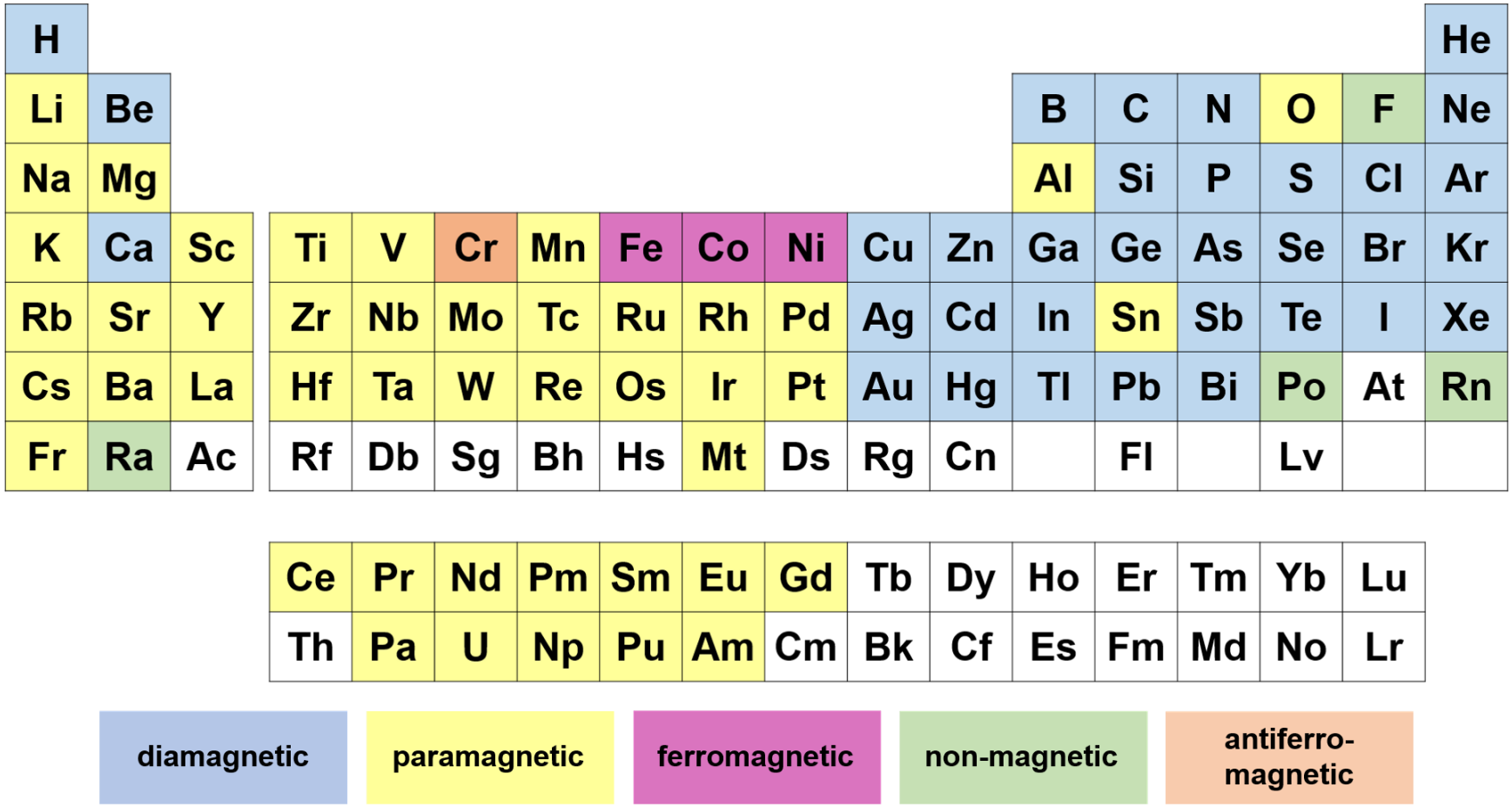

### 5.2.2 Nickel and Permalloy Thin Films

To show that the possibility to manipulate the magnetic properties of cobalt is not a unique occurrence for this element, nickel and Permalloy were also tested. Both also showed great response to the various functional groups and therefore allow the generalization that all ferromagnetic materials can be manipulated in their magnetic properties

#### 5.2.2.1 Nickel

Ferromagnetic metals are an anomaly compared to the other transition metals, as can be seen in **Table 5.2** [8]. Therefore, it was explored if other ferromagnetic metals behave similar to cobalt. However, due to the quick and unpredictable oxidation of iron, this element was neglected and only nickel was used. A 30 nm thin film was measured before and after the application of the chosen series of chemicals with different functionalities. The results were surprising (**Figure 5.9**). The width between the two PHE peaks changed almost twice as much as it did for cobalt. For example, acetic acid showed a change in width of ~11 % on the nickel, while it only showed ~4.5 % for the cobalt sample. In addition, the nice trend of the HSAB concept that could be observed in the cobalt sample was not at all present for nickel. This was a very surprising result and has yet to be explained. This leads to the conclusion, that there are interactions at play that cannot be explained only by the HSAB concept, even though it admirably explains both, the alcohol chain length effect and the results for bare cobalt with various ligands, as well as others discussed below. Statistical Analysis was performed via ANOVA

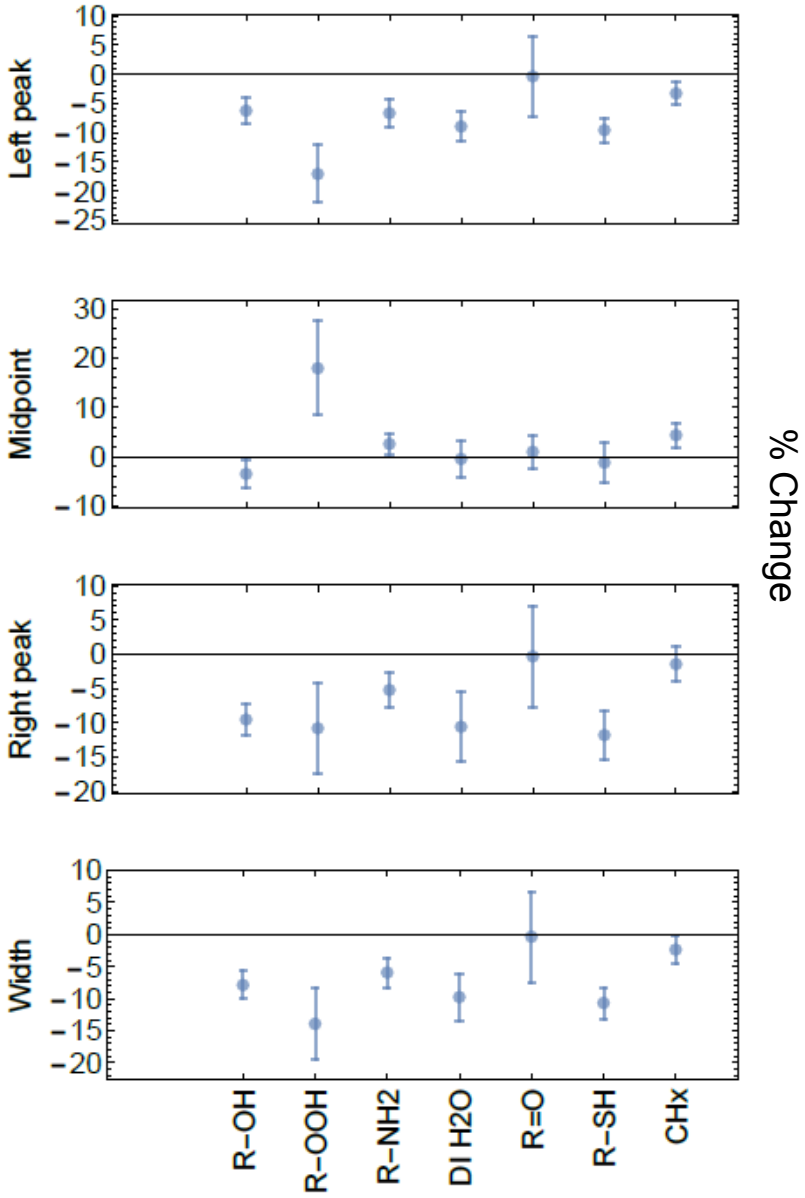


***Figure 5.9: Change in left and right peak, as well as the midpoint and the width between the two peaks for 30 nm nickel thin films after the application of various ligands with different functional groups on the surface. The error bars indicate the standard deviation of the mean.***

single factor analysis and a p-value of p=0.002 was determined for the comparison of all data sets. This p-value indicates that, in this simple analysis, there are no statistically significant differences between the data sets. Again, see appendix F.

5.2.2.2 Permalloy

Wanting another comparison to test for magnetic changes in ferromagnetic materials, Permalloy ($Ni_{0.8}Fe_{0.2}$), a common alloy, which is mainly used for magnetic shielding [9] in various magnetic applications such a hard drives was chosen. Although it has a 20 % iron content, it has a much slower oxidation rate and is therefore much preferred over iron for these experiments, as irons quick and unpredictable oxidation would make it impossible to measure. Looking at **Figure 5.10**, results similar to the ones observed for bare cobalt can been seen. The results vary greatly from the nickel results and the HSAB concept can be employed again to predict the outcome of the ligand deposition on the surface of the Permalloy. Considering the standard deviation, the midpoints of all samples are roughly along one line, with the exception of the hexylamine. While all other ligands have a positive shift in midpoint, the hexylamine has a negative shift. However, looking at the change in width between the two PHE peaks, it now is the 1-dodecylthiol that diverges from the trend, rather than the hexylamine. For now, it cannot be explained why the two exceptions occur for two different ligands.

Overall these measurements lead to the conclusion that the magnetization in ferromagnetic materials can be manipulated by surface modifications. The magnitude of the change is strictly dependent on the metal-ligand interaction and although it roughly follows the trend of the HSAB concept, this cannot be used as an ultimate reliable guide to predict results as the surface chemistry taking place seems to be more complex and needs more investigation. Statistical Analysis was performed via ANOVA single factor analysis and a p-value of p=0.235 was

determined for the comparison of all data sets. This p-value indicates that, in this simple analysis, there are no statistically significant differences between the data sets. Again, see appendix F.

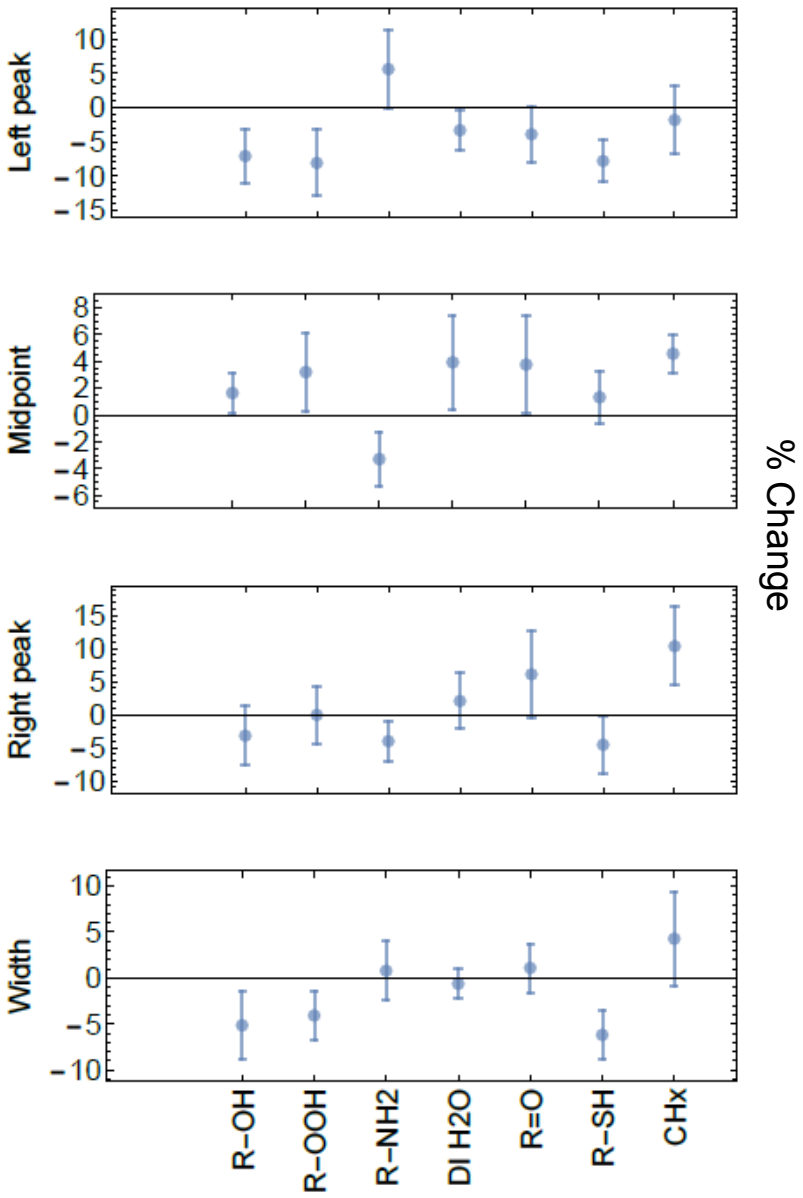


***Figure 5.10: Change in left and right peak, as well as the midpoint and the width between the two peaks for 30 nm Permalloy thin films after the application of various ligands with different functional groups on the surface. The error bars indicate the standard deviation of the mean.***

## 5.3 Ferromagnetic/Diamagnetic Bilayers

Having shown that the magnetization of ferromagnetic thin films can be manipulated by modifying the surface, it was then investigated if it is also possible to manipulate the magnetic properties of diamagnetic elements. Still wanting to use the same method of measurement, bilayers consisting of 30 nm cobalt, topped by the diamagnetic metal were used. This way, if the diamagnetic layer induces a magnetization of its own, this magnetization will influence the overall magnetization of the sample and therefore the position of the PHE. This allows one to use the ferromagnetic thin film as a sensor, as previously shown by Knaus *et al* [1]. For the following experiments I chose the $d^9$ elements copper, silver, and gold. All of them are diamagnetic, even though they have an odd number of electrons.

### 5.3.1 Cobalt/Gold

Gold thin films do not deposit as a uniform layer in our deposition system until a thickness of 30 nm is reached and therefore it must be assumed that some of the cobalt is exposed through pin holes and could cause the shifts recorded for the cobalt/gold bilayers. To see if the shift is caused by the interaction of the exposed cobalt with the ligand or if the gold itself really develops a magnetic moment, it was important to measure various thicknesses of gold on top of the cobalt thin film. Keeping the cobalt thickness steady at 30 nm for all samples, the gold thickness was varied from 0 nm to 50 nm. Due to the high response with the 1-dodeacylthiol on the gold, this chemical was chosen as one of the ligands for the surface modification. Ethanol was chosen as a second ligand since a number of

previous publications applied a thiol to the gold surface using a 1 mM solution of the thiol in ethanol [1, 3]. If ethanol indeed causes a peak shift as well, that could give rise to doubts about the published data, since it cannot be clearly determined which chemical caused the change in magnetic properties.

#### 5.3.1.1 Reach of PHE through Gold on Cobalt using Ethanol

The deposition system does not deposit a homogeneous gold layer until a film thickness of 30 nm is reached. A number of samples were prepared that consisted of 30 nm cobalt as a first layer, which functions as the sensor, topped by different thicknesses of gold. The gold varied from 0 nm to 50 nm in thickness. For gold films thicker than 50 nm the signal-to-noise ratio of the perpendicular voltage was so low that the peak location could not be accurately determined anymore. A reasonable explanation for this is the decrease in sample resistance as more highly conductive gold, copper, or silver, respectively, was added as a parallel conduction path to the cobalt. This in combination with the increasing distance of the treated surface on top of the gold layer to the cobalt sensor layer resulted in a smaller field at the sensor and a corresponding smaller signal.

It is important to understand, that the cobalt layer is still the sensor, even though now there is multiple nm of gold on top, which removes any potential induced magnetic moment from the actual sensor. Because the ligands affect the gold, which is tens of nm away from the cobalt sensor material, the actual change in net magnetic field is larger than the raw measurements suggest. Even though the hysteresis curve shrank by the same 2-3 % seen with bare cobalt, the effect

on the gold must be larger since the sensor is now making a remote measurement and so its sensitivity has decreased.

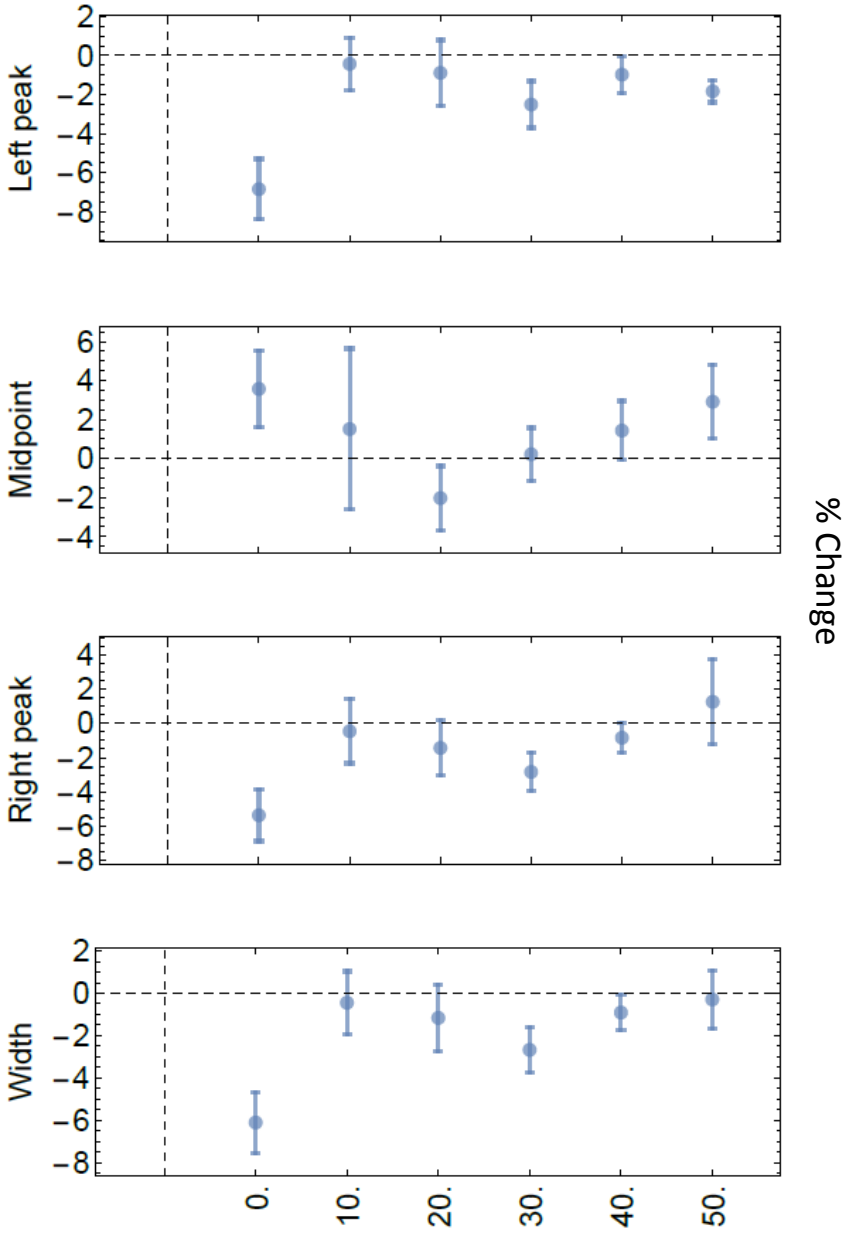


***Figure 5.11: Change in left and right peak, as well as the midpoint and the width between the two peaks for 30 nm cobalt, topped by varying thicknesses of gold in nm, after the application of ethanol on the surface. The error bars indicate the standard deviation of the mean.***

**Figure 5.11** shows the changes in left and right peak, as well as the midpoint and width change for the various thicknesses of gold after the application of ethanol. Following the common hard and soft acids and bases concept (HSAB), it was expected that the ethanol would be more drawn to the cobalt than the gold and therefore the change in width between the two peaks would decrease with increasing gold thickness. However, against the expectation, the change in width showed a maximum for a 30 nm gold thin film on top of 30 nm of cobalt. This indicates a strong interaction between the gold and the ethanol that even surpasses the interaction of the ethanol with the cobalt. The fact that the change in width decreases for 40 nm and 50 nm is likely due to the fact the induced magnetization is getting further removed from the sensor and cannot be detected anymore. This results supports the suggestion that the effect has a very deep reach though the sample. Statistical Analysis was performed via ANOVA single factor analysis and a p-value of p=0.010 was determined for the comparison of all data sets. This p-value indicates that, in this simple analysis, there are no statistically significant differences between the data sets. Again, see appendix F.

#### 5.3.1.2 Reach of PHE through Gold on Cobalt using 1-Dodecylthiol

Since 1-dodecylthiol on gold was the most used ligand in literature [1-3] and it was claimed to be special and required to invoke the effect, the same experiments as previously described for ethanol were performed with the 1-

dodecylthiol to see if there is an influence on the gold from the 1-dodecanethiol. The gold thickness of the samples varied from 0 nm to 50 nm.

Again following the HSAB concept, a better interaction with the gold was expected since thiols are soft bases and gold is a soft acid, according to Pearson [8]. Although there could be a strong metal-organic bond without an induction of magnetism in the gold this interaction would be invisible for the MaRMS measurement and it would be impossible to make a statement about it in this thesis. **Figure 5.12** shows the changes in left and right peak, as well as the midpoint and width change for the various thicknesses of gold after the application of 1-dodecylthiol. The change in width for the 10 nm gold thin film on top of the cobalt is larger than the previously discussed change in width for ethanol. In a similar fashion to the ethanol, the 1-dodecylthiol also increases in width change and peaks at 30 nm of gold on top of the cobalt. Just like before, the fact that the change in width decreases for 40 nm and 50 nm is likely due to the fact the induced magnetization is getting further removed from the sensor and cannot be detected anymore. However, it is important to point out that the change in width for 1-dodecyl thiol is about 50 % more with ~3.8 % than for the ethanol with ~2.6 %. Again considering that the surface modification is removed from the sensor with increasing thickness of the gold, these number are actually higher than what the sensor experiences. Therefore, gold indeed does develop a significant change in magnetization when interacting with a ligand on the surface. It must be pointed out that the positive width change for 50 nm gold was unexpected and cannot be explained at this point in time. Statistical Analysis was performed via ANOVA

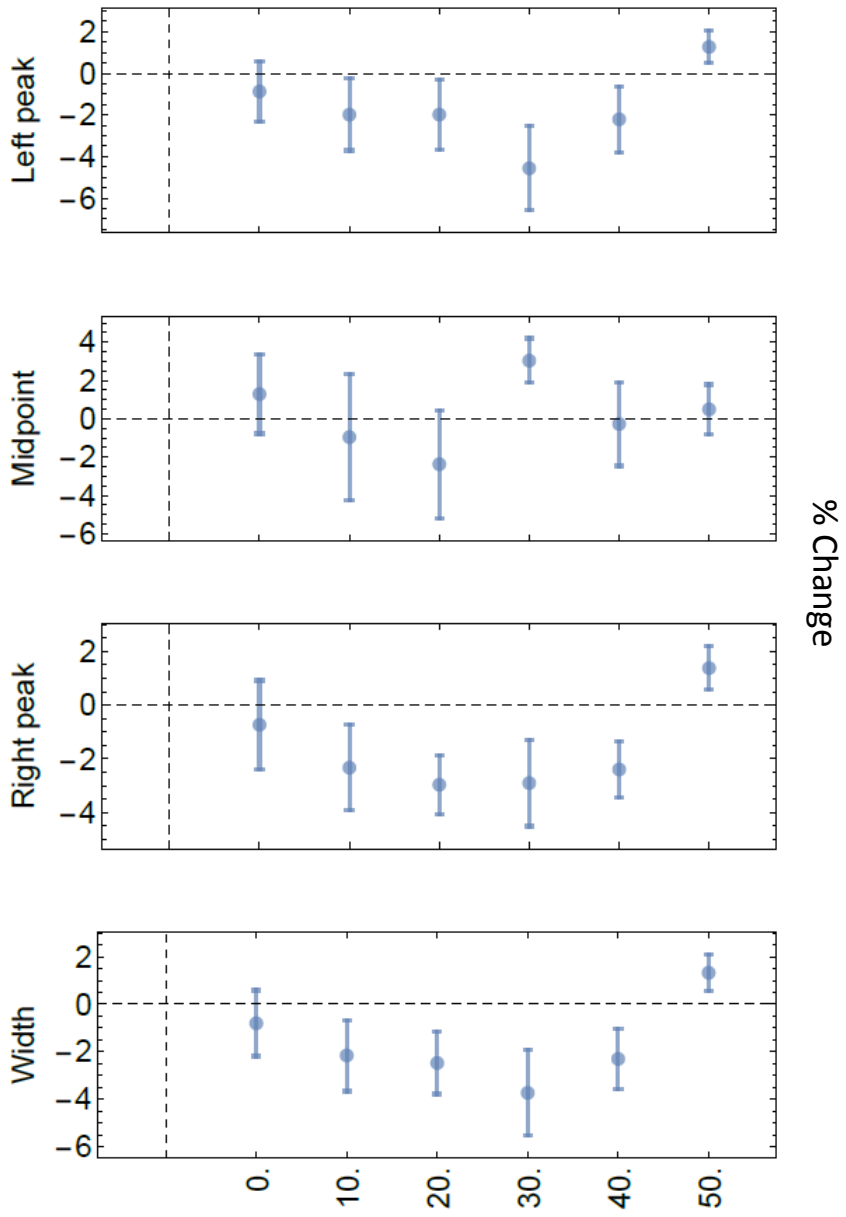


***Figure 5.12: Change in left and right peak, as well as the midpoint and the width between the two peaks for 30 nm cobalt, topped by varying thicknesses of gold, after the application of 1-dodecylthiol on the surface. The error bars indicate the standard deviation of the mean.***

single factor analysis and a p-value of p=0.131 was determined for the comparison of all data sets. This p-value indicates that, in this simple analysis, there are no statistically significant differences between the data sets. Again, see appendix F.

### 5.3.1.3 Thiols on Gold are Different: 1-Dodecylthiol vs. Ethanol

Since separate graphs of ethanol and 1-dodecanethiol with the different gold thicknesses are rather hard to compare, the data was plotted in a 2D graph. In **Figure 5.13** one can see the percent change caused by the ethanol on the x-axes and the percent change caused by the 1-dodecylthiol on the y-axes. The dashed line shows a 1:1 response, which would mean equal responses of both substances

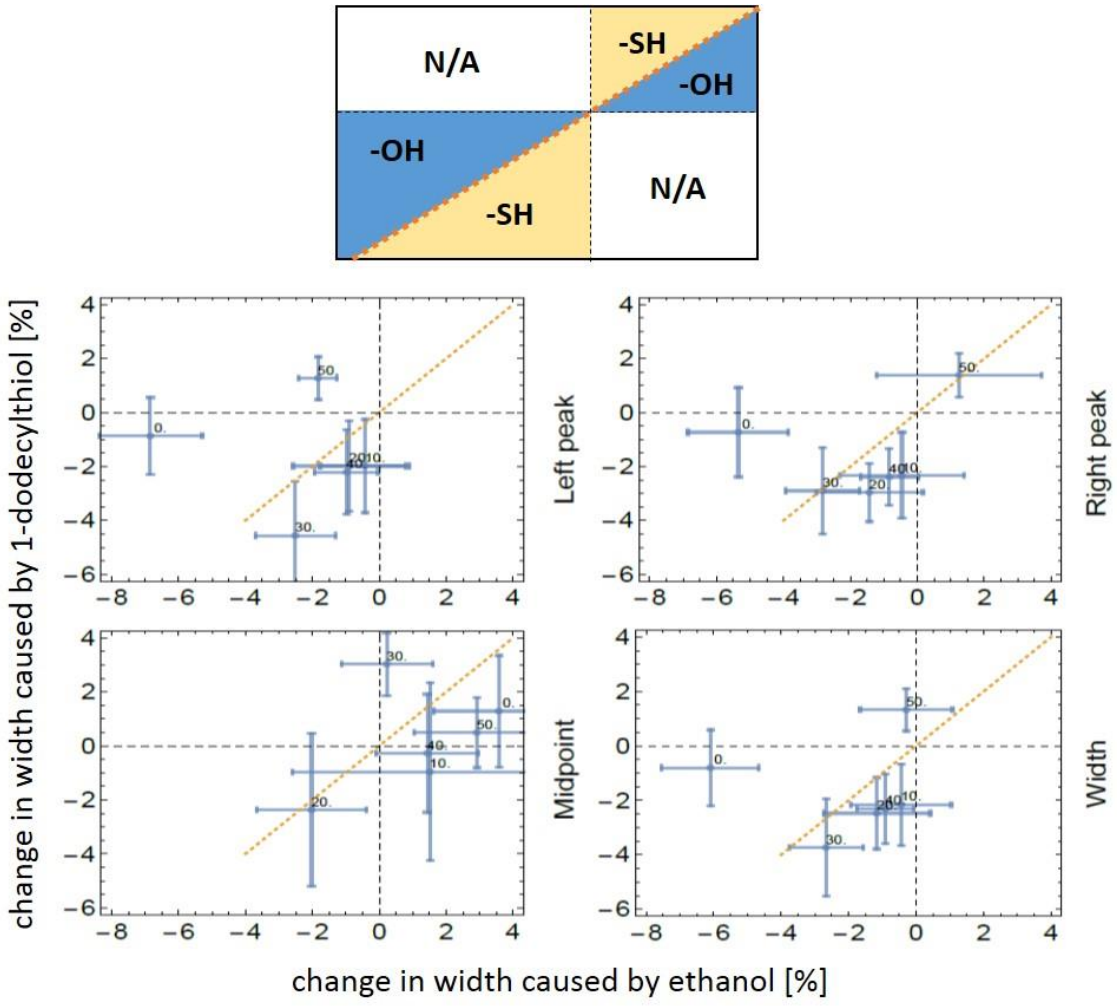


***Figure 5.13: Top: schematic drawing showing which functional group caused the larger percent change after the application. Middle and bottom: 1:1 plot of percent change after the application of ethanol (x-axis) and 1-dodecylthiol (y-axis) with the dotted line indicating an equal response to these ligands.***

to the metals. As can be seen in the scheme on the top of **Figure 5.13**, if the data point falls into the yellow area, the application of 1-dodecylthiol causes a higher percent change, while the blue area marks a bigger percent change with the application of ethanol. The white field marks the area that has an unexplained response, which is marked with N/A (not applicable). Those quadrants would represent a magnetic hardening with one ligand, but a magnetic softening with the other ligand. The change in position of the right peak, the left peak, and the change in width are clearly indicating that the 1-dodecylthiol causes a larger percent change for all thicknesses but 50 nm of gold on cobalt. A reasonable explanation is that the surface is so far removed from the actual cobalt thin layer, which functions as the sensor, that the change in magnetization cannot be detected anymore.

This confirms the previous results reported in literature that thiols induce magnetic moments in gold and changes in the strength of the magnetic moment.

#### 5.3.1.3 Various Solvents on Cobalt/Gold bilayer

Just like on the ferromagnetic metals before, it was important to find out if gold also shows any effect with other ligands than thiol. Therefore, the series of solvents previously chosen was applied to the cobalt/gold bilayer. A new set of samples was evaporated and prepared.

It was expected that thiol would stand out significantly compared to the other ligand systems. However, looking at the change in width between the two peaks as shown in **Figure 5.14**, it looks as if the carboxylic acid as well as the amine

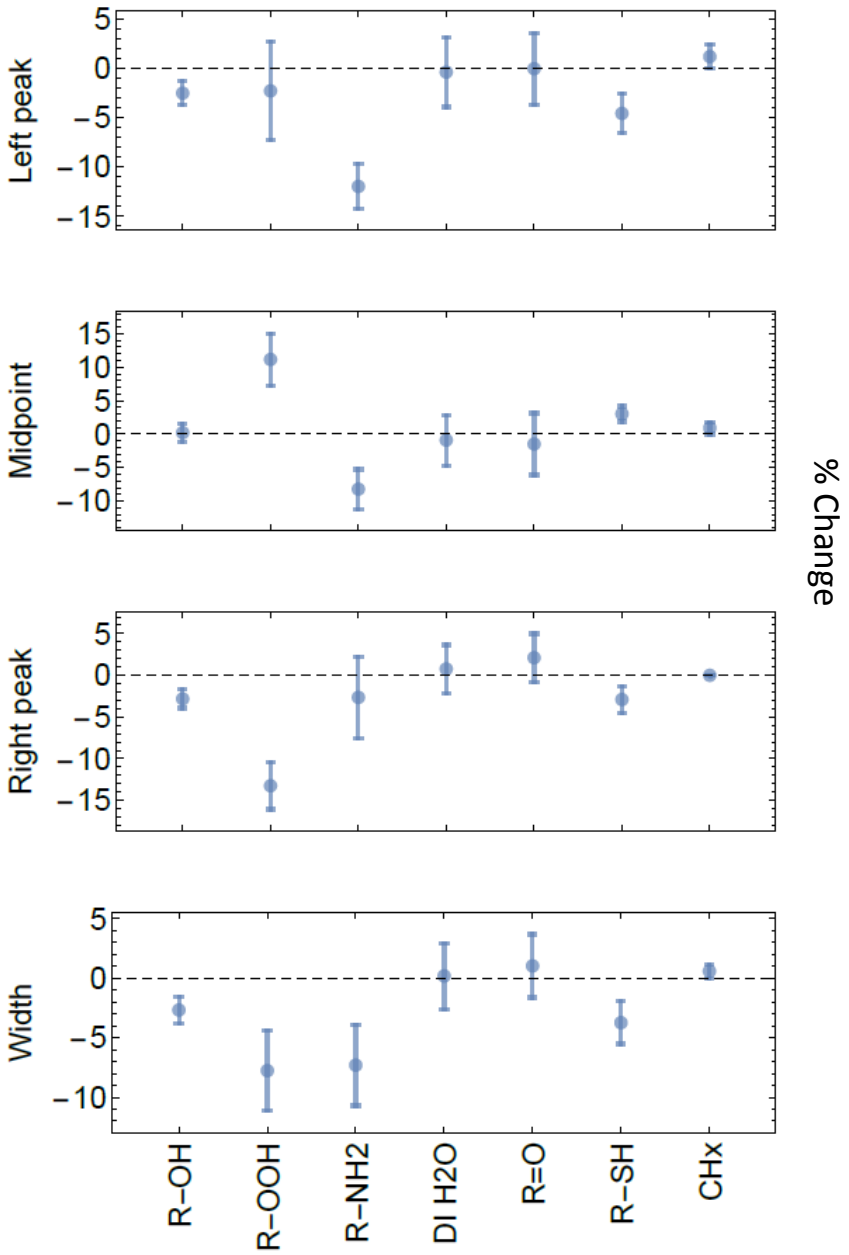


***Figure 5.14: Change in left and right peak, as well as the midpoint and the width between the two peaks for 30 nm cobalt, topped by 30 nm of gold, after the application of various ligands on the surface. The error bars indicate the standard deviation of the mean.***

have equal, if not larger, effects as the thiol. Although not expected, this finding goes along with the results from the ferromagnetic layers, in which these two functional groups also had a large effect on the PHE peak. Statistical Analysis was

performed via ANOVA single factor analysis and a p-value of p=0.048 was determined for the comparison of all data sets. This p-value indicates that there are significant differences between the data sets. More information can be found in Appendix F.

### 5.3.2 Cobalt/Silver and Cobalt/Copper

Just as before, bilayers with 30 nm cobalt and varying thicknesses of the diamagnetic metal were used to measure the PHE. However, for copper and silver it was impossible to find a peak for thicknesses other than 10 nm. For larger thicknesses of silver and copper the peak could not be clearly identified since the signal-to-noise ratio was very poor. Therefore bilayers of 30 nm cobalt and 10 nm of the diamagnetic metal were used. Just as with the ferromagnetic metals, the chosen series of ligands were applied and the shift for the PHE peak was measured.

It was found that the graph shapes for the cobalt/copper and cobalt/silver bilayers are different than for the cobalt/gold bilayer or for any of the ferromagnetic thin films, which are equal in shape to the cobalt/gold thin films (**Figure 5.15**). While the angle dependence of the PHE has a significant influence on the graph shape, they still always follow roughly the same shape. For this particular range of the applied magnetic field, it was always possible to see the slope from the combination of regular Hall effect and AHE, and sticking out from that was the peak for the PHE. For the cobalt/copper and cobalt/silver bilayers, the slope from the

regular Hall effect and AHE disappear and a single peak with a very broad base remains. In addition, the signal-to-noise ratio worsens for these bilayers.

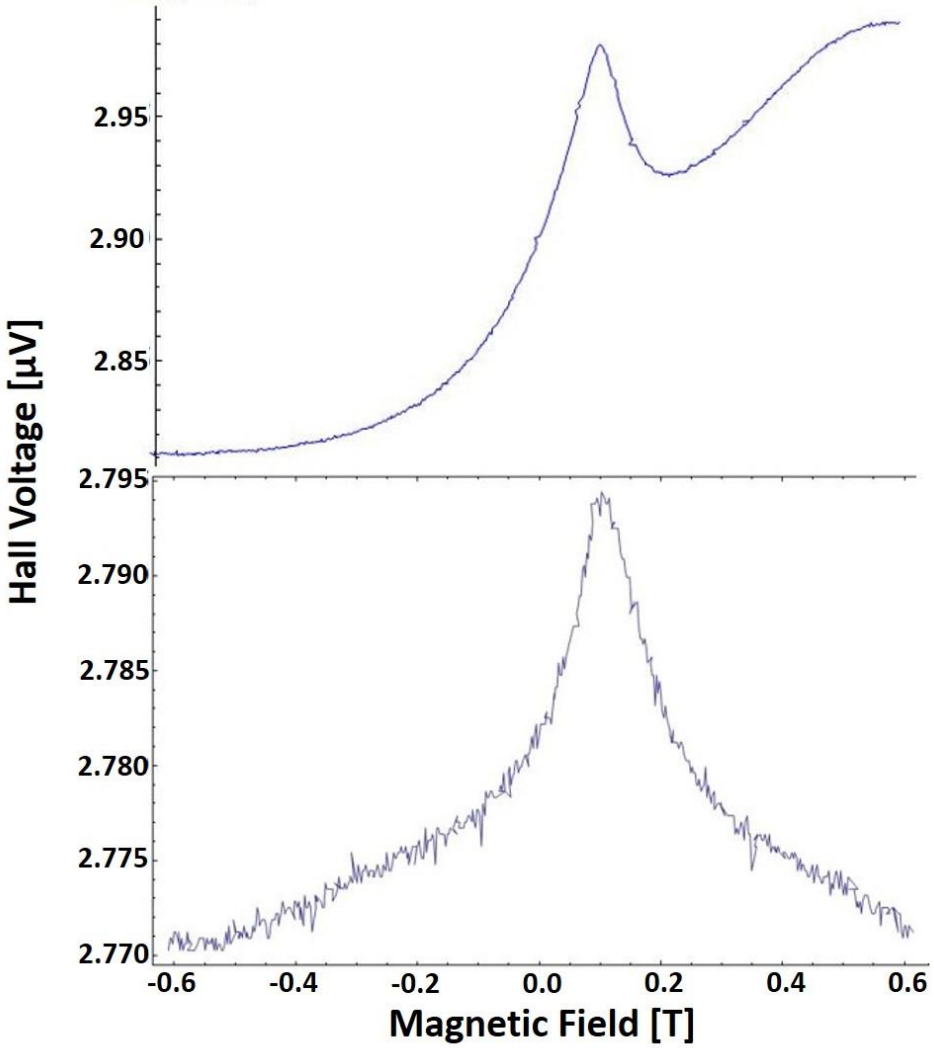


***Figure 5.15: Top: typical graph of the cobalt/gold bilayer, including the positive slope caused by the regular Hall effect and the anomalous Hall effect; bottom: typical graph shape of cobalt/copper and cobalt/silver bilayers, respectively. The slope the regular Hall effect and the anomalous Hall effect seems to have vanished completely.***

For the cobalt/silver thin films the percent changes are significantly lower than for ferromagnetic thin films or the cobalt/gold thin films, yet a slight trend can be seen. The percent change transforms from a negative percent change to a

positive percent change going from strongest to weakest ligand, as can be seen in **Figure 5.16**.

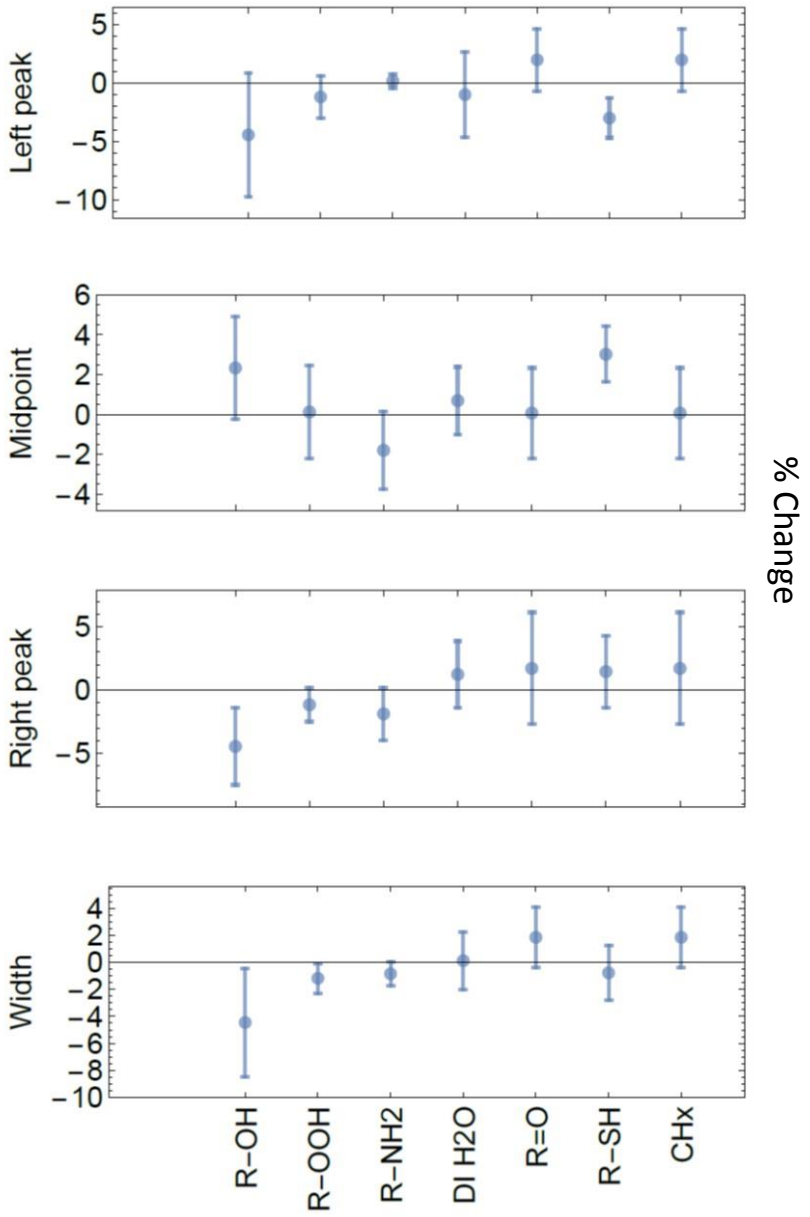


***Figure 5.16: Change in left and right peak, as well as the midpoint and the width between the two peaks for 30 nm cobalt, topped by 10 nm of silver, after the application of ligands with various functional groups on the surface. The error bars indicate the standard deviation of the mean.***

The cobalt/copper thin films show even less of a percent change after the application of the various functional groups, as can be seen in **Figure 5.17**. Considering the standard deviation for the percent change in width between the two peaks, it is basically zero for every applied ligand.

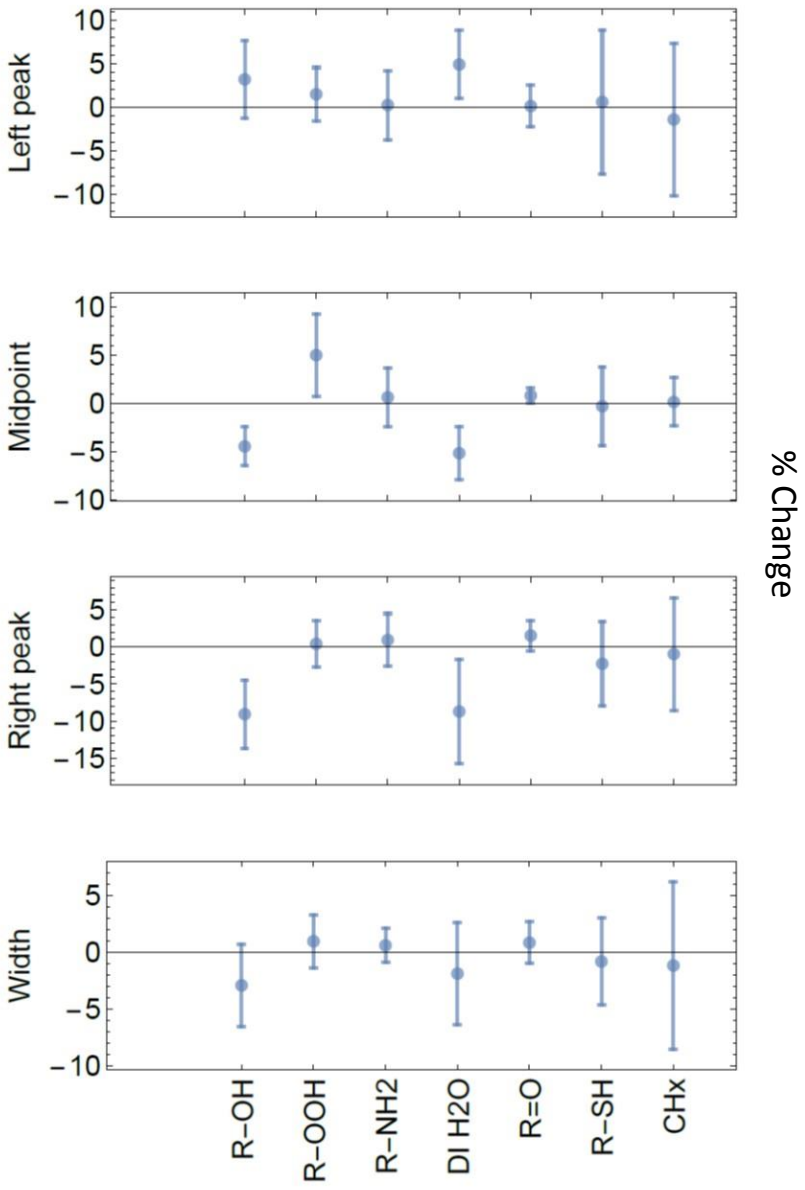


***Figure 5.17: Change in left and right peak, as well as the midpoint and the width between the two peaks for 30 nm cobalt, topped by 10 nm of copper, after the application of ligands with various functional groups on the surface. The error bars indicate the standard deviation of the mean.***

Although the resistivity measurements confirm that there are holes present in the diamagnetic top layer, there should at least be a change in magnetization similar to that of pure cobalt. Therefore the question remains, why silver and copper show such a muted response to the surface modifications. Statistical Analysis was performed via ANOVA single factor analysis and p-values of p=0.540 for the cobalt and silver bilayer and p=0.984 for the cobalt and copper bilayer were determined for the comparison of all data sets. These p-values indi that, in this simple analysis, there are no statistically significant differences be en the data sets. Again, see appendix F.

## 5.4 Future work

This field of study still offers a wide variety of paths to take, especially since there is still controversy about the source of this phenomenon. Looking at future work directly building up on these experiments, a natural question is whether the observed behavior is increased by having an organized crystal structure in the metal thin films. So far the metal patterns used had no particular crystal structure and mostly rough surfaces. Using an organized structure might lead to conclusions similar to Adeagbo *et al.* [10, 11]. For this it would be necessary to design a new deposition system that can guarantee an organized crystal growth when creating the thin films. This system must also be able to introduce an easy axis into the samples so that the PHE can still be measured.

Considering that the magnetism of materials is highly temperature dependent, creating an instrument set up that permits temperature control over a

wide range would also be a possible route for the future. It would be interesting to see, if the surface modification can influence the Curie temperature of the metal thin film. Since iron, nickel, and cobalt have rather high Curie temperatures, gadolinium would be a great choice of metal for this experiment. With a Curie temperature at 18 °C, at which the metal switches from ferromagnetic to paramagnetic properties, this metal would be perfectly suited for this experiment.

Although the deposition of the ligand was improved by using a piezo crystal to evaporate the ligand liquids, no emphasis was put in the creation of a self-assembled monolayer (SAM). However, having an organized monolayer of the ligand system on the surface might improve the responses of the various metals and decrease the standard deviation of the measurements. Even with the methods used up to this point, it was possible to distinguish between different functional groups. Therefore, an organized SAM as a ligand system, in combination with a perfect crystal structure of the thin film, might equip this system to become a highly sensitive sensor, which can find applications in a wide range of settings, reaching from electronics to medical purposes.

Although a large number of functional groups was employed for the presented measurements, there is still room for improvement in order to better compare the different systems. The ligands used in this work were chosen due to their safety, price, and availability. However, in this work it was clearly shown that the tail of the ligand has a significant influence. This fact was, so far, neglected. Using an enclosed system it would make it possible to apply ligand systems that

are gaseous at room temperature or even some that would pose as a safety risk in the open environment in which MaRMS runs at this point.

Another interesting route to take would be the application of magnetic polymers to the surface. Although it was shown that a metal-organic bond is necessary to have an impact on the magnetic properties of the thin film, a magnetic polymer would open up the possibility to introduce a material that can create such a bond on one hand, but also has its own magnetization on the other hand.

Since ferromagnetic and diamagnetic samples have been explored in this work, it would be interesting to expand the elements for the thin films to paramagnetic materials. So far six out of roughly seventy feasible elements have been explored. This would offer a great opportunity to really show whether or not the HSAB concept can be used as a guideline for this type of measurement.

At this point, using MaRMS can only deliver comparative measurements because no definite value for the magnetic moment can be determined. Therefore it is mandatory to get a better understanding physically of the sensor and what causes the peak shifts. Chemically it is necessary to understand the organometallic interaction. It must be determined if the HSAB concept is adequate to use here or if a more in depth theory must be developed. Overall this work is the foundation for a broader field of study.

## 5.5 REFERENCES


1. Knaus, B.; Garzon, S.; Crawford, T.M. Alkenethiol induced changes in the magnetotransport properties of Co/Au bilayers. *J. Appl. Phys.* **2009**, *105*, 07A903

2. Carmeli, I.; Leitus, G.; Naaman, R.; Reich, S.; Vager, Z. Magnetism induced by the organization of self-assembled monolayers. *J. Chem. Phys.* **2003**, *118 (23),* 10372-10375

3. Crespo, P.; Litran, R.; Rojas, T.C.; Multigner, M.; de la Fuente, J.M.; Sanchez-Lopez, J.C.; Garcia, M.A.; Hernando, A.; Penades, S.; Fernandez, A. Permanent magnetism, magnetic anisotropy, and hysteresis of thiol-capped gold nanoparticles. *Phys. Rev. Lett.* **2004**, *93 (8)*, 087204

4. Yamamoto, Y.; Miura, T.; Suzuki, M.; Nawamura, N.; Miyagawa, H.; Nakamura, T.; Kobayashi, K.; Teranishi, T.; Hori, H. Direct observation of ferromagnetic spin polarization in gold nanoparticles. *Phys. Rev. Lett.* **2004**, *93 (11)*, 116801

5. Hernando, A.; Crespo, P.; Garcia, M.A.; Fernandez Pinel, E.; de la Venta, J.; Fernandez, A.; Penades, S. Giant magnetic anisotropy at the nanoscale: Overcoming the superparamagnetic limit. *Phys. Rev. B* **2006** *74*, 052403

6. Verbal communication: Dr. Scott Crittenden

7. Pearson, R. G. Hard and Soft Acids and Bases. *J. Am. Chem. Soc.* **1963**, *85 (22)*, 3533

8. Lide, D. R., ed. *CRC Handbook of Chemistry and Physics, 85th Edition*, CRC Press, Boca Raton, 2004

9. Tumanski, S. The application of Permalloy magnetoresistive sensors for nondestructive testing of electrical steel sheets. *J. Magn. Magn. Mater.* **1988**, *75*, 266

10. Adeagbo, W.A.; Fischer, G.; Ernst, A.; Hergert, W. Magnetic effects of defect pair formation in ZnO. *J. Phys.: Condens. Matter.* **2010**, *22*, 436002

11. Adeagbo, W.A.; Fischer, G.; Hergert, W. First-principle investigation of electronic and magnetic properties of $SrTiO_3$ (001) surfaces with adsorbed ethanol and acetone molecules. *Phys. Rev. B*, **2011**, *83*, 195428

# CHAPTER 6

## SUMMARY AND CONCLUSION

In this dissertation it was shown that the magnetic properties of various metal thin films, both ferromagnetic and diamagnetic, can be manipulated by surface modification via organic ligand. Against common belief, any functional group can cause such a manipulation and not just a particular one such as thiol on gold. However, different ligands have different strengths of influence on the magnetic properties of the thin films and the abilities roughly correlate with the HSAB concept.

Since organometallic bonds are classically based on an interaction of an electron pair from the ligand with the empty orbitals of the metal, and therefore influence the metal's electromagnetic structure, the observed results were in the range of expectations. However, this effect reaches much further than initially expected. In particular, the magnetization of ferromagnetic materials can be manipulated by a variety of surface modifications. In this work, the possibility of manipulation of the magnetization was proven for cobalt, nickel, and Permalloy on a large number of samples, employing the PHE. To understand the reach of the ligand modification, measurements were performed on cobalt thin films with

increasing thickness. These measurements showed that the change in magnetization is much larger than previously expected and had a reach of roughly 30 nm.

While the head functional group involved in the organometallic bond has a very strong influence on the magnitude of the effect, as was shown with a large variety of ligands, the tail group of the ligand also has a significant influence on the manipulation of the magnetic properties of the metal thin film. This was shown by using alcohols with different alkyl chain lengths as ligands on a 30 nm cobalt thin film.

In addition to demonstrating the manipulation of the ferromagnetic thin films, they were also used as sensors to measure the changes in magnetic properties of diamagnetic thin films. While the induction of paramagnetism or even ferromagnetism in otherwise diamagnetic gold has caused excitement in past publications, the problem of contamination in the gold samples did not permit a conclusive answer. The MaRMS system provided the ability to show proof for a change in the magnetic properties of gold. Although it is not possible with this system to distinguish whether gold develops para- or ferromagnetism, it is possible to say without a doubt that it reacts magnetically to the application of a thiol ligand system. Also it must be noted, that the development of a magnetization in gold is not exclusive for the thiol. Other ligands, such as ethanol, also showed a significant peak shift when applied to the cobalt/gold bilayer. In addition, the data presented in this thesis is not consistent with a remarkably larger effect of thiol compared to other ligands on gold or any other tested metal. However, the

presented data shows that thiol does have the largest effect on gold of all molecules investigated, although it has only a moderate effect on other metals, such as cobalt and nickel.

The novel set-up MaRMS was used to detect the changes in planar Hall voltage under standard room conditions. It allowed the modification of the sample surface via solvent application without having to move the sample. A custom sample holder allowed for angle adjustment in the x- and y-directions as little as 0.5 mrad, which can correct an awry sample placement. The inclusion of a piezo crystal to vaporize the desired liquids and creating an airflow to guide the vapors over the sample simplified their application. Although operating with a significantly smaller magnetic field than the commercially available PPMS, MaRMS is compact and eliminates the need for expensive cryogenics. By employing the PHE, the presence of possible paramagnetic contaminations is eliminated.

These selected examples of magnetization manipulation, together with the newly developed instrumentation and optimization, provide the basis for a promising field with applications in sensing and electronics.

# BIBLIOGRAPHY

Abraham, D.W.; Frank, M.M.; Guha, S. Absence of Magentism in Hafnium Oxide Films. *Appl. Phys. Lett.* **2005**, *87*, 252502

Adeagbo, W.A.; Fischer, G.; Ernst, A.; Hergert, W. Magnetic effects of defect pair formation in ZnO. *J. Phys.: Condens. Matter.* **2010**, *22*, 436002

Adeagbo, W.A.; Fischer, G.; Hergert, W. First-principle investigation of electronic and magnetic properties of $SrTiO_3$ (001) surfaces with adsorbed ethanol and acetone molecules. *Phys. Rev. B*, **2011**, *83*, 195428

Anderson, P.W.; Rowell, J.M. Probable observation of the Josephson superconducting tunneling effect. *Phys. Rev. Lett.* **1963**, *10 (6)*, 230-231

BACH beamline of ELETTRA Trieste specifications http://www.elettra.trieste.it

Berger, R.; Delamarche, E.; Lang, H.; Gerber, C.; Gimzewski, J.; Meyer, E.; Guentherodt, H. Surface stress in the self-assembly of alkanethiols on gold. *Science*, **1997**, *276*, 2021

Bianconi, A. Surface X-ray absorption spectroscopy: Surface EXAFS and surface XANES. *Appl. Surf. Sci.* **1980**, *6 (3)*, 392-418

Bigelow, W.C.; Pickett, D.L.; Zisman, W.A. Oleophobic monolayers: Films adsorbed from solution in non-polar liquids. *J. Colloid. Sci.* **1946**, *1 (6)*, 513-538

Blodgett, K.B. Monomolecular films of fatty acids on glass. *J. Am. Chem. Soc.* **1934**, *56*, 495

Blundell, S. *Magnetism in Condensed Matter,* Oxford University Press, Oxford, 2001

Carmeli, I.; Leitus, G.; Naaman, R.; Reich, S.; Vager, Z. Magnetism induced by the organization of self-assembled monolayers. *J. Chem. Phys.* **2003**, *118 (23),* 10372-10375

Chakhalian, J.; Freeland, J.W.; Srajer, G.; Strempfer, J.;Khaliullin, G.; Cezar, J.C.; Charlton, T.; Dalgliesh, R.; Bernhard, C.; Cristiani, G.; Habermeier, H.-U.; Keimer, B. Magnetism at the interface between ferromagnetism and superconducting oxides. *Nature Phys.* **2006**, *2*, 244-248

Chang, C.-R. A hysteresis model for planar Hall effect in thin films *IEEE Trans. Magn.* **2000**, *36*, 1214

Crespo, P.; Litran, R.; Rojas, T.C.; Multigner, M.; de la Fuente, J.M.; Sanchez-Lopez, J.C.; Garcia, M.A.; Hernando, A.; Penades, S.; Fernandez, A. Permanent magnetism, magnetic anisotropy, and hysteresis of thiol-capped gold nanoparticles. *Phys. Rev. Lett.* **2004**, *93 (8)*, 087204

Crespo, P.; Garcia, M.A.; Fernandez Pinel, E.; Multigner, M.; Alcantara, D.; de la Fuente, J.M.; Penades, S.; Hernando, A. Fe Impurities Weaken the Ferromagnetic Behavior in Au Nanoparticles. *Phys. Rev. Lett.* **2006**, *97*, 177203

Crespo, P.; de la Presa, P.; Marin, P.; Multigner, M.; Alonso, J.M.; Rivero, G.; Yndurain, F.; Gonzalez-Calbet, J.M.; Hernando, A. Magnetism in Nanoparticles: Tuning Properties with Coatings. *J. Phys. Cond. Matt.* **2013**, *25*, 484006

Cuadrado, R.; Puerta, J.M.; Soria, F.; Cerda, J.I. A First Principle Study of Thiol-Capped Au Nanoparticles: Structural, Electronic, and Magnetic Properties as a Function of Thiol Coverage. *J. Chem. Phys.* **2013**, *139*, 034319

Elfimov, I.S.; Yunoki, S.; Sawatzky, G.A. Possible path to a new class of ferromagnetic and half-metallic ferromagnetic materials. *Phys. Rev. Lett.* **2002**, *89*, 216403

Epshtein, E.M.; Krikunov, A.I.; Ogrin, Y.F. Planar Hall effect in thin-film magnetic structures. Cobalt films on silicon substrates. *J. Magn. Magn. Mater* **2003**, *258*, 80

Esquinanzi, P.; Hergert, W.; Spemann, D.; Setzer, A.; Ernst, A. Defect-induced magnetism in solids. *IEEE Trans. Magn.* **2013**, *49 (8)*, 4668

Fischer, G.; Sanchez, N.; Adeagbo, W.A.; Lueders, M.; Szotek, Z.; Temmerman, W.M.; Ernst, A.; Hergert, W.; Munoz, M.C. Room-temperature p-induced surface ferromagnetism: First principle study. *Phys. Rev. B*, **2011**, *84*, 205306

Fried, G.; Zhang, Y.; Bohn, P. Effect of molecular adsorption at the liquid-metal interface on electronic conductivity: The role of surface morphology. *Thin Solid Films* **2001**, *401 (1)*, 171-178

Garcia, M.A.; Merino, J.M.; Fernandez Pinel, E.; Quesada, A.; de la Venta, J.; Ruiz Gonzales, M.L.; Castro, G.R.; Crespo, P.; Llopis, J.; Gonzales-Calbet, J.M.

Hernando, A. Magnetic Properties of ZnO Nanoparticles. *Nano Lett.* **2007**, *7*, 1489-1494

Garcia, M.A.; Fernandez Pinel, E.; de la Venta, J.; Quesada, A.; Bouzas, V.; Fernandez, J.F.; Romero, J.J.; Martin Gonzalez, M.S.; Costa-Krämer, J.L. Sources of Experimental Errors in the Observation of Nanoscale Magnetism. *J. Appl. Phys.* **2009**, *105*, 013925

Garitaonandia, J.S.; Insausti, M.; Goikolea, E.; Suzuki, M.; Cashion, J.D.; Kawamura, N.; Ohsawa, H.; Gil de Muro, I.; Suzuki, K.; Plazaola, F.; Rojo, T. Chemically Induced Permanent Magnetism in Au, Ag, and Cu Nanoparticles: Localization of the Magentism by Element Selective Techniques. *Nano Lett.* **2008**, *8*, 661-667

Garitaonandia, M.; Goikolea, E.; J.S.; Insausti, Suzuki, M.; Kawamura, N.; Ohsawa, H.; Gil de Muro, I.; Suzuki, K.; Cashion, J.D.; Gorria, C.; Plazaola, F.; Rojo, T. Thiol-capped ferromagnetic Au nanoparticles investigated by Au $L_3$ X-ray absorption spectroscopy. *J. Appl. Phys.* **2009**, *105*, 07A907

Glinchuk, M.D.; Eliseev, E.A.; Khist, V.V.; Morozovska, A.N. Ferromagnetism Induced by Magnetic Vacancies as a Size Effect in Thin Films of Non-Magnetic Oxides. *Thin Solid Films* **2013**, *534*, 658-692

Godin, M.; Williams, P.; Tabard-Cossa, V.; Laroche, O.; Beaulieu, L.; Lennox, R.; Gruetter, P. Surface stress, kinetics, and structure of alkanethiol self-assembled monolayers. *Langmuir*, **2004**, *20*, 7090-7096

Grant, J.T.; Briggs, D. *Surface Analysis by Auger and X-ray Photoelectron Spectroscopy*, IM Publications and Surface Spectra Ltd, Manchester 2003

Guerrero, E.; Munoz-Marquez, M.A.; Fernandez, A.; Crespo, P.; Hernando, A.; Lucena, R.; Conesa, J.C. Magnetometry and Electron Paramagnetic Resonance Studies of Phosphine- and Thiol-Capped Gold Nanoparticles. *J. Appl. Phys.* **2010**, *107*, 064303

Häkkinen, H.; Barnett, R.N.; Landman, U. Electronic Structure of Passive $Au_{38}(SCH_3)_{24}$. *Phys. Rev. Lett.* **1999**, *82*, 3264

Häkkinen, H. The Gold-Sulfur Interface at the Nanoscale. *Nat. Chem.* **2012**, *4*, 443-455

Hall E. On a new action of the magnet on electric currents. *Amer. J. Math.* **1879**, *2 (3)*, 287-292

Hegner, M.; Wagner, P.; Semenza, G. Ultralarge atomically flat template-stripped Au surfaces for scanning probe microscopy. *Surf. Sci.*, **1993**, *291*, 39

Heisenberg, W. Zur Theorie des Ferromagnetismus. *Z. Phys.* **1928**, *49*, 619-639

Hernando, A.; Crespo, P.; Garcia, M.A.; Fernandez Pinel, E.; de la Venta, J.; Fernandez, A.; Penades, S. Giant magnetic anisotropy at the nanoscale: Overcoming the superparamagnetic limit. *Phys. Rev. B* **2006** *74*, 052403

Hernando, A.; Garcia, M.A. Comment on “Bosons as the origin for giant magnetic properties of organic monolayers” *Phys. Rev. Lett.* **2006**, *96 (2)*, 029703

Hori, H.; Teranishi, T.; Nakae, Y.; Seino, Y.; Miyake, M.; Yamada, S. Anomalous magnetic polarization effect of Pd and Au nano-particles. *Phys. Lett. A* **1999**, *263*, 406-410

Hori, H.; Yamamoto, Y.; Iwamoto, T.; Miura, T.; Teranishi, T.; Miyake, M. Diameter Dependence of Ferromagnetic Spin Moment in Gold Nanocrystals. *Phys. Rev. B* **2004**, *69*, 174411

Information found in the brochure for Bruker Aurora Elite: http://www.bruker.com/aurora_elite_icpms (accessed August23, 2014)

Jackson, J. D. *Classical Electrodynamics 3rd Edition*, Wiley & Sons, Inc., New York 1998

Jaklevic, R.C.; Lambe, J.; Silver, A.H.; Mercereau, J.E. Quantum interference effects in Josephson tunneling. *Phys. Rev. Lett.* **1964**, *12 (7)*, 159-160

Khalid, M.; Setzer, A.; Ziese, M.; Esquinazi, P.; Spemann, D.; Poeppl, A.; Goering, E. Ubiquity of ferromagnetic signals in common diamagnetic oxide crystals. *Phys. Rev. B*, **2010**, *81 (21)*, 214414

Knaus, B.; Garzon, S.; Crawford, T.M. Alkenethiol induced changes in the magnetotransport properties of Co/Au bilayers. *J. Appl. Phys.* **2009**, *105*, 07A903

Langmuir, I. The mechanism of the surface phenomenon of flotation. *Trans. Faraday Soc.* **1920**, *15*, 62-74

Lawrence Berkeley National Laboratory X-ray specifications http://xraysweb.lbl.gov/ (accessed August 30, 2014)

Lide, D. R., ed. *CRC Handbook of Chemistry and Physics, 85th Edition*, CRC Press, Boca Raton, 2004

Litran, R.; Sampedro, B.; Rojas, T.C.; Multigner, M.; Sanchez-Lopez, J.C.; Crespo, P.; Lopez-Cartes, C.; Garcia, M.A.; Hernando, A.; Fernandez, A. Magnetic and Microstructural Analysis of Palladium Nanoparticles with Different Capping Systems. *Phys. Rev. B* **2006**, *73*, 054404

Liu, Y.; Zhou, W.; Wu, P. Tuning of Magentism of $SrTiO_3$ by Site-Specific Doping. *Mater. Chem. Phys.* **2015**, *160*, 80-86

Mataga, N. Possible “ferromagnetic states” of some hypothetical hydrocarbons. *Theoret. Chim. Acta*, **1968**, *10*, 372-376

Mathon, O.; Baudelet, F.; Itie, J.-P.; Pasternak, S.; Polian, A.; Pascarelli, S. XMCD under pressure at the Fe K edge on the energy-dispersive beamline of the ESRF. *J. Synchrotron Rad*. **2004**, *11*, 423-427

Montaser, A.; Golightly, D.W. *Inductively Coupled Plasma in Analytical Atomic Spectroscopy*, VCH Publisher Inc., New York, 1992

Montgomery, D.M. *Design and Analysis of Experiments*, Wiley, New York, 1997

Morozovska, A.N.; Eliseev, E.A.; Glinchuk, M.D.; Blinc, R. Surface-Induced Magnetism of the Solids with Impurities and Vacancies. *Phys. B* **2011**, *406*, 1673-1688

Nakamura, T.; Suzuki, M. Recent Progress of the X-Ray Magnetic Circular Dichroism Technique for Element-Specific Magnetic Analysis. *J. Phys. Soc. Jap.* **2013**, *82*, 021006

Ogrin, F.Y.; Lee, S.L.; Ogrin, Y.F. Investigation of perpendicular anisotropy of a thin film using the planar Hall effect. *J. Magn. Magn. Mater.* **2000**, *219*, 331-339

Ovchinnikov, A.A. Multiplicity of the ground state of large alternant organic molecules with conjugated bonds. *Theoret. Chim. Acta*, **1978**, *47*, 297-304

Ovchinnikov, A.A.; Shamovsky, I.L. The structure of ferromagnetic phase of carbon. *J. of Molecular Structure*, **1991**, *251*, 133-140

Ovchinnikov, A.A.; Spector, V.N. Organic ferromagnets – new results. *Synth. Metals*, **1988**, *27*, 615-624

Pavao, A.C.; Santos, J.R.S.; Taft, C.A. Ab initio calculation of magnetism in Fe, Co and Ni. *Molecular Simulations* **2009**, *35 (4)*, 287-291

Pavlenko, N.; Kopp, T.; Mannhart, J. Emerging magnetism and electronic phase separation at titanate interfaces. *Phys. Rev. B*, **2013**, *88*, 201104

Pearson, R. G. Hard and Soft Acids and Bases. *J. Am. Chem. Soc.* **1963**, *85 (22)*, 3533

Potzger, K.; Osten, J.; Levin, A.A.; Shalimov, A.; Talut, G.; Reuther, H.; Arpaci, S.; Bürger, D.; Schmidt, H.; Nestler, T.; Meyer, D.C. Defect-Induced Ferromagnetism in Crystalline $SrTiO_3$. *J. Magn. Magn. Mater.* **2011**, *323*, 1551-1562

Quantum Design, Product Introduction for MPMS SQUID VSM http://www.qd-china.com/download/squid_vsm/squidvsm.pdf (accessed September 16, 2014)

Rajca, A.; Rajca, S. Intramolecular antiferromagnetic vs ferromagnetic spin coupling through the biphenyl unit. *J. Am. Chem. Soc.* **1996**, *118 (34)*, 8121-8126

Rajca, A.; Utamapanya, S.; Xu, J. Control of magnetic interactions in polyarylmethyl triplet diradicals using steric hindrance. *J. Am. Chem. Soc.* **1991**, *113 (24)*, 9235-9241

Rajca, A.; Wongsriratanakul, J.; Rajca, S. Magnetic ordering in an organic polymer. *Science* **2001**, *294*, 1503-1505

Reich, S.; Leitus, G.; Feldman, Y. Observation of Magnetism in Au Thin Films. *Appl. Phys. Lett.* **2006**, *88*, 222502

Samant, M.G.; Stoehr, J.; Parkin, S.S.P.; Held, G.A.; Hermsmeier, B.D.; Herman, F.; Van Schilfgaarde, M.; Duda, L.-C.; Mancini, D.C.; Wassdahl, N.; Nakajima, R. Induced spin polarization in Cu spacer layers in Co/Cu multilayers. *Phys. Rev. Lett.* **1994**, *72 (7)*, 1112

Shein, I.R.; Ivanovskii, A.L. First Principle Prediction of Vacancy-Induced Magnetism in Non-Magnetic Perovskite $SrTiO_3$. *Phys. Lett. A* **2007**, *371*, 155-159

Stamenov, P.; Coey, J.M.D. Sample Size, Position, and Structure Effects on Magnetization Measurements using Second-Order Gradiometer Pickup Coils. *Rev. Sci. Inst.* **2006**, *77*, 015106

Suzuki, K.; Zhang, H.; Saito, K.; Garitaonandia, J.S.; Goikolea, E.; Insausti, M. Ferromagentism of Polythiophene-Capped Au Nanoparticles. *J. Appl. Phys.* **2011**, *109*, 07E328

Teo, B.K. *EXAFS: Basic Principles and Data Analysis*, Springer-Verlag, Berlin 1986

Teranishi, T.; Hori, H.; Miyake, M. ESR Study on Palladium Nanoparticles. *J. Phys. Chem. B* **1997**, *101 (30)*, 5774-5776

Thomson, W. On the electro-dynamic qualities of metals: Effects of magnetization on the electric conductivity of nickel and iron. *Proc. Royal Soc.* **1857**, *8*, 546-550

Tippler, P. A. *Physik*, Spektrum Akademischer Verlag, Heidelberg, Berlin, Oxford 1994

Tromas, C.; Eaton, P.; Mimault, J.; Rojo, J.; Penade, S. Structural characterization of self-assembles monolayers of neoglycoconjugates using atomic force microscopy. *Langmuir*, **2005**, *21*, 6142

Trudel, S. Unexpected magnetism in gold nanostructures: making gold even more attractive. *Gold Bull.* **2011**, *44*, 3-13

Tumanski, S. The application of Permalloy magnetoresistive sensors for nondestructive testing of electrical steel sheets. *J. Magn. Magn. Mater.* **1988**, *75*, 266

Tyutyulkov, N.; Bangov, I. Electronic Structure of some hypothetical polymeric non-classical hydrocarbons. *Compt. Rend. Acad. Bulg. Sci.*, **1974**, *27*, 1517-1524

Ulman, A. Formation and Structure of self-assembled monolayers. *Chem. Rev.* **1996**, *96(4)*, 1533-1554

Vager, Z.; Naaman, R. Bosons as the origin for giant magnetic properties of organic monolayers. *Phys. Rev. Lett.* **2004**, *92 (8)*, 087205

Vager, Z.; Naaman, R. Reply *Phys. Rev. Lett.* **2006**, *96 (2)*, 029704

Venkataramanan, M.; Pradeep, T. A method to study the phase transition and desorption of self-assembled monolayers on planar gold surfaces *Anal. Chem.* **2000**, *72*, 5852-5856

Versluijs, J. J.; Bari, M. A.; Coey, J. M. D. Magnetoresistance of Half-Metallic Oxide Nanocontacts, *Phys. Rev. Lett.,* **2001**, *87*, 026601

Wolf, S. A.; Awschalom, D. D.; Buhrman, R. A.; Daughton, J. M.; von Molnár, S.; Roukes, M. L.; Chtchelkanova, A. Y.; Treger, D. M. Spintronics: A Spin-Based Electronics from the Furture, *Science,* **2001**, *294*, 1488

Yamamoto, Y.; Miura, T.; Suzuki, M.; Nawamura, N.; Miyagawa, H.; Nakamura, T.; Kobayashi, K.; Teranishi, T.; Hori, H. Direct observation of ferromagnetic spin polarization in gold nanoparticles. *Phys. Rev. Lett.* **2004**, *93 (11)*, 116801

Zhang, P.; Sham, T.K. Tuning the electronic behavior of Au nanoparticles with capping molecules. *Appl. Phys.* Lett **2002**, *81*, 736-738

Zhang, Y.; Hu, J.; Cao, E.; Sun, L.; Qin, H. Vacancy Induced Magnetism in $SrTiO_3$. *J. Magn. Magn. Mater.* **2012**, *324*, 1770-1775

Zunger A.; Lany, S.; Raebiger, H. The quest for dilute ferromagnetism in semiconductors: Guides and misguides by theory. *Physics*, **2010**, *3*, 53

Zutic J. F.; Sarma, S. D. Spintronics: Fundamentals and Applications Rev. Mod. Phys. 76, 323 (2004).

# APPENDIX A

## PREVIOUSLY USED TECHNIQUES

The influences of self-assembled monolayers on the magnetic properties of different metals has not been widely investigated and the existing publications vary greatly in their results, which was discussed in chapter 3. To understand how these authors gathered the data and therefore where potential errors might stem from, it is necessary to review the methods used.

### A.1 SUPERCONDUCTING QUANTUM INTERFERENCE DEVICES (SQUIDS)

The superconducting quantum interference device was first developed in 1964 in the Ford Laboratories in Michigan [1, 2]. A standard SQUID can measure very small magnetic fields down to the aT range ($10^{-18}$ T). It consists of a superconducting ring, which is interrupted by parallel Josephson junctions (**Figure A.1**). When a current is applied in the absence of an external magnetic field, the current splits into two equal parts to run through the parallel circuit. One of the properties of a superconductor is that when a magnetic field is applied a screening current begins to circulate in order to create a magnetic field in the opposite direction of the applied one and therefore to cancel the applied field out. The applied current runs in the same direction through both junctions and the screening current runs in a loop. The addition of the screening current causes an increase in the current through the Josephson junction in one side of the loop, while the other

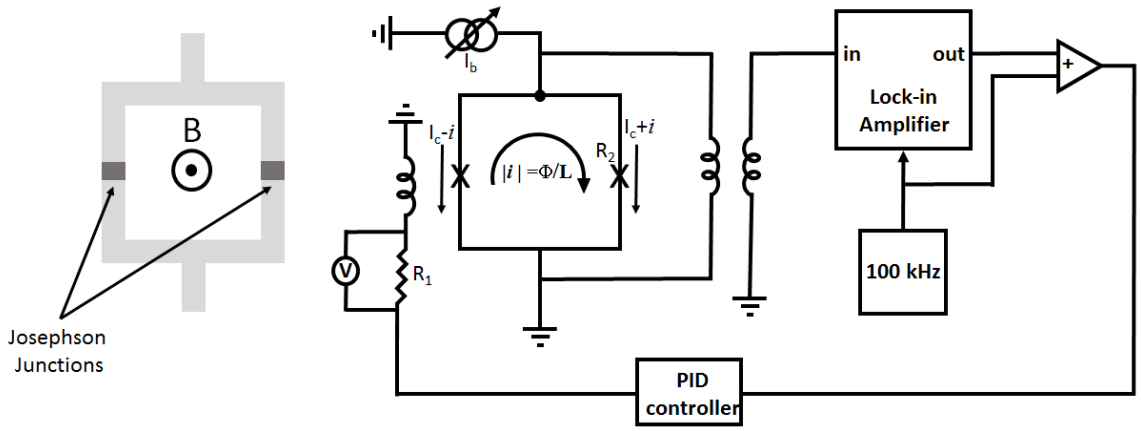


***Figure A.1: left: Schematic function of a SQUID. A current enters and splits into the two paths; right: A current is send through the coil on the far left where it creates a magnetic flux Φ. This magnetic flux causes a supercurrent in the ring of the SQUID. The ring is in a parallel circuit with a second coil which causes mutual inductance with the third coil on the right. The current created by the inductance (L) of the third coil runs through a lock-in amplifier (LIA) where its amplitude is read out. Coming out of the LIA this current is added to a reference current which runs into a proportional-integral-derivative controller (PID controller). The PID controller calculates the difference between the current from the LIA and the reference and reduces or increases it by the difference. The current coming out of the PID controller runs through a resistor, over which the voltage is measured, and from there through the first coil where it restarts the process. The current running through the first coil must be just strong enough to create a field with opposite direction to the sample field but with equal value to cancel it out.***

side experiences a decrease. The created magnetic flux, which is the sum of the magnetic field lines through a surface, can only exist as quantized values. Therefore it can happen that a flux quantum value does not quite match the applied field and the screening current increases to hit the next flux current value, which might be too high. This causes a fluctuation in the flux, which can be measured [3].

The sensitivity of a SQUID varies with sample size and material. In the following appendix chapter, if not otherwise stated, the following standard sample geometry will always be assumed: 1 cm length, 1 cm width, and 100 nm thickness. As a standard impurity I will consider iron. A gold sample of standard size has 6 x

$10^{17}$ gold atoms, considering the lattice parameter of a face centered cubic (fcc) crystal. Bulk iron has a magnetic moment of 2.2 $\mu_B$ ($\mu_B$ = 9.3 x $10^{-24}$ $Am^2$) per atom [4], which converts into 2.05 x $10^{-20}$ emu per atom. The reference SQUID considered here is manufactured by Quantum Design and has a resolution of $10^{-8}$ emu, therefore 3 ppm of iron would be the detection limit of the SQUID for our standard sample. This reference SQUID is a typical instrument for a lab setting and therefore serves well for this calculation to give an idea of a SQUID resolution.

## A.2 X-RAY PHOTOELECTRON SPECTROSCOPY (XPS)

X-Ray photoelectron spectroscopy is an elemental analysis technique that employs the interaction of X-rays with the electrons of the substance of interest. A X-ray photon provides the energy during a collision to eject a core electron out of the substance's orbitals (**Figure A.2**). A photodetector measures the kinetic

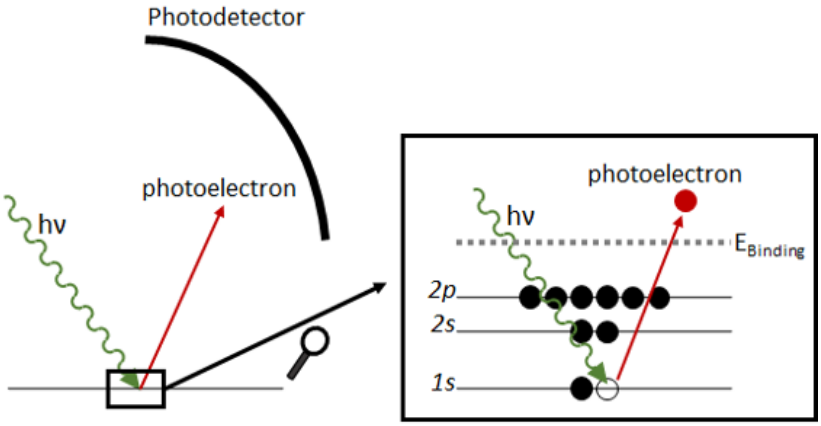


***Figure A.2: Schematic drawing of the XPS process; a X-ray photon incident causes a core electron to be emitted, which is then in turn captured by a photo-detector.***

energy of the ejected electron, which allows one to calculate the binding energy ($E_{binding}$) of each element by using energy conservation. All energies are given with

respect to the vacuum energy as zero. Therefore the energy of the photon (hv) impinging on the material must equal the sum of the binding energy $E_{binding}$, which is the energy needed to eject an electron from the ground state to the vacuum level, and the remaining kinetic energy ($E_{kin}$) which is measured by the photodetector. Since the system is not ideal there is a small loss of kinetic energy during the absorption of the photoelectron into the spectrometer, the work function of the spectrometer, Φ, which needs to be accounted for. Therefore the binding energy can be calculated by subtracting the measured kinetic energy and the work function of the instrument from the energy of the incident photon:

$$\mathbf{E_{Binding} = hv - (E_{kin} + \Phi)} \qquad \mathbf{(12)}$$

Since the binding energy of the core electrons varies for different elements it allows one to obtain information about the composition of a substance. XPS is a surface technique and generally analyzes only the first 20 atomic layers, which causes problems in thicker samples. In addition it has a fairly low detection limit of parts per thousand [5]. Better detection limits can be achieved with extremely long measuring times (several hours). This technique is designed to be used on solids like metals or polymers as well as on highly viscous oils. Low viscosity materials like liquids cannot be analyzed since it has to be operated under high vacuum conditions. Since this technique is highly depending on the energy of the incoming photons, which in turn interacts with the emitted photoelectron, the sensitivity can vary over a large range.

## A.3 X-RAY MAGNETIC CIRCULAR DICHROISM TECHNIQUE (XMCD)

For the X-ray magnetic circular dichroism technique the difference between two X-ray absorption spectra of circularly polarized light is measured while an external magnetic field is applied. Using polarized light, the excitation is spin dependent and a certain spin reacts better to one polarization direction while its opposite spin will react to the other polarization direction (**Figure A.3**). This causes a difference in the absorption spectrum. By subtracting the two absorption spectra

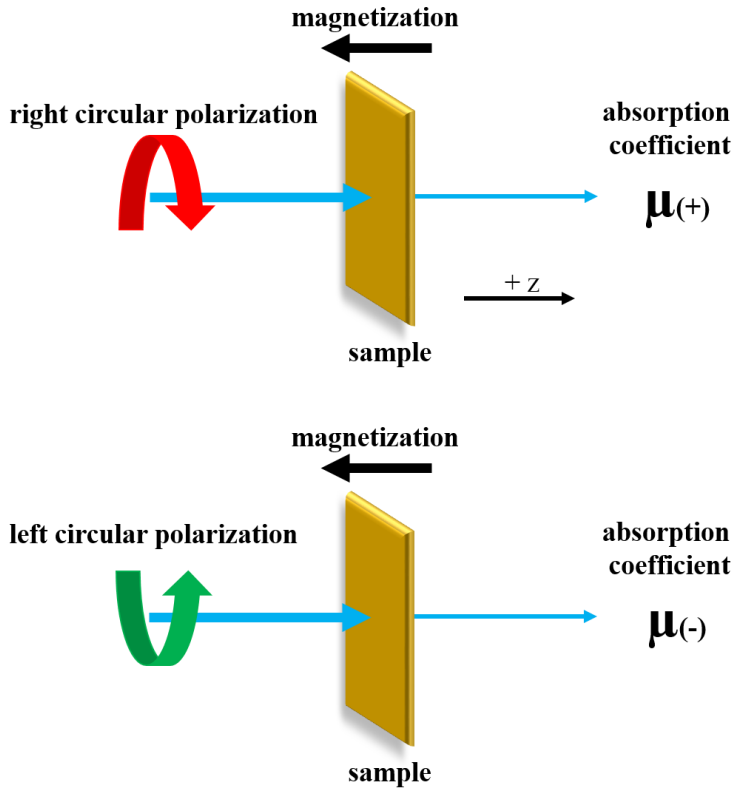


***Figure A.3: Schematic drawing of the XMCD process; while a sample is strongly magnetized, it is exposed to right and left circularly polarized light. Each polarization direction interacts differently with the magnetized material, which results in different absorption coefficients. The difference of the two directions can give information about the spin orientation and orbital momentum of the material.***

it is possible to get an idea of the difference in spin population. A difference other than zero indicates the presence of magnetism. Depending on the element, the atoms will absorb the light at a different wavelength. The large external magnetic field allows one to align the electrons of the outer orbitals. Therefore the resulting signal will have the same polarization signal and therefore is easier to detect. In general, an electron from a p orbital gets excited into one of the d orbitals. Shining polarized light on the atoms allows one to get information about the spin orientation and the orbital magnetic moment of the atom. XMCD is not only used in the identification of metal properties, but is also a very powerful tool in biology where different complex structures can be analyzed with respect to their oxidation and spin state. The X-ray's deep penetration depth of several hundred Ångstrom [6] allows for bulk measurements. XMCD can measure in steps as little as $0.01\mu_B$ per 2000 $nm^2$ circular focal area [7], which translate to 1 ppb of iron in a 100 nm thick sample.

## A.4 X-Ray Absorption Near-Edge Structure (XANES)

The X-ray absorption near-edge structure technique is a high energy version of standard absorption techniques. The main difference between XANES and common photoemission spectroscopy is that in the latter an electron is ejected due to a collision with a photon and the ejected electron is directly measured. In XANES the incoming photon penetrates deep and ejects a core electron, leaving a hole behind. An electron from a higher state drops down and fills the core hole under emission of energy. This energy generally can be either released as a

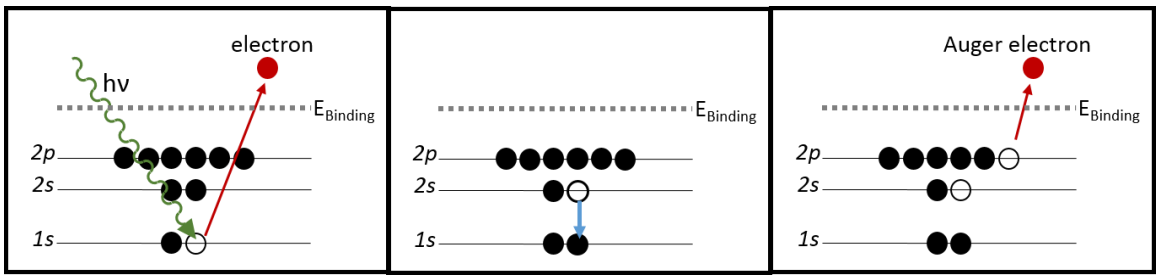


***Figure A.4: Schematic drawing of the Auger process; an incoming photon ejects a core electron (left); the hole is filled by an electron from a higher shell, which drops down in energy (middle); to release the excess energy remaining from the higher shell, an electron from the valence shell is ejected (right).***

photon or as emission of an electron from a high state, which both can be measured (**Figure A.4**). This process is also known as the Auger process and the finally emitted electron is called an Auger electron. Just like in common photoelectron spectroscopy the binding energy can be calculated by subtracting the measured kinetic energy of the Auger electron or the emitted photon and the work function of the instrument from the X-ray photon energy. The scattering of the electron inside the solid state structure can be measured by the interference pattern it causes in the signal. Therefore this technique allows a more in-depth analysis then regular light absorption techniques. XANES uses relatively low energy X-rays which are close to the absorption edge of the electrons in an atom. Since each element has a different absorption edge pattern, this technique not only gives information about oxidation states of the atoms, but also about the elemental composition of the structure. In fact, the scattering pattern varies with the environment of the atom. Therefore it can be very useful to obtain the complex coordination in novel substances [8]. Although it is impossible to determine a magnetic moment with this technique, it is vital to this field to determine the purity of metal substrates.

## A.5 Extended X-Ray Absorption Fine Structure (EXAFS)

The extended X-ray absorption fine structure technique is similar to the XANES technique. The main difference between the two is the excitation energy. While XANES excited around the edge of the electronic structure, EXAFS excites at higher energies [9] (**Figure A.5**). The EXAFS signal is caused by a scattering of the ejected electron off of the neighboring atoms, which causes it to return to the initial absorbing atom. This modulates the amplitudes of the initial wave-function of the ejected electron and causes the spectra to have peaks rather than being a smooth graph. Since the wavelength of the backscattering depends on the energy of the incoming X-ray photon, XANES scattering has bigger wavelength in the backscattering. In addition, EXAFS considers a single scattering event, while

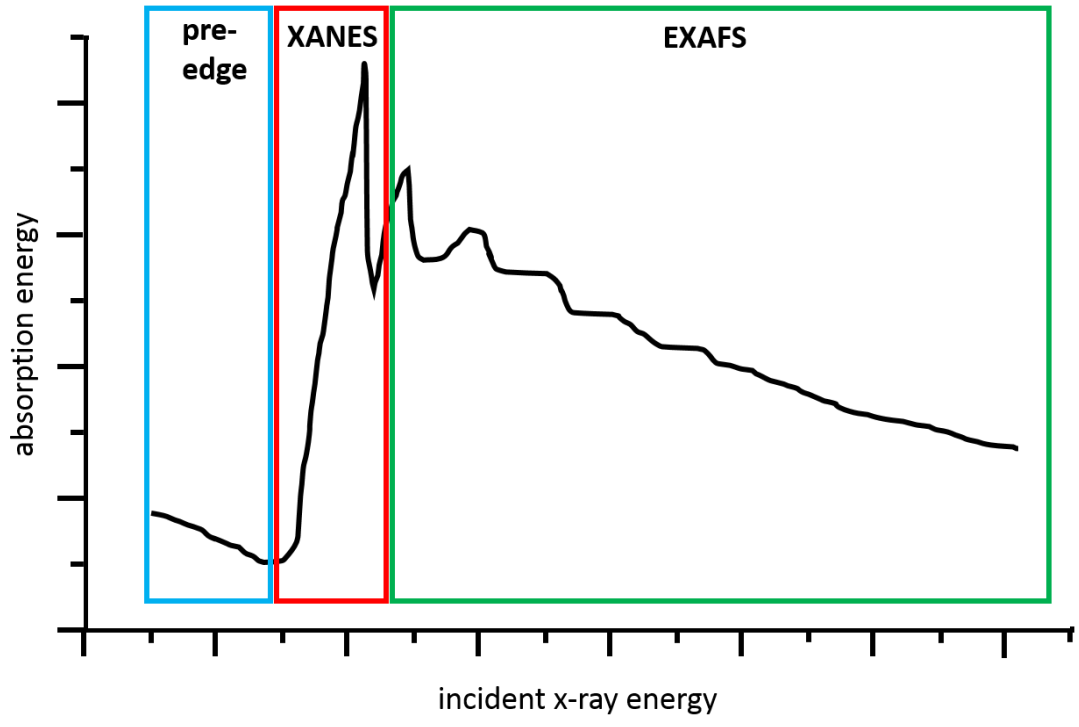


***Figure A.5: Full absorption spectrum in which both, the XANES and EXAFS, as well as the pre-edge are shown.***

XANES considers multiple scattering events until a new photon or Auger electron is released. Therefore, the resulting signal varies in the number of interferences. A Fourier transformation of the data can provide real space information. This technique, similar to the XANES, also serves to determine the purity of a metal substrate.

## A.6 Inductively Coupled Plasma-Mass Spectrometry (ICP-MS)

The inductively coupled plasma-mass spectrometry is an accurate technique to track trace elements. Under high vacuum ($10^{-5}$ Torr) a plasma, most commonly an argon plasma, is created by electromagnetic induction and high temperatures of up to 7,000 °C are reached in this plasma [10]. The sample is introduced through a nebulizer into the plasma and due to the heat, it will evaporate and break down into atoms. The heat also causes the atoms to lose their outermost electrons and ionize. An oscillating magnetic field created by a quadrupole allows separation of the ions based on their mass-to-charge ration (m/z). Eventually the ions reach a detector where a collision of the ion with the detector causes an analog signal proportional to their relative quantity is created. A standard ICP-MS can detect concentrations at the parts per trillion level ($10^{-12}$) [10, 11]. Using this technique, it is possible to determine the purity of the liquid ligand systems.

## A.7 REFERENCES


1. Jaklevic, R.C.; Lambe, J.; Silver, A.H.; Mercereau, J.E. Quantum interference effects in Josephson tunneling. *Phys. Rev. Lett.* **1964**, *12 (7)*, 159-160

2. Anderson, P.W.; Rowell, J.M. Probable observation of the Josephson superconducting tunneling effect. *Phys. Rev. Lett.* **1963**, *10 (6)*, 230-231

3. Quantum Design, Product Introduction for MPMS SQUID VSM http://www.qd-china.com/download/squid_vsm/squidvsm.pdf

4. Pavao, A.C.; Santos, J.R.S.; Taft, C.A. Ab initio calculation of magnetism in Fe, Co and Ni. *Molecular Simulations* **2009**, *35 (4)*, 287-291

5. Grant, J.T.;Briggs, D. *Surface Analysis by Auger and X-ray Photoelectron Spectroscopy*, IM Publications and Surface Spectra Ltd, Manchester 2003

6. Chakhalian, J.; Freeland, J.W.; Srajer, G.; Strempfer, J.;Khaliullin, G.; Cezar, J.C.; Charlton, T.; Dalgliesh, R.; Bernhard, C.; Cristiani, G.; Habermeier, H.-U.; Keimer, B. Magnetism at the interface between ferromagnetism and superconducting oxides. *Nature Phys.* **2006**, *2*, 244-248

7. Mathon, O.; Baudelet, F.; Itie, J.-P.; Pasternak, S.; Polian, A.; Pascarelli, S. XMCD under pressure at the Fe K edge on the energy-dispersive beamline of the ESRF. *J. Synchrotron Rad*. **2004**, *11*, 423-427

8. Bianconi, A. Surface X-ray absorption spectroscopy: Surface EXAFS and surface XANES. *Appl. Surf. Sci.* **1980**, *6 (3)*, 392-418

9. Teo, B.K. *EXAFS: Basic Principles and Data Analysis*, Springer-Verlag, Berlin, 1986

10. Montaser, A.; Golightly, D.W. *Inductively Coupled Plasma in Analytical Atomic Spectroscopy*, VCH Publisher Inc., New York, 1992

11. Information found in the brochure for Bruker Aurora Elite: http://www.bruker.com/aurora_elite_icpms (accessed August23, 2014)

# APPENDIX B

## CODE USED FOR ANALYSIS IN WOLFRAM MATHEMATICA

```
(*sets path where desired files are located*)
SetDirectory["C:\\Users\\oxsher\\Desktop\\*date*"]

(***Manipulative Plot to find the peak tip***)

(*defines desired data sets*)
filesa = {425, 427, 429, 446, 495};
(*creates a table of all imported data sets*)
a = Table[
    (*<>ToString allows import of multiple data sets without typing
     every single one*)
    Import["Run " <> ToString[filesa[[n]]], "TSV"]
     (*first data point to use;;last data point to use;;in steps of X,
     items 2 to 3 of every group in data set*)
     [[1649 ;; 3654 ;; 5, 2 ;; 3]],
    (*defines n to be used, first data set, last data set data set*)
    {n, 1, Length[filesa]}];
(*allows manipualtion of item in data set
  → e.g. aV= apply it(#) to the second item in all pairs of a,
multiply with 1000*)
aV = #[[All, 2]] & /@ a * 1000;
aH = #[[All, 1]] & /@ a;
(*creats new table of manipulated data*)
A = Table[
    (*Transposes forms pairs of the two previously manipulated data points*)
    Transpose[{aH[[n]], aV[[n]]}],
    {n, 1, Length[filesa]}];
(*Manipulate allows to *)
Manipulate[
 ListLinePlot[A,
  (*Defines properties of the plot*)
  ImageSize → 800,
  PlotRange → All,
  AxesLabel → {"Filed in Amps", "Hall Voltage in μV"},
  (*GridLines are the movable lines and require a manipulatable plot*)
  GridLines -> {{x}, {y}}],
 (*definition of GridLines, from value, to value, in steps of*)
 {x, -3, 3, 0.01},
 {y, 1.5, 2.5, 0.01}]
```

```
(***Error Plot***)

(*ErrorBarPlots needs to be inserted into Mathematica*)
Needs["ErrorBarPlots`"]
(*Creates Plot with error bars*)
ErrorListPlot[
 (*{x and y value of data point}, length of error bar*)
 {{{1, 2.096}, ErrorBar[0.452]},
  {{2, 1.495}, ErrorBar[0.340]}},
 (*Replaces original tick values with any other word or number*)
 Ticks → {{
    {1, "Water"},
    {2, "Acetone"}},
   Automatic},
 PlotRange → All,
 AxesOrigin → {0, 0},
 AxesLabel → {None, "% Change"},
 LabelStyle → Directive[Black, Bold, Small],
 PlotStyle → Directive[PointSize[Large], Blue],
 AspectRatio → 1 / 3
]
```

```
(***3D Plot***)

files = {(*run number*)};
a = Table[
    Import["Run " <> ToString[files[[n]]], "TSV"][[1256 ;; 3756 ;; 10, 2 ;; 3]],
    {n, 1, Length[filesa]}
  ];
(*Flatten unravels lists of lists
  → e.g. Flatten[{{a,{b},c}d}]={a d,b d,c d} *)
A = Flatten[
    Table[{n, #[[1]], #[[2]]} & /@ a[[n]], {n, 1, 41}], 1];
ListPointPlot3D[A,
 ImageSize → 1200,
 AxesLabel → {"Number of Data Set", "H-Field in Ampere",
   "Hall Voltage in mV"},
 LabelStyle → Directive[Black, Bold]]
```

```
(***2D error plot***)

(*d1&2 present mean data values*)
d1 = {4.698, 3.430, 2.864};
d2 = {3.628, 3.239, 2.946};
(*e1&2 present standard mean deviation values for d1&2*)
e1 = {0.712, 0.756, 0.667};
e2 = {0.750, 0.453, 0.444};
(*creates pairs of the two data points*)
d12 = {d1, d2}^T;
(*creates 2 errorbars for each d12 data point*)
e12 = ErrorBar[#[[1]], #[[2]]] & /@ ({e1, e2}^T);
(*combines the data point with the according error bars*)
p = {d12, e12}^T;
(*"Show" allows to combine the error plot with a secondary graph,
here: dashed line*)
Show[
 ErrorListPlot[p,
  ImageSize → 1000,
  AspectRatio → 0.8,
  PlotRange → {{0, 5.5}, {0, 4.5}},
  AxesLabel → {"% Change w/ Ethanol", "% Change w/ 1-Dodecanethiol"},
  LabelStyle → Directive[Black, Bold, Large],
  AxesOrigin → {0, 0}],
 (*inserts dashed line into error plot*)
 Plot[x, {x, 0, 5},
  PlotStyle → {Black, Dashed, Thickness[0.001]}]
]
```

# APPENDIX C

## EDS SPECTRA

To show the absence of parasite atoms, energy dispersive spectra (EDS) of different cobalt and gold samples were recorded. To achieve a good sensitivity, all samples were tested to 10000 counts. As expected, the silica substrate can be found in all of the sample spectra in form of signal for Si and O due to the penetration depth of the EDS, which reaches way past the sample thickness. In addition, carbon was detected, which resulted from the tape that affixed the sample to the holder. All samples were measured with a FEI Quanta 200 SEM. Overall it was concluded that no impurities in form of other metals are present in the thin film samples.

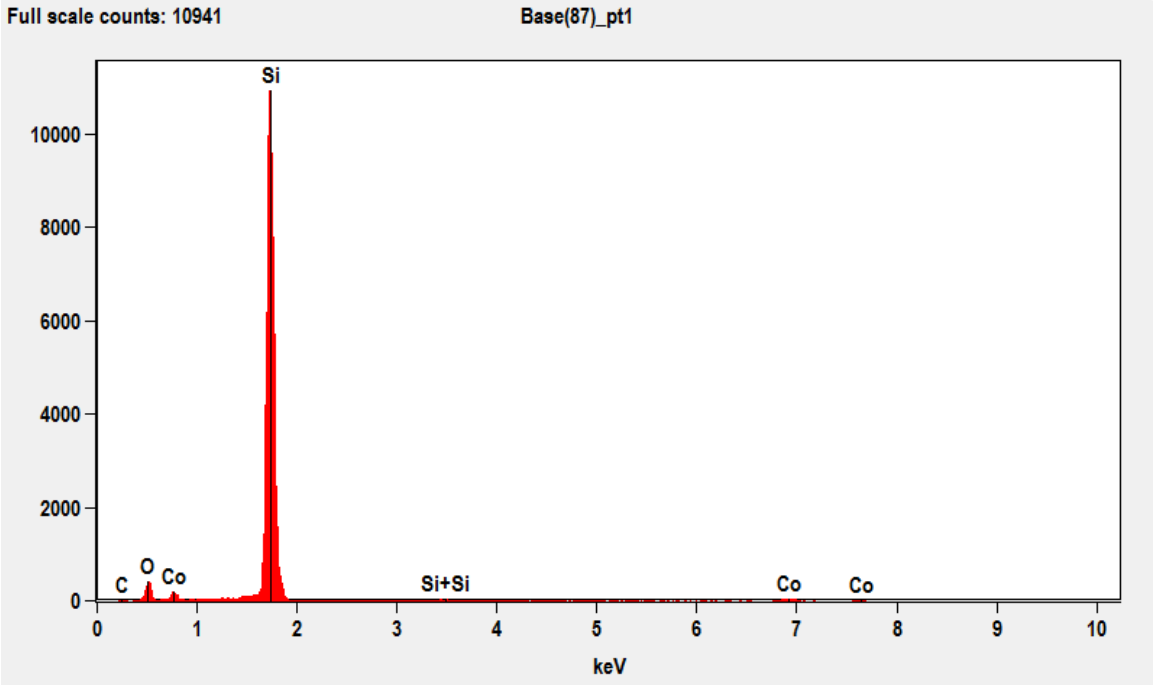


| Element | Net Counts | Net Counts Error | Weight % | Weight % Error | Atom % | Atom % Error |
|---|---|---|---|---|---|---|
| C | 173 | ± 29 | 6.67 | ± 1.12 | 13.10 | ± 2.20 |
| O | 2672 | ± 86 | 15.87 | ± 0.51 | 23.39 | ± 0.75 |
| Si | 93128 | ± 348 | 73.93 | ± 0.28 | 62.09 | ± 0.23 |
| Si | 0 | 0 | --- | --- | --- | --- |
| Co | 997 | ± 87 | 3.53 | ± 0.31 | 1.41 | ± 0.12 |
| Co | 1407 | ± 96 | --- | --- | --- | --- |
| Total | | | 100.00 | | 100.00 | |

***Figure C.1: top: EDS spectrum of 30 nm cobalt; bottom: quantitative results for same sample***

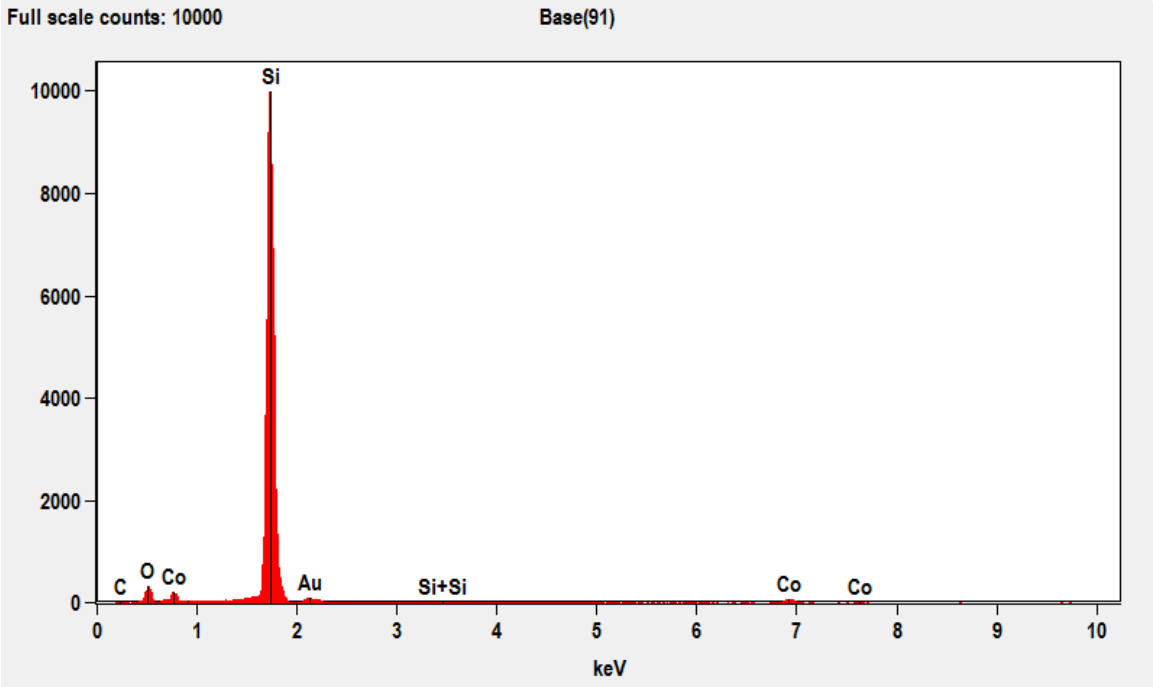


| Element | Net Counts | Net Counts Error | Weight % | Weight % Error | Atom % | Atom % Error |
|---|---|---|---|---|---|---|
| C | 162 | ± 31 | 6.60 | ± 1.26 | 13.52 | ± 2.59 |
| O | 2053 | ± 83 | 13.55 | ± 0.55 | 20.83 | ± 0.84 |
| Si | 83478 | ± 330 | 72.66 | ± 0.29 | 63.65 | ± 0.25 |
| Si | 0 | 0 | --- | --- | --- | --- |
| Co | 984 | ± 90 | 3.76 | ± 0.34 | 1.57 | ± 0.14 |
| Co | 1442 | ± 97 | --- | --- | --- | --- |
| Au | 183 | ± 50 | 3.44 | ± 0.94 | 0.43 | ± 0.12 |
| Au | 1619 | ± 76 | --- | --- | --- | --- |
| Total | | | 100.00 | | 100.00 | |

***Figure C.2: top: EDS spectrum of 30 nm cobalt topped by 10 nm gold; bottom: quantitative results for same sample***

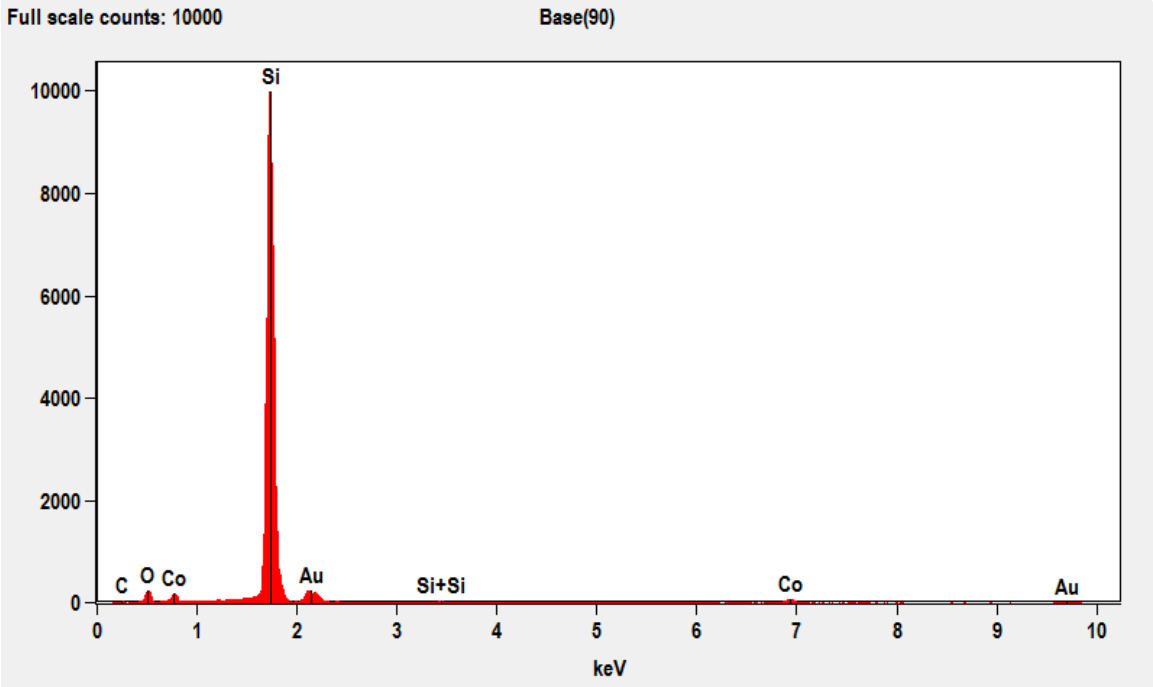


| Element | Net Counts | Net Counts Error | Weight % | Weight % Error | Atom % | Atom % Error |
|---|---|---|---|---|---|---|
| C | 228 | ± 34 | 8.00 | ± 1.19 | 17.52 | ± 2.61 |
| O | 1417 | ± 78 | 9.21 | ± 0.51 | 15.14 | ± 0.83 |
| Si | 83690 | ± 339 | 68.82 | ± 0.28 | 64.47 | ± 0.26 |
| Si | 0 | 0 | --- | --- | --- | --- |
| Co | 912 | ± 96 | 3.20 | ± 0.34 | 1.43 | ± 0.15 |
| Co | 1259 | ± 94 | --- | --- | --- | --- |
| Au | 625 | ± 101 | 10.78 | ± 1.74 | 1.44 | ± 0.23 |
| Au | 4328 | ± 194 | --- | --- | --- | --- |
| Total | | | 100.00 | | 100.00 | |

***Figure C.3: top: EDS spectrum of 30 nm cobalt topped by 30 nm gold; bottom: quantitative results for same sample***

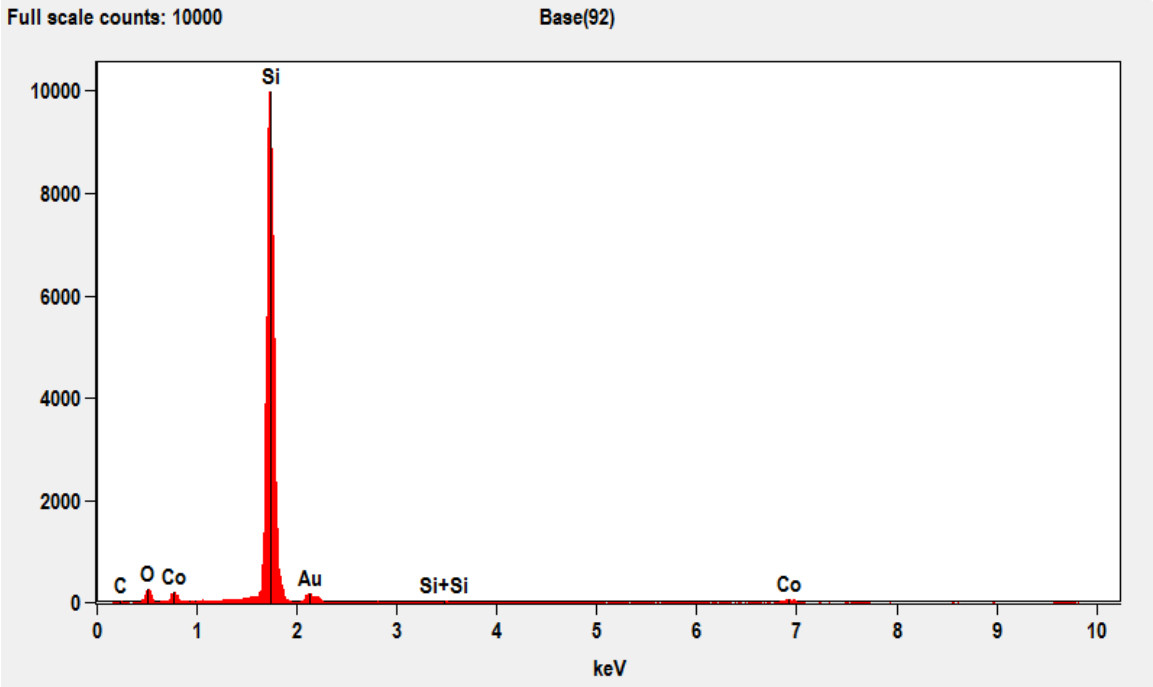


| Element | Net Counts | Net Counts Error | Weight % | Weight % Error | Atom % | Atom % Error |
|---|---|---|---|---|---|---|
| C | 216 | ± 33 | 7.96 | ± 1.22 | 16.61 | ± 2.54 |
| O | 1801 | ± 80 | 11.47 | ± 0.51 | 17.97 | ± 0.80 |
| Si | 85093 | ± 338 | 70.41 | ± 0.28 | 62.84 | ± 0.25 |
| Si | 0 | 0 | --- | --- | --- | --- |
| Co | 1211 | ± 59 | 4.32 | ± 0.21 | 1.84 | ± 0.09 |
| Co | 1493 | ± 96 | --- | --- | --- | --- |
| Au | 332 | ± 61 | 5.84 | ± 1.07 | 0.74 | ± 0.14 |
| Au | 3066 | ± 95 | --- | --- | --- | --- |
| Total | | | 100.00 | | 100.00 | |

***Figure C.4: top: EDS spectrum of 30 nm cobalt topped by 50 nm gold; bottom: quantitative results for same sample***

# APPENDIX D

## NMR SPECTRA

After showing the purity of the metal samples, the next concern was the purity of the ligand liquids. To show the ligand purity, nuclear magnetic resonance (NMR) spectra were recorded for each ligand. For this, all ligands were dissolved in an appropriate deuterated solvent and measured in a Bruker Avance III HD at 300 MHz. For all recorded spectra, it was shown that no impurities are present in the liquid according to the present peaks.

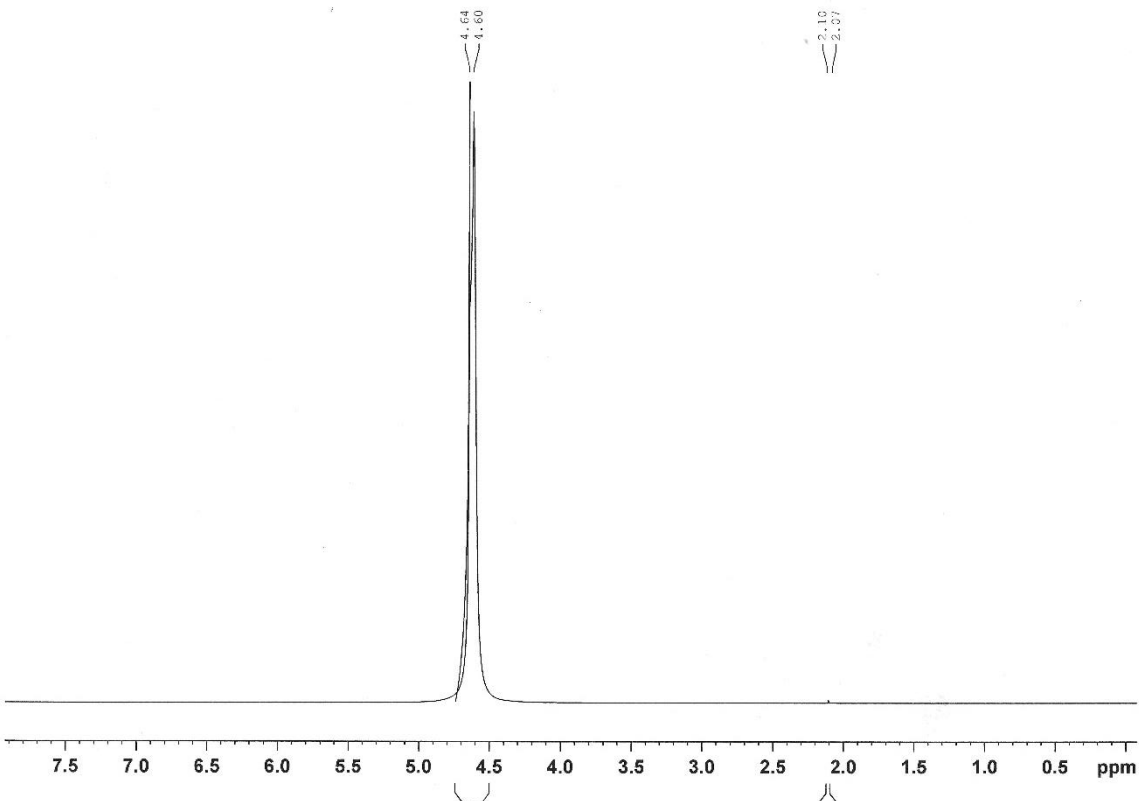


***Figure D.1: $^{1}$H-NMR of DI water at 300 MHz in deuterated acetone ($(CD_3)_2CO$) $\delta$ = 4.60 (s, 2H, $H_2O$)***

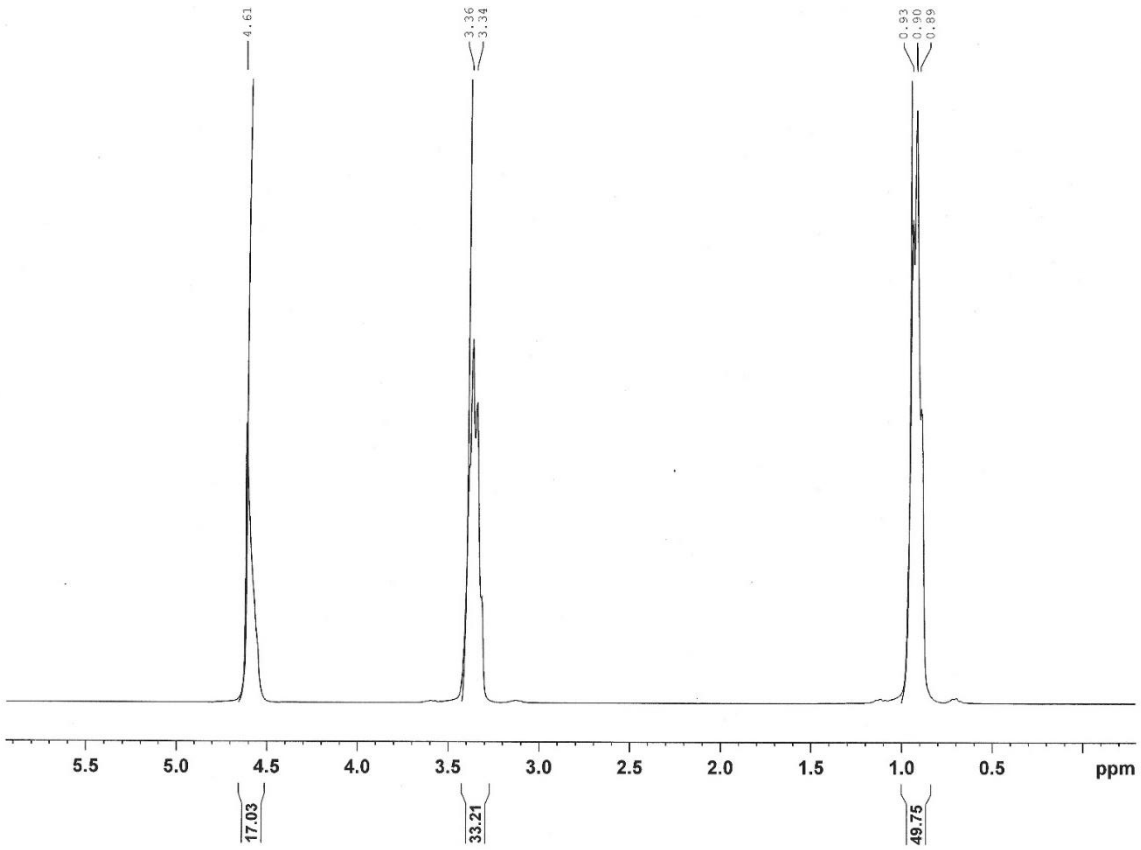


***Figure D.2 $^{1}$H-NMR of ethanol at 300 MHz in deuterated chloroform ($CDCl_3$) δ = 4.61 (s, 2H, $H_2O$), 3.35 (q, 2H, -$CH_2$-), 0.90 (t, 3H, -$CH_3$)***

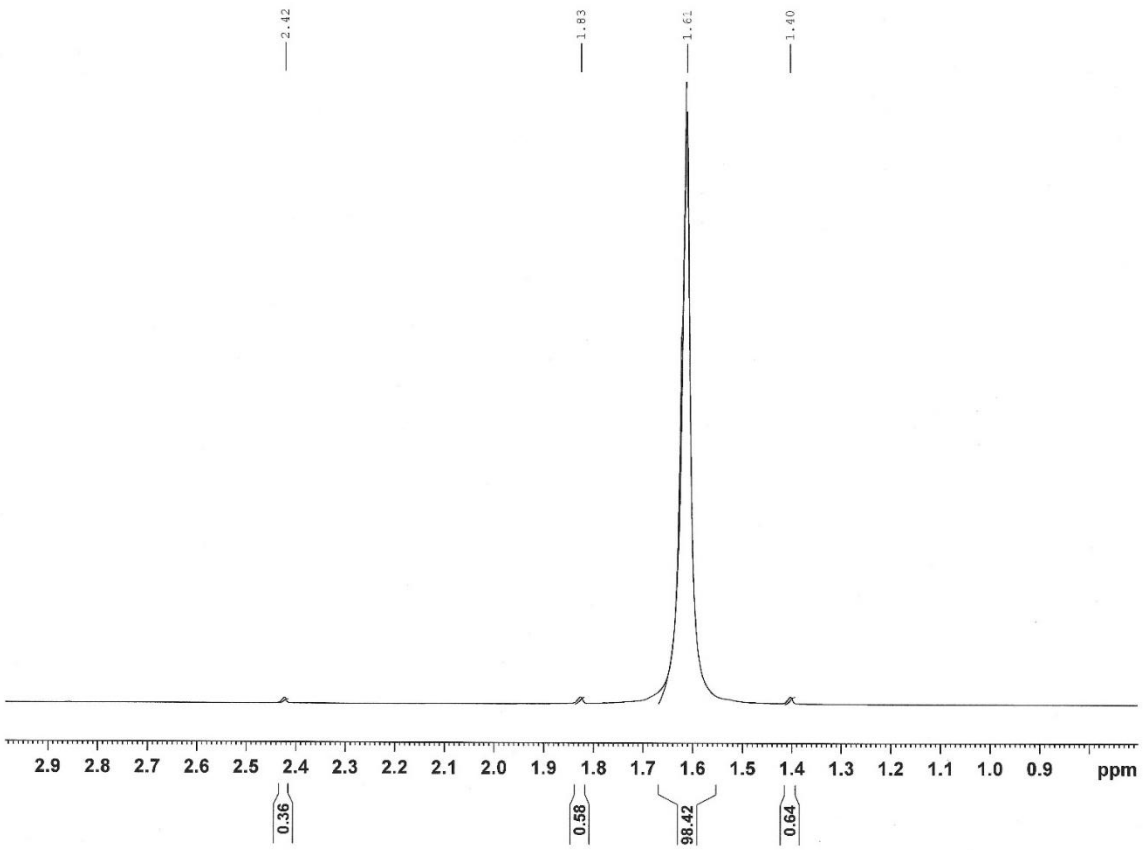


***Figure D.3 $^{1}$H-NMR of acetone at 300 MHz in deuterated chloroform ($CDCl_3$) δ = 1.61 (s, 6H, -$CH_3$)***

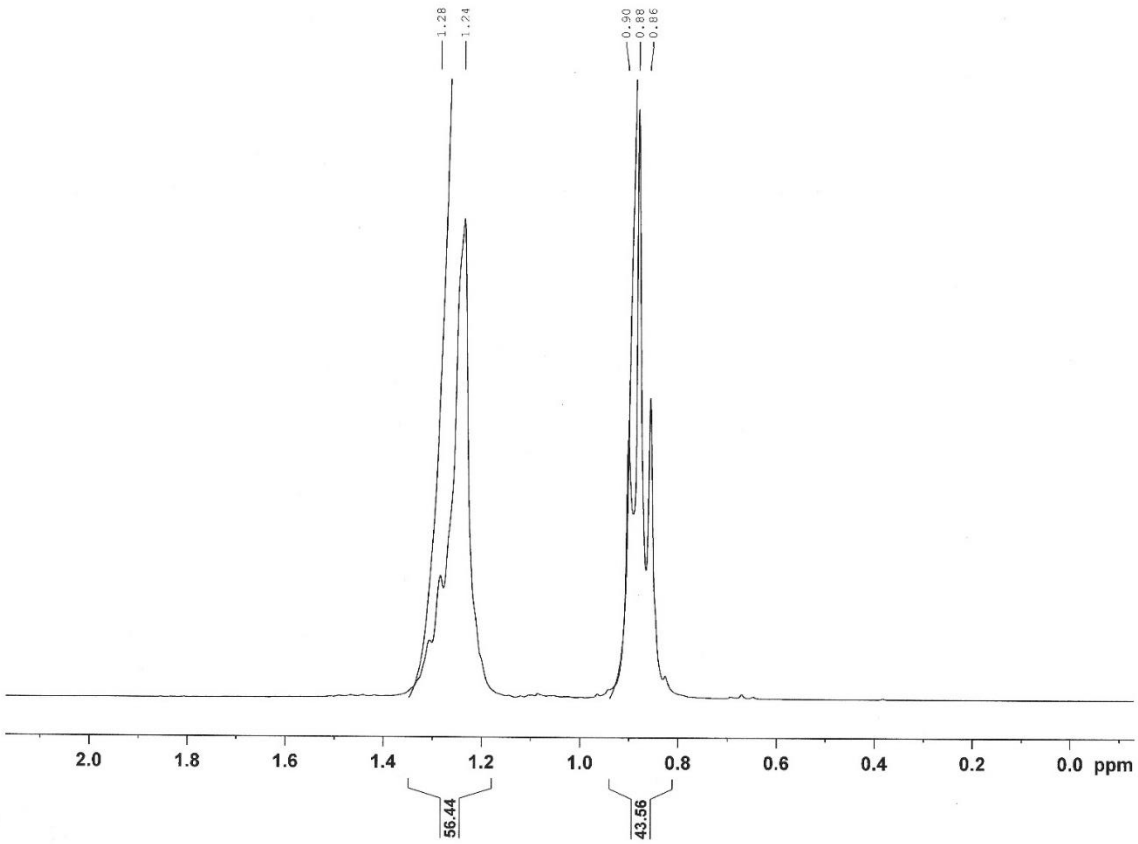


***Figure D.4 $^{1}$H-NMR of hexane at 300 MHz in deuterated benzene ($C_6D_6$) δ = 1.24 (s, 8H, -$CH_2$-), 0.88 (t, 6H, -$CH_3$)***

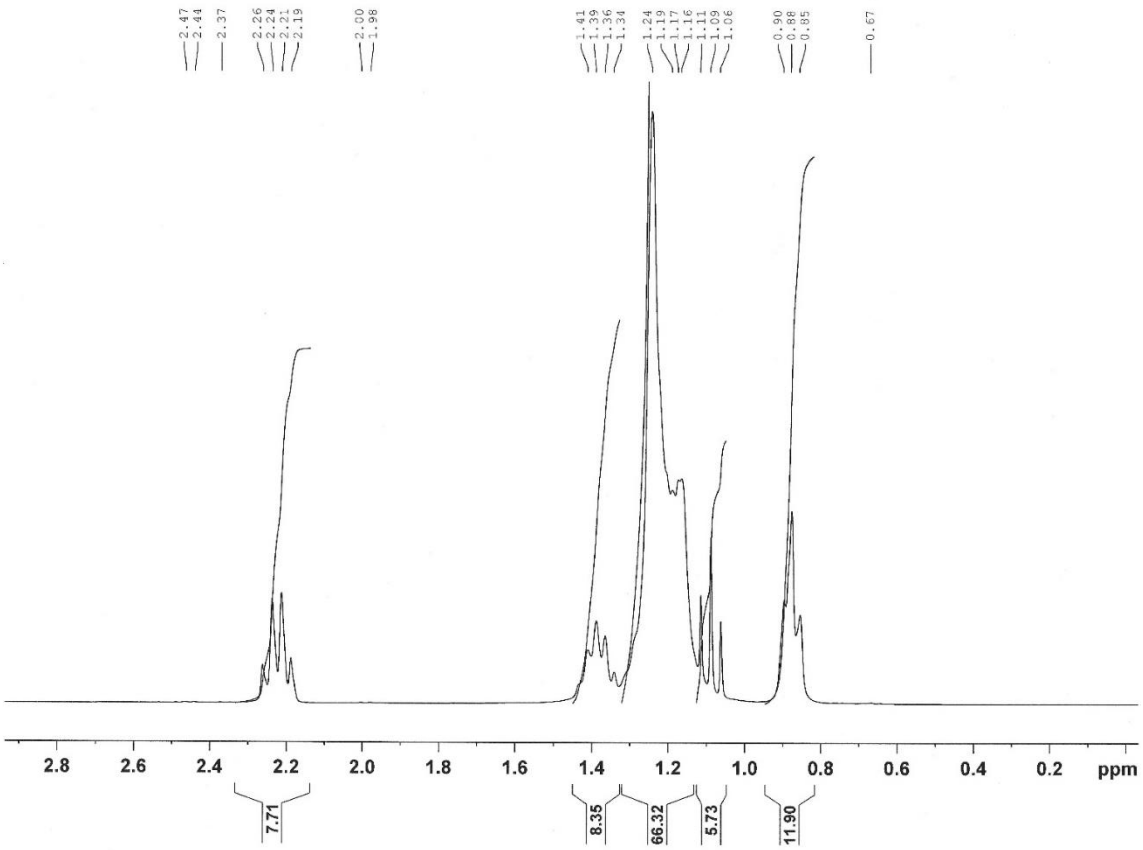


***Figure D.5 $^{1}$H-NMR of 1-dodecylthiol at 300 MHz in deuterated chloroform ($CDCl_3$) δ = 2.22 (q, 2H, -$CH_2$), 1.39 (t, 2H, -$CH_2$), 1.34 (s, 1H, -SH), 1.24 (m, 16H, -$CH_2$), 1.09 (t, 2H, -$CH_2$), 0.88 (t, -$CH_3$)***

# APPENDIX E

## CONVERSION OF EMU TO $\mu_B$

The magnetics community often turns away from using SI units and rather uses the Gaussian system. This can easily lead to problems with comparing data sets or even in calculating various values for one data set. In chapter 3.2.3 a publication by Hernando *et al.* [1] was discussed, in which the conversion became a problem and led to a result that was reduced by a factor of $4\pi$. Looking at the conversion between SI units and Gaussian units, $4\pi$ is a repeating conversion factor [2]. Therefore it was assumed that it was used in error, although not necessary.

For this particular calculation, from emu/cm$^2$ to $\mu_B$/atom, there was actually no conversion between the two systems necessary. The following values need to be considered:

- 1 emu = $1 \times 10^{-3}$ J/T
- 1 $\mu_B$ = $9.274 \times 10^{-24}$ J/T
- The above leads to: 1 $\mu_B$ = $9.274 \times 10^{-21}$ emu
- The number of gold atoms per cm$^2$ is $2 \times 10^{14}$ atoms/cm$^2$
- From the presented data (**Figure E.1**) it can be seen, that the hysteresis curves reach a maximum at $2 \times 10^{-3}$ emu/cm$^2$, which is here indicated by the pink dotted lines

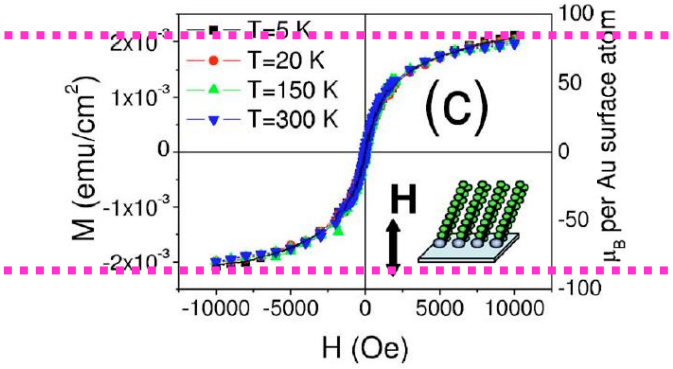


***Figure E.1: The pink dotted lines indicate the maxima of the hysteresis curves used by Hernando et al. to determine the magnetization per surface atom. Copyright 2006 by the American Physical Society***

Considering these statements, first the emu/cm$^2$ can be converted into $\mu_B$/cm$^2$:

$$\frac{2 \times 10^{-3} \frac{emu}{cm^2}}{9.274 \times 10^{-21} \frac{emu}{\mu B}} = 2.157 \times 10^{17} \frac{\mu B}{cm^2} \qquad \textbf{(13)}$$

In a second step, the number of gold atoms per cm$^2$ is taken into consideration:

$$\frac{2.157 \times 10^{17} \frac{\mu B}{cm^2}}{2 \times 10^{14} \frac{atoms}{cm^2}} = 1078.5 \frac{\mu B}{atom} \qquad \textbf{(14)}$$

This value divided by 4π leads to the reported 86 $\mu_B$/atom. However, since no conversion between Gaussian and SI system was necessary, the scale factor of 4π is really not needed here and lead to a reduced result.

## E.1 REFERENCES

1. Hernando, A.; Crespo, P.; Garcia, M.A.; Fernandez Pinel, E.; de la Venta, J.; Fernandez, A.; Penades, S. Giant magnetic anisotropy at the nanoscale: Overcoming the superparamagnetic limit. *Phys. Rev. B* **2006** *74*, 052403

2. Tippler, P. A. *Physik*, Spektrum Akademischer Verlag, Heidelberg, Berlin, Oxford 1994

# APPENDIX F

## STATISTICAL DATA ANALYSIS

The data presented below was created by using ANOVA single factor in Microsoft Excel. Each p-value was determined by comparing two different data sets. In addition for each complete experiment an overall p-value was determined with the same method.

The null hypothesis is that the data sets are all from the same sample pool, which is reflected by a p-value of $p>0.1$. The alternative hypothesis is that the data sets are actually taken from different sample pools, which is reflected by a p-value of $p<0.1$ marked in red. Both of these limitations were chosen by me at will.

It must be stated that this analysis is an optimistic alpha testing method and a more elaborate method of statistical analysis is needed in the future to better determine the significant differences between the various sample pools.

| 30 nm cobalt modified with various ligands | | | | | | |
|---|---|---|---|---|---|---|
| p(all)=0.085 | | | | | | |
| | **R-OOH** | **R-SH** | **R-NH2** | **R=O** | **DI H2O** | **CHx** |
| **R-OH** | 0.656 | 0.117 | 0.239 | 0.071 | 0.061 | 0.119 |
| **R-OOH** | | 0.096 | 0.068 | 0.082 | 0.271 | 0.172 |
| **R-SH** | | | 0.846 | 0.578 | 0.767 | 0.789 |
| **R-NH2** | | | | 0.744 | 0.905 | 0.931 |
| **R=O** | | | | | 0.934 | 0.851 |
| **DI H2O** | | | | | | 0.948 |

| Various thicknesses of cobalt modified with ethanol | | | | |
|---|---|---|---|---|
| p(all)=0.809 | | | | |
| | **20 nm** | **30 nm** | **40 nm** | **50 nm** |
| **10 nm** | 0.853 | 0.797 | 0.792 | 0.041 |
| **20 nm** | | 0.838 | 0.730 | 0.043 |
| **30 nm** | | | 0.524 | 0.217 |
| **40 nm** | | | | 0.769 |

| 30 nm Co with various alcohols | | | |
|---|---|---|---|
| p(all)=0.125 | | | |
| | **ethanol** | **propanol** | **hexanol** |
| **methanol** | 0.042 | 0.029 | 0.061 |
| **ethanol** | | 0.484 | 0.297 |
| **propanol** | | | 0.395 |

| 30 nm nickel modified with various ligands | | | | | | |
|---|---|---|---|---|---|---|
| p(all)=0.002 | | | | | | |
| | **R-OOH** | **R-SH** | **R-NH2** | **R=O** | **DI H2O** | **CHx** |
| **R-OH** | 0.260 | 0.124 | 0.012 | 0.009 | 0.645 | 0.161 |
| **R-OOH** | | 0.655 | 0.637 | 0.932 | 0.009 | 0.293 |
| **R-SH** | | | 0.190 | 0.468 | 0.117 | 0.903 |
| **R-NH2** | | | | 0.513 | 0.012 | 0.170 |
| **R=O** | | | | | 0.326 | 0.276 |
| **DI H2O** | | | | | | 0.133 |

| 30 nm permalloy modified with various ligands | | | | | | |
|---|---|---|---|---|---|---|
| p(all)=0.235 | | | | | | |
| | **R-OOH** | **R-SH** | **R-NH2** | **R=O** | **DI H2O** | **CHx** |
| **R-OH** | 0.832 | 0.823 | 0.243 | 0.194 | 0.287 | 0.152 |
| **R-OOH** | | 0.594 | 0.299 | 0.201 | 0.267 | 0.176 |
| **R-SH** | | | 0.120 | 0.073 | 0.097 | 0.074 |
| **R-NH2** | | | | 0.942 | 0.709 | 0.551 |
| **R=O** | | | | | 0.586 | 0.562 |
| **DI H2O** | | | | | | 0.321 |

| Bilayer: 30 nm cobalt topped with varying thicknesses of gold modified with ethanol | | | | | |
|---|---|---|---|---|---|
| p(all)=0.010 | | | | | |
| | **10 nm** | **20 nm** | **30 nm** | **40 nm** | **50 nm** |
| **0 nm** | 0.026 | 0.054 | 0.123 | 0.037 | 0.011 |
| **10 nm** | | 0.743 | 0.225 | 0.792 | 0.940 |
| **20 nm** | | | 0.424 | 0.891 | 0.680 |
| **30 nm** | | | | 0.236 | 0.187 |
| **40 nm** | | | | | 0.734 |

| Bilayer: 30 nm cobalt topped with varying thicknesses of gold modified with 1-dodecylthiol | | | | | |
|---|---|---|---|---|---|
| p(all)=0.131 | | | | | |
| | **10 nm** | **20 nm** | **30 nm** | **40 nm** | **50 nm** |
| **0 nm** | 0.518 | 0.401 | 0.224 | 0.438 | 0.178 |
| **10 nm** | | 0.878 | 0.516 | 0.941 | 0.044 |
| **20 nm** | | | 0.600 | 0.928 | 0.018 |
| **30 nm** | | | | 0.517 | 0.015 |
| **40 nm** | | | | | 0.025 |

| Bilayer: 30 nm cobalt topped with 30 nm gold modified with various ligands | | | | | | |
|---|---|---|---|---|---|---|
| p(all)=0.048 | | | | | | |
| | **R-OOH** | **R-SH** | **R-NH2** | **R=O** | **DI H2O** | **CHx** |
| **R-OH** | 0.074 | 0.602 | 0.102 | 0.157 | 0.275 | 0.122 |
| **R-OOH** | | 0.266 | 0.926 | 0.076 | 0.107 | 0.026 |
| **R-SH** | | | 0.323 | 0.150 | 0.237 | 0.079 |
| **R-NH2** | | | | 0.090 | 0.126 | 0.034 |
| **R=O** | | | | | 0.831 | 0.862 |
| **DI H2O** | | | | | | 0.880 |

| Bilayer: 30 nm cobalt topped with 10 nm silver modified with various ligands | | | | | | |
|---|---|---|---|---|---|---|
| p(all)=0.540 | | | | | | |
| | **R-OOH** | **R-SH** | **R-NH2** | **R=O** | **DI H2O** | **CHx** |
| **R-OH** | 0.621 | 0.433 | 0.496 | 0.199 | 0.368 | 0.199 |
| **R-OOH** | | 0.866 | 0.835 | 0.249 | 0.578 | 0.249 |
| **R-SH** | | | 0.979 | 0.405 | 0.769 | 0.405 |
| **R-NH2** | | | | 0.373 | 0.712 | 0.373 |
| **R=O** | | | | | 0.591 | 1.000 |
| **DI H2O** | | | | | | 0.591 |

| Bilayer: 30 nm cobalt topped with 10 nm copper modified with various ligands | | | | | | |
|---|---|---|---|---|---|---|
| p(all)=0.984 | | | | | | |
| | **R-OOH** | **R-SH** | **R-NH2** | **R=O** | **DI H2O** | **CHx** |
| **R-OH** | 0.391 | 0.699 | 0.427 | 0.408 | 0.862 | 0.819 |
| **R-OOH** | | 0.701 | 0.904 | 0.969 | 0.588 | 0.752 |
| **R-SH** | | | 0.757 | 0.724 | 0.861 | 0.964 |
| **R-NH2** | | | | 0.921 | 0.642 | 0.799 |
| **R=O** | | | | | 0.616 | 0.775 |
| **DI H2O** | | | | | | 0.932 |